Department of Physics
and Astronomy

Heidelberg University

Master's thesis in Physics
submitted by Manuel Reichert
born in Stuttgart
Submission: April 2015

Asymptotic Safety of Local Quantum Gravity coupled to Matter

This Master's thesis
has been carried out by Manuel Reichert
at the Institute for Theoretical Physics
under the supervision of
Prof. Dr. Jan M. Pawlowski

Asymptotische Sicherheit von lokaler Quantengravitation gekoppelt an Materie:

Wir untersuchen asymptotisch sichere Quantengravitation mit einer Vertexentwicklung anhand einer Einstein-Hilbert ähnlichen Wirkung. Wir verwenden einen selbstkonsistenten Ansatz für die Vertices und berechnen das Laufen der Gravitationskonstanten durch die Gravitations-drei-Punkt-Funktion. Wir bauen den Beweis von lokalen Korrelationen im Impulsraum von dem Gravitationspropagator hin zum drei-Graviton-Vertex aus. Damit setzen wir die Basis für eine wohldefinierte, lokale Theorie der Quantengravitation. Weiterhin untersuchen wir das Phasendiagramm von Quantengravitation im Rahmen unserer Theorie und finden einen voll attraktiven ultraviolett (UV) Fixpunkt. Damit haben wir einen weiteren Hinweis für das asymptotisch sichere Szenario gesammelt. Zusätzlich finden wir einen metastabilen Fixpunkt in allen Approximationen, was auf seine physikalische Relevanz hindeuten könnte. Im Infraroten (IR) finden wir, dass die Kopplungen klassisch skalieren, und können damit klassische, allgemeine Relativitätstheorie reproduzieren. Zudem binden wir fermionische und skalare Materie in die Theorie ein und untersuchen den Effekt auf den UV Fixpunkt. Fermionen stabilisieren die Existenz des Fixpunktes und schwächen die Gravitationskrafts ab, während Skalare genau den gegenteiligen Effekt erzeugen. Schließlich analysieren wir kurz unimodulare Quantengravitation und finden einen attraktiven UV Fixpunkt, obwohl die Theorie nicht die gewünschte Eigenschaft der Lokalität besitzt.

Asymptotic Safety of Local Quantum Gravity coupled to Matter:

We investigate asymptotically safe quantum gravity using a vertex expansion of an action similar to Einstein-Hilbert. We implement a self-consistent ansatz for the vertices and compute the running of Newton's coupling from the graviton three-point function. We extend the proof of local correlators in momentum space from the graviton propagator to the graviton three-point function. Thus, we set the foundation for a well-defined, local formulation of quantum gravity. Furthermore, we investigate the phase diagram of quantum gravity in this truncation and find a fully attractive ultraviolet (UV) fixed point. Hence, we find further evidence for the asymptotic safety scenario. Additionally, we find a metastable fixed point in all approximations, which hints towards its physical relevance. In the infrared (IR), we find classical scaling of the couplings and hence regain classical general relativity. On top of that, we include fermionic and scalar matter and investigate the effects on the UV fixed point. Fermionic matter stabilizes the existence of the UV fixed point and weakens the gravitational force while scalar matter has the opposite effect. Finally, we briefly analyse unimodular quantum gravity and find an attractive UV fixed point, despite the fact that the theory misses the property of locality.

Contents

1 Introduction

Since one century Einstein's theory of general relativity is remarkably successful in describing the gravitational force with high precision. It covers an enormous range of length scales, from solar systems to galaxy clusters. Until today, it is verified by all measurements. Nevertheless, it is still believed to break down at some high energy scale, i.e. the Planck scale at 10^{19} GeV. This scale is far away from the energy than can be achieved by any measurement in the near future, e.g. the LHC can achieve 14 TeV. The reason for the breakdown is inherent in the theory: Just quantum theories are believed to describe physical phenomena on small length scales. General relativity, however, is a classical field theory. The believe in quantum theories originates from its big success covering the other three fundamental forces, which are the electromagnetic, the strong and the weak force. They are all well described by a renormalizable quantum field theory in the setup of the Standard Model of particle physics. It is a long sought aim of theoretical physics to unify physics in one theory and for this purpose only a quantized version of general relativity is missing. The resulting theory might even be a fundamental one, valid on all length scales.

But the quantization of gravity is not only an academic problem. It can reveal many insights into the physics of inflation [1] and black holes [2]. Furthermore, quantum gravity effects could already dominate at lower energy scales under the assumption that more spacetime dimensions exist [3]. However, the problem of the quantization is that general relativity is perturbatively non-renormalizable due to the negative mass dimension of Newton's constant,

$$[G_N] = -2 \, . \tag{1.1}$$

For this reason, a canonical quantum field theory approach fails since it would require infinitely many measurements to determine the complete theory, i.e. the theory would have no predictive power [4]. Nevertheless, there are many different approaches to find a theory of quantum gravity. The most popular alternative is string theory, others are quantum loop gravity or causal dynamical triangulation.

In this work, we study the asymptotic safety scenario, which is in particular interesting since it made recently a lot of progress. It was first proposed by Weinberg in 1976 [5] and came up when the whole understanding of renormalization changed. In the early days of quantum field theory, renormalization was merely a method to remove the infinities from the perturbative calculation. Then, effective field theories were taken more seriously. A physical cutoff was introduced and the theory was not expected to describe physics above that energy scale. It was Wilson's pioneering work [6] that showed that lowering the cutoff of the theory, i.e. integrating out momentum shells, leads to a new effective Lagrangian with modified couplings. The couplings of

the theory can thus be seen as a function of the cutoff, i.e. as scale dependent quantities. This is the principle of the renormalization group flow. Weinberg's idea of asymptotic safety states that the renormalization group flow could hit a non-trivial ultraviolet (UV) fixed point and therefore prevent couplings with a negative mass dimension from diverging on large energy scales, in our case it prevents the divergence of Newton's coupling. This UV fixed point might lay in the non-perturbative region, which would lead to the above mentioned breakdown of the canonical perturbative approach.

In the Wilsonian picture, the renormalization group flow is usually a perturbative statement. It took some more time until exact renormalization group equations were developed. Examples for this are the Polchinski equation [7] or the Wetterich equation [8–10]. The latter one is the tool of our choice. It is an exact, non-perturbative evolution equation for an effective average action. Furthermore, it allows a large variety of systematic approximation schemes. With these properties it is well suited for studying not only quantum gravity but also condensed matter and many body systems as well as strongly coupled systems like quantum chromodynamics [11]. Due to this development, the first equations for asymptotically safe quantum gravity were set up by Martin Reuter [12]. Its first solution [13] and also the first phase diagram [14] gave hints that a non-trivial UV fixed point might exist. Over the years many improvements followed and more hints towards asymptotic safety of quantum gravity were gathered [15–18].

One of the most problematic topics of asymptotic safety is the disentanglement of the background and the fluctuating metric. In many approximations they are simply identified with each other. Several ideas to resolve this interplay were put forward, for example the bi-metric approach [19], the use of the geometrical flow equation [20] or a vertex expansion [21]. In this work, we improve the latter and implement the first fully self-consistent ansatz for an asymptotically safe theory of quantum gravity. This involves the use of a self-consistent vertex construction [21] and the computation of the vertex expansion up to the graviton three-point function, which is the first vertex that contains information about the running of Newton's coupling.

The starting point is the gauge fixed Einstein-Hilbert action, which is expanded around a flat Euclidean background. The flow of the graviton and the ghost propagator are computed with fully momentum dependent anomalous dimensions [21]. The flow of the graviton three-point function is determined for a special set of tensor and momentum projections that is expected to capture the physically most relevant degrees of freedom. Importantly, this work addresses the topic of local flows in momentum space. Locality is a desired property of the theory. Without locality the whole concept of renormalization group flows becomes questionable since it would imply that a renormalization group step in the low energy regime can change the physics in the UV. In [22], it was shown that the flow of the graviton propagator is local in momentum space. We address the question of locality to the graviton three-point function.

As a second topic, this work is concerned with the inclusion of matter in the theory of quantum gravity. Graviton-matter interactions are interesting for both sides, the

matter theory and the gravitational theory: In matter theories, the gravitational interaction might change basic properties of a theory e.g. effect the Landau pole [23] or induce chiral symmetry breaking [24] can be investigated. In the gravitational theory, the interactions can have severe effects on the UV fixed point and might even spoil asymptotic safety.

For the latter exits an analogy in Yang-Mills theories, where too many fermion flavours spoil asymptotic freedom. For gravity, the interesting question is: Which numbers of matter flavours are compatible with asymptotic safety? This question was first discussed in [25] where the general signs of matter contributions to the running of Newton's constant were determined. Bounds on the number of matter flavours were found in [26] and their follow-up [27] where all types of matter were coupled to gravity and the existence of a UV fixed point was investigated. These works state that the Standard Model is compatible with asymptotic safety while supersymmetric theories and grand unified theories are not.

In this work, we test these statements in a different approximation, but limiting ourselves to scalar and fermionic matter. For the first time, the technique of the vertex expansion is extended to the matter sector In consequence, the background dependence is also disentangled in the matter sector. In the fermionic sector, we discard the usual vielbein formalism and apply instead the lately developed spin-base invariance formalism [28]. All matter is minimally coupled and no matter-matter interactions are taken into account.

This thesis is structured in the following way: In chapter 2, we introduce basic methods of quantum field theory and use them to derive the Wetterich equation. Furthermore, we discuss some properties of the equation and introduce compatible approximation schemes. In chapter 3, we display ingredients we need from classical general relativity. Since we later briefly investigate unimodular quantum gravity, we also introduce the classical version of it in this chapter and show the equivalence to general relativity. In chapter 4, the asymptotic safety scenario is introduced. First the general idea is explained and then we recap the recent work and progress in this field. We put some focus on the inclusion of matter. In chapter 5, we present our setup, i.e. the vertex expansion and the construction of the flow for correlation functions. We present the derivation of the flow equations and for each running quantity we display different versions due to different projection possibilities. Especially for the running of Newton's coupling we have two choices e.g. the geometrical flow equation or the graviton three-point function. Additionally, we compute matter-graviton interactions. In chapter 6, we discuss some details of our calculation i.e., the computation of the vertices, and the evaluation of the diagrams. We put emphasis on the derivation of analytic equations. In chapter 7, we display our results, namely the locality of the three-point function and the UV fixed point of the pure gravity system. We present the evolution of the UV fixed point under matter inclusions. We also describe the possibility of a UV fixed point with non-vanishing matter masses. At the end of the chapter, we briefly discuss unimodular quantum gravity and display the UV fixed point in this system. In chapter 8, we summarize and give an outlook on further projects.

Part I

Basics and Revision

2 The Functional Renormalization Group

In this chapter, the most important tool of this thesis is introduced, the functional renormalization group. It is already known that perturbative methods face severe problems in quantum gravity and hence non-perturbative methods are required. The Wetterich equation fulfils this requirement. This chapter goes along the same lines as [29] and [30].

Modern quantum fields theories are formulated with a generating functional. There are different generating functionals, e.g., the generating functional of all n-point correlators $\mathcal{Z}$, the generating functional of connected correlators $\mathcal{W}$ or the effective action Γ, which generates one particle irreducible correlators. We are especially interested in the latter one, but it is only known in very simple systems. Since the derivation of the Wetterich equation goes hand in hand with these functionals, we shortly introduce them here.

The basic objects of a quantum field theory are the n-point correlators. In the Euclidean case for the action $S[\varphi]$ they are given by

$$\langle \varphi(x_1) \dots \varphi(x_n) \rangle := \mathcal{N} \int \mathcal{D}\varphi \, \varphi(x_1) \dots \varphi(x_n) \mathrm{e}^{-S[\varphi]} \,, \tag{2.1}$$

with some normalization $\mathcal{N}$. As already stated, all n-point correlators can be generated from a functional $\mathcal{Z}$ by functional differentiation

$$\langle \varphi(x_1) \dots \varphi(x_n) \rangle = \frac{1}{\mathcal{Z}[0]} \left(\frac{\delta^n \mathcal{Z}[J]}{\delta J(x_1) \dots \delta J(x_n)} \right)_{J=0} \,, \tag{2.2}$$

if $\mathcal{Z}$ is given by

$$\mathcal{Z}[J] = \int \mathcal{D}\varphi \, \mathrm{e}^{-S[\varphi] + J \cdot \varphi} \,, \tag{2.3}$$

with the short hand notation $J \cdot \varphi = \int d^4x \, J(x)\varphi(x)$. The functional of connected correlators $\mathcal{W}$ emerges by taking the logarithm

$$\mathcal{W}[J] \equiv \ln \mathcal{Z}[J] \,. \tag{2.4}$$

The advantage of $\mathcal{W}$ is that it only generates connected correlators. Non-connected correlators are discarded anyway and consequently it is often said that $\mathcal{W}$ stores the information about the system more efficiently. A further upgrade is the effective action, which is obtained by performing a Legendre transformation

$$\Gamma[\phi] = \sup_J \left(J \cdot \phi - \mathcal{W}[J] \right) \,. \tag{2.5}$$

This automatically guarantees that the effective action is a convex functional. The value of J that fulfils the supremum condition is now a functional of the field ϕ. At the supremum equation

$$0 \stackrel{!}{=} \frac{\delta}{\delta J} \left(J \cdot \phi - \mathcal{W}[J] \right) \tag{2.6}$$

holds. With this it is possible to establish a connection between the fields ϕ and φ, namely,

$$\phi = \frac{\delta \mathcal{W}[J]}{\delta J} = \frac{1}{\mathcal{Z}[J]} \frac{\delta \mathcal{Z}[J]}{\delta J} = \langle \varphi \rangle_J \,. \tag{2.7}$$

In the last step, the one-point correlator as in equation (2.2) with a non-vanishing source was introduced. So the field ϕ is the expectation value of the field φ in presence of a source. With all these ingredients we turn now to the functional renormalization group and derive the exact evolution equation for the effective average action, the so called Wetterich equation.

2.1 The Wetterich Equation

In the framework of the functional renormalization group one usually initiates a theory at some high momentum scale $k = \Lambda$. At this momentum scale the theory should be well described, i.e. dominated by classical physics. So this is the bare microscopic action S_{bare}, which needs to be quantized. The idea is now to successively change the momentum scale. In the limit where the momentum scale goes to zero one would like to obtain the effective action Γ. For the interpolation between these two actions one defines the effective average action Γ_k, where k is again the momentum scale parameter. The effective average action needs to fulfils the limits $\Gamma_{k \to \Lambda} = S_{\text{bare}}$ and $\Gamma_{k \to 0} = \Gamma$. The momentum scale dependence is introduced via a modification of the action

$$S \to S + \Delta S_k \,. \tag{2.8}$$

The modification ΔS_k should be quadratic in the fields in order to act like a momentum dependent mass term. In particular it should act as a mass term for the infrared (IR) modes and therefore suppress them. If the field is split into a background field $\bar{\varphi}$ and a dynamical field φ, as it is necessary in gauge theories, one has to be a little more precise. The modification should be quadratic in the dynamical field:

$$\Delta S_k[\varphi] = \frac{1}{2} \int \frac{\mathrm{d}^4 q}{(2\pi)^4} \varphi(-q) R_k[\bar{\varphi}](q) \varphi(q) \,. \tag{2.9}$$

The regulator function R_k should just depend on the background field and should also fulfil some other requirements.

- $$\lim_{q^2/k^2 \to 0} R_k(q) > 0 \tag{2.10}$$

  This ensures that IR modes are suppressed with a mass-like term.

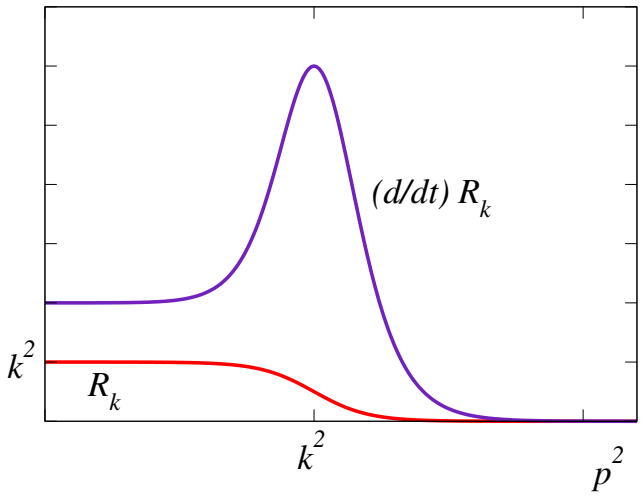

Figure 2.1: The shape of a typical regulator function and its derivative with respect to the RG-time t is shown. The regulator has a finite value in the IR and acts as a mass term. The derivative is peaked around $p^2 = k^2$, which implements the integration of that momentum shell according to the Wilsonian idea. From [29].

- $$\lim_{k^2/q^2 \to 0} R_k(q) = 0 \tag{2.11}$$

  This ensures that the regulator dependence vanishes in the limit $k \to 0$ and hence ensures that the full effective action is approached in this limit.

- $$\lim_{k \to \Lambda \to \infty} R_k(q) = \infty \tag{2.12}$$

  This ensures that the classical action is recovered in the limit $k \to \Lambda$ since the effective average action can be written as $\Gamma_{k \to \Lambda} \to S + \text{constant}$.

The typical shape of the regulator function and its derivative is shown in figure 2.1. It nicely displays the finite value of the regulator in the IR, which in consequence acts like a mass term for these modes. Further it shows the peak of the derivative of the regulator at $p^2 = k^2$, which implements the integration of that momentum shell according to the Wilsonian idea. Note that the derivative is taken with respect to the dimensionless RG-time t which is defined as

$$t = \ln \frac{k}{\Lambda}\,, \qquad \partial_t = k \partial_k\,, \tag{2.13}$$

where Λ is some chosen momentum scale. The derivative with respect to t is sometimes represented with a dot, i.e. $\partial_t f = \dot{f}$. A detailed discussion about different regulator functions follows later in section 2.3.

Now we have to look again at the generating functionals with the modified action. All functionals are now k dependent, but the source term J is still fixed and k independent. Hence, we obtain

$$\mathcal{Z}_k = \mathrm{e}^{\mathcal{W}_k} = \int \mathcal{D}\varphi\, \mathrm{e}^{-S-\Delta S_k+J\cdot\varphi} = \exp\left(\Delta S_k\left[\frac{\delta}{\delta J}\right]\right)\mathrm{e}^{\mathcal{W}[\varphi,J]}\,. \tag{2.14}$$

Before we compute the flow of the generating functional we introduce the connected propagator, which is

$$\begin{aligned}\mathcal{W}_k^{(2)} &= \frac{\delta^2\mathcal{W}_k}{\delta J\delta J} = \frac{\delta^2\ln\mathcal{Z}_k}{\delta J\delta J} = \frac{\delta}{\delta J}\left(\frac{1}{\mathcal{Z}_k}\frac{\delta\mathcal{Z}_k}{\delta J}\right)\\ &= \left(\frac{\delta}{\delta J}\frac{1}{\mathcal{Z}_k}\right)\frac{\delta\mathcal{Z}_k}{\delta J} + \frac{1}{\mathcal{Z}_k}\frac{\delta^2\mathcal{Z}_k}{\delta J\delta J} = -\phi\phi + \langle\varphi\varphi\rangle_J\,.\end{aligned} \tag{2.15}$$

With this object the flow of the generating functional can be computed to

$$\begin{aligned}\partial_t\mathcal{W}_k = \partial_t\ln\mathcal{Z}_k &= \frac{1}{\mathcal{Z}_k}\int\mathcal{D}\varphi\,\partial_t(-\Delta S_k)\mathrm{e}^{\mathcal{W}_k}\\ &= -\frac{1}{2}\int\frac{\mathrm{d}^4q}{(2\pi)^4}\dot{R}_k\langle\varphi\varphi\rangle_J\\ &= -\frac{1}{2}\int\frac{\mathrm{d}^4q}{(2\pi)^4}\dot{R}_k\mathcal{W}_k^{(2)} - \partial_t\left(\Delta S_k[\phi]\right)\,.\end{aligned} \tag{2.16}$$

Ultimately we want to compute the flow of the effective action, hence we have to do a modified Legendre transformation:

$$\Gamma_k[\phi] = \sup_J\left(J\cdot\phi - \mathcal{W}_k[J]\right) - \Delta S_k[\phi]\,. \tag{2.17}$$

The supremum is now dependent on the momentum scale k but the expectation value of the field φ is still determined by

$$\phi(x) = \langle\varphi(x)\rangle_J = \frac{\delta\mathcal{W}_k[J]}{\delta J(x)}\,, \tag{2.18}$$

in analogy to the usual quantum field theory in equation (2.7). Taking the functional derivative of equation (2.17) with respect to ϕ at the supremum of J leads to the quantum equation of motion, which receives a modification compared to the standard quantum field theory equation

$$J(x) = \frac{\delta\Gamma_k[\phi]}{\delta\phi} + (R_k\phi)(x)\,. \tag{2.19}$$

We deduce now a connection between the connected propagator and the propagator of the effective average action, before we ultimately compute the flow of the effective average action. From equation (2.18) and (2.19) one can derive the following

identities by taking functional derivatives with respect to ϕ and J, respectively:

$$\frac{\delta J(x)}{\delta \phi(y)} = \frac{\delta^2 \Gamma_k[\phi]}{\delta \phi(x) \delta \phi(y)} + R_k(x,y)\,, \tag{2.20}$$

$$\frac{\delta \phi(y)}{\delta J(x)} = \frac{\delta^2 \mathcal{W}_k[J]}{\delta J(x) \delta J(y)}\,. \tag{2.21}$$

Together, they lead to the identity

$$\begin{aligned}\delta(x-y) = \frac{\delta J(x)}{\delta J(y)} &= \int \mathrm{d}^4 z\, \frac{\delta J(x)}{\delta \phi(z)} \frac{\delta \phi(z)}{\delta J(y)} \\ &= \int \mathrm{d}^4 z\, \left(\frac{\delta^2 \Gamma_k[\phi]}{\delta \phi(x) \delta \phi(z)} + R_k(x,z) \right) \frac{\delta^2 \mathcal{W}_k[J]}{\delta J(z) \delta J(y)}\,.\end{aligned} \tag{2.22}$$

Or in different notation

$$\mathcal{W}_k^{(2)} = \left(\Gamma_k^{(2)} + R_k \right)^{-1}\,. \tag{2.23}$$

Now we can finally compute the flow of the effective average action for fixed ϕ. We first use the definition in equation (2.17), switch one term to fixed J, then use the equations (2.16) and (2.18) and finally use equation (2.23):

$$\begin{aligned}\partial_t \Gamma_k[\phi] &= \phi \cdot \partial_t J - \partial_t \mathcal{W}_k[J]\Big|_{\phi=\text{const.}} - \partial_t \left(\Delta S_k[\phi] \right) \\ &= \phi \cdot \partial_t J - \partial_t \mathcal{W}_k[J]\Big|_{J=\text{const.}} - \frac{\delta \mathcal{W}_k[J]}{\delta J} \cdot \partial_t J - \partial_t \left(\Delta S_k[\phi] \right) \\ &= -\left(-\frac{1}{2} \int \frac{\mathrm{d}^4 q}{(2\pi)^4} \dot{R}_k \mathcal{W}_k^{(2)} - \partial_t \left(\Delta S_k[\phi] \right) \right) - \partial_t \left(\Delta S_k[\phi] \right) \\ &= \frac{1}{2} \int \frac{\mathrm{d}^4 q}{(2\pi)^4} \dot{R}_k \left(\Gamma_k^{(2)} + R_k \right)^{-1} \\ &= \frac{1}{2} \mathrm{STr} \left[\frac{1}{\Gamma_k^{(2)} + R_k} \dot{R}_k \right]\,.\end{aligned} \tag{2.24}$$

In the last step, we introduced the supertrace, which involves the contraction and integration about all internal indices and momenta and also a minus sign for Grassmann valued fields. This equation is also known as the Wetterich equation. It is the central equation of this work and hence some of its properties are discussed here.

- The Wetterich equation has a nice diagrammatic representation similar to Feynman diagrams. The fully dressed propagator $\left(\Gamma_k^{(2)} + R_k \right)^{-1}$ is represented as a usual propagator. Depending on the field content this can be a line, two lines, a curly or a dashed line. The vertices, which are also fully dressed, are represented as usual vertices by a dot where the propagator field lines meet. The regulator insertion, i.e. the derivative of the regulator, is always represent

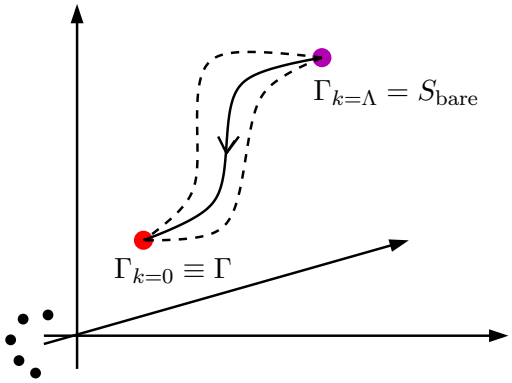

Figure 2.2: Sketch of the possible RG flows of the effective average action in theory space. Each axis represents the value of a dimensionless coupling and there are infinitely many axis. The different trajectories represent different regulators but still all trajectories must end at the full quantum effective action as long as the system is not truncated. From [29].

by a crossed circle although the regulator depends on the propagator it is inserted in. Each diagram contains exactly one regulator insertion and there are just one-loop diagrams. With these diagrammatic rules the Wetterich equation can be written as

$$\dot{\Gamma}_k = \frac{1}{2}$$ 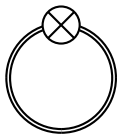 . (2.25)

- The Wetterich equation is an exact equation. At no point of the derivation we have made any approximation and the modification ΔS_k drops out in the limit $k \to 0$. So in this limit we are indeed approaching the full quantum effective action if we do not truncate our system, which is unfortunately necessary in non-trivial cases. Furthermore it is an one-loop equation and nevertheless takes higher loop effects into account since the flow encodes the evolution of the bare vertices to the fully dressed vertices.

- In principle, all allowed operators must be considered in the flow. These are evidently infinitely many. Each of those has a coupling, which can be made dimensionless. The space of all those dimensionless couplings is called theory space. It is a infinite dimensional space. The bare action is one point in this space and the quantum effective action is another one. So the solution to the Wetterich equation is a trajectory connecting those two points. While moving along this trajectory one is subsequently integrating out momentum shells according to the Wilsonian idea. A sketch of theory space is displayed in figure 2.2.

- The Wetterich equation is obviously regulator dependent and this choice is completely arbitrary as long as they fulfil the before mentioned conditions of equation (2.10) until (2.12). Different regulators correspond to different trajectories in theory space. Nevertheless the end point of all trajectories is the same, i.e. the full quantum effective action $\Gamma_{k=0}$, as long as the regulator requirements are respected. This behaviour is nicely displayed in figure 2.2. If the system is truncated, which is a necessity, the end point is not unique anymore and one should pay particular attention to the choice of regulator in order to minimize the error. Evidently a study of the regulator dependence is helpful in this case.

- It is possible to regain perturbation theory from the Wetterich equation. One can impose a loop expansion

$$\Gamma_k = S + \Gamma_{k,1-\text{loop}} + \text{higher loops} \tag{2.26}$$

and insert it into the Wetterich equation. The bare action is not scale dependent and drops out on the left hand side. The right hand side is already one loop and hence $\Gamma_k^{(2)}$ is replaced by $S^{(2)}$ to stay at one loop order. So the resulting equation is

$$\partial_t \Gamma_{k,1-\text{loop}} = \frac{1}{2}\text{Tr}\left[\partial_t R_k \left(S^{(2)} + R_k\right)^{-1}\right] = \frac{1}{2}\partial_t \text{Tr}\ln\left(S^{(2)} + R_k\right). \tag{2.27}$$

This equation can be trivially integrated to $k = 0$ where the regulator is zero and $\Gamma_{k,1-\text{loop}}$ turns into the one-loop effective action

$$\Gamma_{1-\text{loop}} = S + \frac{1}{2}\text{Tr}\ln S^{(2)} + \text{constant}\,. \tag{2.28}$$

With this we have arrived back at the standard one-loop effective action from perturbation theory.

2.2 Approximation Schemes

As already mentioned, the Wetterich equation cannot be solved exactly, except in some trivial cases. But one of its advantages is that there are several systematic approximation schemes that can be applied to it.

A first example is the derivative expansion. The effective average action is constructed from operators with increasing numbers of derivatives. For example in case of one real scalar field it is

$$\Gamma_k[\phi] = \int \mathrm{d}^4x \left(V_k(\phi) + \frac{1}{2}Z_k(\phi)(\partial_\mu\phi)^2 + \mathcal{O}(\partial^4)\right), \tag{2.29}$$

where V_k is the effective potential and Z_k is the wavefunction renormalization. This

truncation scheme is solved by projecting the flow of the effective average action onto the effective potential, the wavefunction renormalization, etc. To solve the resulting flow equations one has to eventually make an ansatz.

A second example, which is used throughout this thesis, is the vertex expansion for effective average action

$$\Gamma_k[\phi] = \sum_{n=0}^{\infty} \frac{1}{n!} \int \mathrm{d}^4x_1 \dots \mathrm{d}^4x_n \Gamma_k^{(n)}(x_1, \dots, x_n)\phi(x_1)\dots\phi(x_n)\,. \tag{2.30}$$

This ansatz for the effective average action is inserted into the Wetterich equation, then functional derivatives with respect to the fields are taken on both sides and all other fields are set to zero. This way flow equations for each vertex are obtained. It is important to note that the flow equation of n-th vertex $\Gamma_k^{(n)}$ depends on all vertices from $\Gamma_k^{(2)}$ until $\Gamma_k^{(n+2)}$, which means one ends up with an unsolvable infinite tower of differential equations. The next step of approximation is to cut this tower at some level n and to make an ansatz about the behaviour of $\Gamma_k^{(n+1)}$ and $\Gamma_k^{(n+2)}$.

The differential flow equations for the n-point vertex can be visualized with the diagrammatic representation introduced above. For the simple example of a single bosonic matter field the two-point function is

∂_t 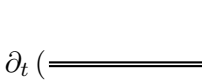 $= -\frac{1}{2}$ 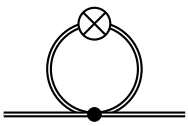 . (2.31)

In principle, all possible one-loop diagrams with two external legs are displayed. The exact prefactor of the diagrams are explained in the next paragraph. The diagrams are usually called the self-energy-diagram and the tadpole-diagram in this order. For later convenience, we also present the flow of the three-point function for a single bosonic matter field, which is

∂_t 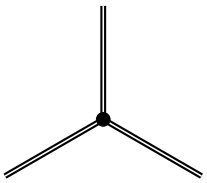 $= 3$ 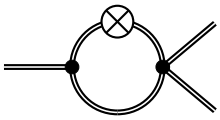 $- 3$ 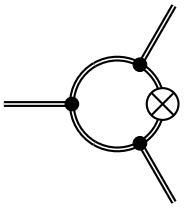 $-\frac{1}{2}$ 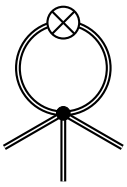 . (2.32)

Again, we give names to the diagrams, i.e. they are called the swordfish-diagram, the star-diagram, and again the tadpole-diagram in this order. For different types of fields it is necessary to write down all possible one loop diagrams. It just involves loops of other fields. Note that the prefactor for a fermionic or a Grassmann valued field in the loop has to be multiplied by minus two. The minus sign arises from the supertrace in the Wetterich equation and the factor two is caused by the fact that there is the $\psi\bar{\psi}$ contribution as well as the $\bar{\psi}\psi$ contribution. This heuristic argument does not hold anymore if, for example, a four-fermion interaction is considered. Since

in this thesis the diagrams are quite simple we stick to that argument.

The prefactors of the diagrams can be derived from a general formula [31, 32] or from some simple combinatorial arguments. We start from the Wetterich equation so the canonical prefactor is $1/2$ for bosonic loops and -1 for fermionic loops. Now, functional derivatives have to be taken of this equation. The first derivative acts on a propagator, the only field dependent quantity, and evolves it to

$$\frac{\delta}{\delta\phi}(\Gamma^{(2)}+R_k)^{-1} = -(\Gamma^{(2)}+R_k)^{-1}\Gamma^{(3)}(\Gamma^{(2)}+R_k)^{-1}\,. \tag{2.33}$$

Hence, a minus sign appears. The next functional derivative may act on each of the propagators or on the three-point vertex. In case of a propagator, again a minus sign, etc. appear. In case of the three-point vertex, it evolves it to a four-point vertex and no minus sign appears. Like this, one has just to go through all possible combinations, count all appearing minus signs and unify identical diagrams and one eventually arrives at the appropriate signs for the diagrams.

2.3 Regulators

In the last section, we already mentioned the importance of the regulator. In this section, we shed some light one the different classes of regulators.

In [16] they suggested to distinguish between *type I* , *type II* and *type III* regulators. We quickly recapitulate what they mean by that. The regulator is quadratic in the fields and enters as an addition in the propagator. The two-point function is a function of the Laplacien plus a linear map, which can contain curvature terms or couplings like the mass. They write it as $-\nabla^2 + E_1 + E_2$ where E_1 does not contain any couplings but all other linear maps, for example curvature scalars. The factor E_2 on the other hand contains all couplings. We now define the regulator to be a function of this. If it is a function of the whole expression, then they call a *type III* regulator. If E_2 is set to zero, then they call it a *type II* regulator and if it just a function of the Laplacien then they call it a *type I* regulator. In the present work, we just use *type I* regulators, which we express as

$$R_k(p^2) = \Gamma_k^{(2)}(p^2)\Big|_{m=0} r\left(\frac{p^2}{k^2}\right)\,, \tag{2.34}$$

where r is some dimensionless shape function that must fulfil similar requirements as mentioned in the equations (2.10) until (2.12). The two-point function evaluated at vanishing mass is in our case just a function of the Laplacien since we are expanding around the flat Euclidean background $\bar{g}_{\mu\nu} = \delta_{\mu\nu}$, which is commented in detail later. In consequence, possible terms linear in the Ricci scalar are vanishing.

An interesting aspect of different types of regulators was discussed in [33]. There the usage of type one and type two regulator for fermions resulted in different signs in the contribution to the beta function of Newton's constant. Unfortunately, we are

not able to resolve this issue since we are expanding around the flat background and hence type one and type two regulators are just identical. Nevertheless, we pick this issue up again later.

There are different classes of dimensionless shape functions that can be used. The most popular is the Litim regulator, often called the optimized regulator [34]

$$r_{\text{opt}}\left(\frac{p^2}{k^2}\right) = \left(\frac{k^2}{p^2} - 1\right)\Theta\left(k^2 - p^2\right) , \tag{2.35}$$

where Θ is the Heaviside step function. The optimized cut-off is especially useful for analytic calculations. For numerical purposes it is not the most recommendable one due to its non-analytic behaviour. This regulator is used in most cases in this thesis. An alternative is the exponential regulator

$$r_a\left(x\right) = \frac{1}{x\left(2\mathrm{e}^{x^a} - 1\right)} , \tag{2.36}$$

where $x = p^2/k^2$ and a is some positive number, usually in the range between two and six. This regulator is more useful for numerical approaches.

Note, that in case of fermions the whole analysis is slightly different since the two-point function is not a function of the Laplacien but of $\not{\nabla}$. In this case the Litim regulator has the shape

$$r_{\text{opt,ferm}}\left(\frac{p^2}{k^2}\right) = \left(\sqrt{\frac{k^2}{p^2}} - 1\right)\Theta\left(k^2 - p^2\right) . \tag{2.37}$$

3 General Relativity

In this chapter, we shortly introduce the basics of general relativity. We don't present a lot of details, rather the things that are used in this work. General relativity is based on the Einstein-Hilbert action

$$S_{\mathrm{EH}} = \frac{1}{16\pi G_N} \int \mathrm{d}^4x \sqrt{-\mathrm{det} g}(2\Lambda - R)\,, \tag{3.1}$$

where G_N is Newton's constant, Λ is the cosmological constant and R is the Ricci scalar. The field content of the action is the metric field $g_{\mu\nu}(x)$, which appears in the covariant invariant integral measure with $\sqrt{-\mathrm{det} g}$ and also the Ricci scalar is a functional of it. One comment about $\sqrt{-\mathrm{det} g}$ is necessary. Usually, general relativity is defined in a Minkowski-like space where the metric is actually a pseudo metric with signature $(-,+,+,+)$ or the other way round. Hence the square root returns a real value. In this work, we work in Euclidean-like space and the metric is an actual metric with signature $(+,+,+,+)$. So the minus sign under the square root should be dropped in order that everything stays real. As a shorthand notation, we write $\sqrt{g}$ referring to the determinant of the metric with the appropriate sign.

The Ricci scalar is defined as the trace of the Ricci tensor

$$R = \mathrm{Tr}\ \mathrm{Ric}\,. \tag{3.2}$$

In turn, the components of the Ricci tensor are defined via the Riemann tensor

$$\mathrm{Ric}_{\mu\nu} = R^{\alpha}_{\mu\alpha\nu}\,. \tag{3.3}$$

Eventually, the Riemann tensor is given by

$$R^{\alpha}_{\beta\mu\nu} = \partial_\mu \Gamma^{\alpha}_{\nu\beta} - \partial_\nu \Gamma^{\alpha}_{\mu\beta} + \Gamma^{\gamma}_{\nu\beta}\Gamma^{\alpha}_{\mu\gamma} - \Gamma^{\gamma}_{\mu\beta}\Gamma^{\alpha}_{\nu\gamma}\,, \tag{3.4}$$

with the Christoffel symbols Γ. They have the coordinate representation

$$\Gamma^{\alpha}_{\mu\nu} = \frac{1}{2} g^{\alpha\beta}\left(\partial_\mu g_{\nu\beta} + \partial_\nu g_{\mu\beta} - \partial_\beta g_{\mu\nu}\right)\,. \tag{3.5}$$

The spacetime covariant derivative gets a contribution of the Christoffel symbols depending on the object it acts on. In case of a scalar the covariant derivative equals the partial derivative and in case of a vector v^μ or a tensor $t^{\mu\nu}$it is

$$\mathcal{D}_\mu v^\nu = \partial_\mu v^\nu + \Gamma^{\nu}_{\mu\rho} v^\rho\,, \tag{3.6}$$

$$\mathcal{D}_\mu t^{\alpha\beta} = \partial_\mu t^{\alpha\beta} + \Gamma^{\alpha}_{\mu\nu} t^{\nu\beta} + \Gamma^{\beta}_{\mu\nu} t^{\alpha\nu}\,. \tag{3.7}$$

In order to derive the equations of motion one has to vary the action with respect to the field content, which is the metric field $g_{\mu\mu}$, i.e.,

$$\frac{\delta S_{\mathrm{EH}}}{\delta g_{\mu\nu}} \stackrel{!}{=} 0\,. \tag{3.8}$$

What follows are the well known Einstein equations

$$R_{\mu\nu} + \left(\Lambda - \frac{1}{2}R\right) g_{\mu\nu} = 8\pi G_N T_{\mu\nu}\,, \tag{3.9}$$

where $T_{\mu\nu}$ is the energy-momentum tensor, which is zero for an empty universe, but in case we include some matter Lagrangian $\mathcal{L}_m$ it is given by

$$T_{\mu\nu} = -\frac{2}{\sqrt{g}}\frac{\delta \mathcal{L}_m}{\delta g^{\mu\nu}}\,. \tag{3.10}$$

The Einstein-Hilbert action is constructed such that it respects diffeomorphism symmetry. In fact it is the simplest possible action that is invariant under the diffeomorphism group. Higher order operators of R could be included without spoiling the symmetry. The symmetry is later important when quantizing it. For example it could be a reasonable demand that the quantized theory should still respect the symmetry or at least should not violate it too much.

The generator of a diffeomorphism symmetry is the Lie derivative. The Lie derivative is generated by a vector ϵ_μ. Making a coordinate transformation

$$x_\mu \to x_\mu + \epsilon_\mu \tag{3.11}$$

and changing the metric accordingly with the Lie derivative $\mathcal{L}_\epsilon$

$$g_{\mu\nu} \to g_{\mu\nu} + \mathcal{L}_\epsilon g_{\mu\nu} \tag{3.12}$$

leaves the equation of motion invariant. It can be shown that the Lie derivative has a local coordinate representation

$$\mathcal{L}_\epsilon g_{\mu\nu} = \mathcal{D}_\mu \epsilon^\sigma g_{\sigma\nu} + \mathcal{D}_\nu \epsilon^\sigma g_{\sigma\mu}\,. \tag{3.13}$$

3.1 Unimodular Gravity

In unimodular gravity, the determinant of the metric is fixed to a certain number ϵ [35], i.e.

$$\sqrt{g} = \epsilon\,. \tag{3.14}$$

This implies that the volume of the space time is fixed and this is also the reason why unimodular gravity is inherent different to general relativity. The fixing of the volume corresponds to fixing an observable and can hence not be achieved by

any kind of gauge fixing. Nevertheless, unimodular gravity is equivalent to general relativity on a classical level. However, it differs on the quantum level and thus it is particularly interesting to investigate the differences between Einstein quantum gravity and unimodular quantum gravity.

There are also other reasons to be interested in unimodular gravity. One is linked to the nature of quantum vacuum fluctuation, i.e. the fine-tuning problem of the cosmological constant. The mass dimension of the cosmological constant is two, $[\Lambda] = 2$, and therefore the canonical running would drive its value to be approximately the square of the physical mass of the theory, which is the Planck mass with $M_{\text{Pl}} \approx 10^{19}\,\text{GeV}$. The experimental value however differs about 120 orders of magnitudes from that expectation. One can either just accept this difference and say fine-tuning is acceptable or otherwise one has to find a theoretical explanation. Unimodular gravity offers a possible explanation due to an idea, which was again proposed by Weinberg [36]. This idea states that the cosmological constant should not be taken as a coupling of the action but rather a constant of integration that just arises at the equation of motion. In the latter case the cosmological constant does not exhibit any running and hence, there is no fine-tuning problem.

Now we want to show the classical equivalence of general relativity and unimodular gravity. The equations of motion of general relativity are displayed in equation (3.9). It is crucial to note that, together with the Bianchi identities

$$\mathcal{D}^\mu \left(R_{\mu\nu} - \frac{1}{2} g_{\mu\nu} R \right) = 0\,, \tag{3.15}$$

it follows straight forward the conservation of the energy-momentum tensor,

$$\mathcal{D}^\mu T_{\mu\nu} = 0\,, \tag{3.16}$$

by taking the covariant derivative of equation (3.9) and using equation (3.15). Also in unimodular gravity we demand conservation of the energy-momentum tensor. The equation of motion look slightly different

$$R_{\mu\nu} - \frac{1}{4} g_{\mu\nu} R = 8\pi G_N \left(T_{\mu\nu} - \frac{1}{4} g_{\mu\nu} T^\alpha_\alpha \right)\,. \tag{3.17}$$

If we now follow the same procedure as before and demand that the energy-momentum tensor is again conserved, we arrive at the identity

$$\mathcal{D}_\mu \left(R + 8\pi G_N T^\alpha_\alpha \right) = 0\,. \tag{3.18}$$

This identity can be integrated and consequently the expression in the brackets is zero up to a constant of integration, which we choose to call 4Λ. Inserting this back into the equation of motion (3.17) leads precisely to the equation of motion of general relativity (3.9). This proves the equivalence of the theories but only up to the postulate of a conserved energy-momentum tensor in unimodular gravity.

Furthermore, this illustrates the unusual appearance of the cosmological constant and the fact that it is no running parameter. A more general proof for the equivalence in case of $f(R)$ gravity can be found in [37].

4 The Asymptotic Safety Scenario

In this section, we introduce the Asymptotic Safety Scenario. On the one hand we show the physical requirements and implications and on the other hand we give a brief historical review.

The asymptotic safety scenario was first proposed by Steven Weinberg in 1979 [5]. He proposed that a quantum field theory of gravity could be renormalizable despite the known fact of its perturbatively non-renormalizability due to the mass dimension of Newton's constant. Perturbation theory always expands around the so called Gaussian fixed point, which is the fixed point where all couplings are zero. So a non-Gaussian fixed point could be unobserved by perturbation theory. If this non-Gaussian fixed point is UV attractive it can render the theory finite for arbitrary high scales. In case of gravity, this can prevent Newton's coupling from diverging, which is usually expected due to its mass dimension. In this case, the momentum scale k can be taken to infinity without facing any divergences and consequently a theory of gravity is obtained that is valid on all scales. This resulting theory is called a *fundamental* theory due to its validity on all scales.

Let's return to more general considerations, i.e. let's look at the infinite dimensional theory space of dimensionless couplings, which contains for example the dimensionless Newton's coupling $g = G_N k^2$ and the dimensionless cosmological constant $\lambda = \Lambda k^{-2}$. It can contain a more general version of these couplings as we see later, or higher order couplings of e.g. $f(R)$ gravity. But for the moment we restrict ourselves to this finite dimensional subset. For an attractive UV fixed point we require

$$\partial_t g \equiv \beta_g(g,\lambda) \xrightarrow{k\to\infty} \beta_g(g^*,\lambda^*) = 0\,, \tag{4.1}$$

$$\partial_t \lambda \equiv \beta_\lambda(g,\lambda) \xrightarrow{k\to\infty} \beta_\lambda(g^*,\lambda^*) = 0 \tag{4.2}$$

for suitable initial conditions of g and λ. To shed light on this issue of attractiveness we make a small variation of the couplings value around the fixed point values

$$g = g^* + \delta g\,, \tag{4.3}$$

$$\lambda = \lambda^* + \delta\lambda\,. \tag{4.4}$$

This variation is inserted this back into the beta-functions and expanded around the fixed point, which leads to

$$\begin{pmatrix}\beta_g(g,\lambda)\\ \beta_\lambda(g,\lambda)\end{pmatrix} = \begin{pmatrix}\beta_g(g^*,\lambda^*)\\ \beta_\lambda(g^*,\lambda^*)\end{pmatrix} + \underbrace{\begin{pmatrix}\frac{\partial\beta_g}{\partial g} & \frac{\partial\beta_g}{\partial\lambda}\\ \frac{\partial\beta_\lambda}{\partial g} & \frac{\partial\beta_\lambda}{\partial\lambda}\end{pmatrix}}_{\equiv B}(g^*,\lambda^*)\begin{pmatrix}\delta g\\ \delta\lambda\end{pmatrix} + \mathcal{O}(\delta g^2,\delta\lambda^2)\,. \tag{4.5}$$

The first term vanishes due to the definition of a fixed point and second term contains the so called stability matrix B. The eigenvalues of this stability matrix determine if the fixed point is attractive or repulsive. Lets call the eigenvalues b_n and the eigenvectors e_n, hence they are solutions to the eigenvalue problem

$$Be_n = b_n e_n \,. \tag{4.6}$$

Then the real part of b_n determines the stability, which can be easily seen by solving the linearized differential equations. If all real parts are negative, then the fixed point is fully UV attractive or IR repulsive, and if all real parts are positive, then the fixed point is fully UV repulsive or IR attractive. Otherwise it is a saddle point or a metastable fixed point.

The UV fixed point is a point in theory space. Lets assume not every direction of this fixed point is UV attractive. Then the set of initial conditions that create trajectories that flow into the UV fixed point can be defined. In other words the flow equation is solved for different initial values and all initial values that create a trajectory that leads into the UV fixed point are unified in one set. It is evident that this set is not disconnected but forms a surface. This surface is called the UV critical surface. The dimensionality of the surface is exactly the number of attractive directions.

We want our theory to have predictive power, hence, we want to know via experiments, which trajectory connects the UV fixed point and the IR fixed point, which represents general relativity. It is necessary to make experiments and measurements to determine the physical trajectory since a priori non of the infinite amount of trajectory is predestined. Evidently, the number of measurements to be done is exactly the dimensionality of the critical surface, therefore we demand that the critical surface is finite dimensional. This is the second and last criteria of asymptotic safety. Usually one can just solve truncations that contain finitely many directions and so this criterion is trivially fulfilled. But especially in $f(R)$ gravity one demands that at some point all higher orders in R are not increasing the dimensionality of the critical surface. This is exactly what computations have shown e.g. in [18, 38, 39], where just the lowest three powers in R were relevant.

4.1 Background Flow Method

In this section, we present the standard approach to the asymptotic safety scenario, the background flow method. Afterwards, we give a small summery what has been done so far by other research groups and discuss in the end why and how we think we can improve on these truncations.

The starting point is a diffeomorphism invariant bare action. The easiest choice is the Einstein-Hilbert action. The two coupling constants G_N and Λ are promoted to

running, scale dependent couplings i.e.

$$S_{\text{EH}} \longrightarrow \Gamma_k = \frac{1}{16\pi G_{N,k}} \int \mathrm{d}^4x\sqrt{g}(2\Lambda_k - R) \; . \tag{4.7}$$

As already mentioned before, in theories with a gauge symmetry one has to introduce a gauge fixing and a ghost action. To treat this appropriate it is necessary to split the field content into a background field and in a fluctuating field. Consequently the metric is split into

$$g_{\mu\nu} = \bar{g}_{\mu\nu} + h_{\mu\nu} \; . \tag{4.8}$$

The details of the split as well as gauge fixing and ghosts are discussed in the next chapter. Here, we want to emphasize that the background metric can be arbitrary chosen and there is no necessity for the fluctuating field to be small.

A wavefunction renormalization for the fluctuating field has to be introduced. But since the action is a very complicated functional of the fluctuating field it is an easier first shot to introduce it as an overall factor via Newton's constant i.e.

$$G_{N,k} := \frac{G_N}{Z_{g,k}} \; . \tag{4.9}$$

We furthermore introduce the commonly used abbreviation

$$\kappa^2 := \frac{1}{32\pi G_N} \; . \tag{4.10}$$

Now it is easy to write down the left hand side of the Wetterich equation, which is the scale derivative of the effective average action, which we already evaluated at vanishing fluctuations i.e. $\bar{g} = g$

$$\partial_t \Gamma_k \left[g, \bar{g}\right] \Big|_{g=\bar{g}} = 2\kappa^2 \int \mathrm{d}^4x\sqrt{\bar{g}} \left(2\partial_t \left(Z_{g,k}\Lambda_k\right) - \bar{R}\partial_t\Lambda_k\right) \; . \tag{4.11}$$

Note, that this equation is also true if we would have included ghost and gauge fixing contributions because they are vanishing when evaluated at $g = \bar{g}$. On the right hand side we have

$$\partial_t \Gamma_k \left[g, \bar{g}\right] \Big|_{g=\bar{g}} = \frac{1}{2}\mathrm{Tr}\left[\left(\frac{\delta^2}{\delta g^2}\Gamma_k\left[\bar{g}, g\right]\Big|_{g=\bar{g}} + R_k\right)^{-1} \partial_t R_k\right] \; . \tag{4.12}$$

At this point, we want to put focus on the approximation that in done in the background flow method. The problematic gets clear if one observes the metric dependencies on both sides. The left hand side depends only on one metric, since it is evaluated at $g = \bar{g}$, while the right hand side still depends on both metrics since first the functional derivative has to be performed. With other words, the result of the functional derivative can not be resolved with the information that appears on

the left hand side i.e. the flow is not closed. To put it once more differently, the background metric is basically running since it is identified with the full metric but as an input for the regulator, gauge fixing and ghosts it should be set to a constant. Here it is important to note that the full effective action can not be written just in terms of the full metric but is indeed a functional of two metrics separately. To summarize, the error that is implicitly done by the background flow method is

$$\frac{\delta^2}{\delta g^2}\Gamma_k[\bar{g},g]\bigg|_{g=\bar{g}} \approx \frac{\delta^2}{\delta g^2}\Gamma_k[g,g] \; . \tag{4.13}$$

Equation (4.11) is combined with (4.12) and then the inversion of the propagator $(\Gamma_k^{(2)}+R_k)^{-1}$ is performed, which is a non-trivial task due to the tensor structure. The inversion be discussed in section 6.2. Afterwards the equation is expanded in powers of R. We already know that the left hand side only contains terms independent of R and linear in R and hence we can neglect all higher orders on the right hand side. What is left is the evaluation of the functional trace, which is again non trivial and can be done with heat kernel methods. Since this method is not used in the present work, we are referring the reader to e.g [40, 41] for details. Eventually comparing left hand side and right hand side leads to equations for the dimensionless cosmological constant $\lambda := \Lambda_k k^{-2}$ and for the anomalous dimension of Newton's constant $\eta_g := -\dot{Z}_{g,k}/Z_{g,k}$. The flow equation of Newton's constant is then finally

$$\dot{g} = (2-\eta_g)g \; . \tag{4.14}$$

These equation were set up for the first time by Martin Reuter in 1996 [12].[1] He used an exponential cut-off (compare equation (2.36)) and was therefore just able to give convergent but uncalculable integral equations. In [13] the equations were solved numerically. A non-trivial UV fixed point was found and the attractiveness in both directions confirmed. In [14] Martin Reuter and Frank Saueressig discussed the flow in great detail and used a sharp cut-off (compare equation (2.35) instead of an exponential one. The trajectories were numerically integrated and the phase diagram of quantum gravity computed. In figure 4.1 this phase diagram is shown. Besides the fully attractive UV fixed point it displays the expected Gaussian fixed point but no IR fixed point that corresponds to classical general relativity. Instead, the whole region close to $g = 0$ is considered to be equivalent to classical general relativity.

Over the last decade, the system has been improved in many different directions:

- One of the first extensions was an additional term proportional to R^2 in the action [42]. A non-trivial UV fixed point was found also in this truncation and later the whole phase diagram was investigated in detail [43]. This was later extended to higher powers of R, first up to R^7 [18] and later up to R^{34} [39]. In all cases, just the first three orders gave relevant directions.

[1] It involved more elaborate details about gauge fixing and ghosts, etc.

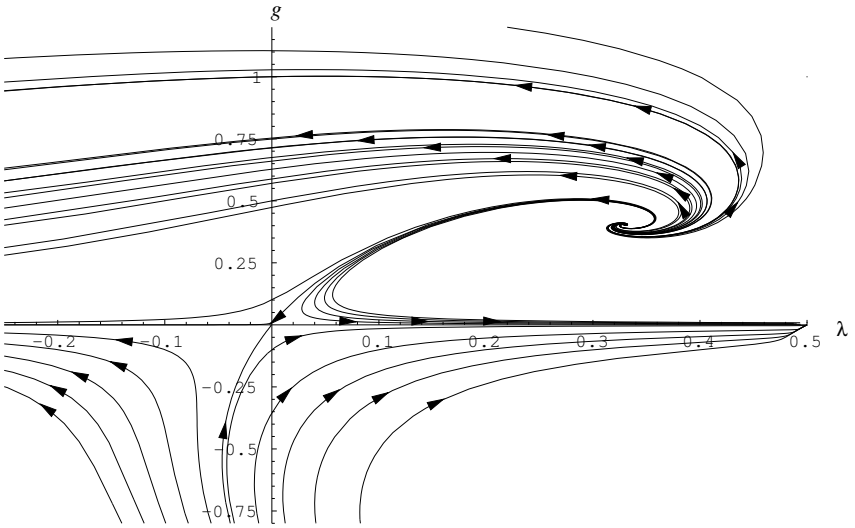

Figure 4.1: The phase diagram of quantum gravity in a background flow truncation is shown. The arrows are pointing in the IR direction. The Gaussian fixed point at $g^* = 0 = \lambda^*$ is visible as well as the fully attractive, non-trivial, interacting UV fixed point at $g^* \approx 0.3$ and $\lambda^* \approx 0.3$. From [14].

- The ghost sector, which was first of all just treated non-dynamical, was improved by a coupling to the curvature [44] and by including the wavefunction renormalization and the anomalous dimension [45, 46].

- It was tried to cure the unphysical background dependence due to the background flow method. One attempt was the so called bi-metric approach [19, 47, 48] where two full Einstein-Hilbert actions are treated at the same time. Other approaches involved the use of Nielsen identities [20] or a vertex expansion [21]. The latter is used in this thesis. General background independence for conformally reduced Einstein-Hilbert gravity was discussed in [49].

- In [50] higher dimensions in Einstein-Hilbert quantum gravity were studied and in all dimensions, from $d = 4$ until $d = 11$, a non-trivial UV fixed point was found.

- Applications of asymptotically safe quantum gravity involve e.g. the physics of black holes since the entropy is directly linked to Newton's constant, which is now a running coupling [2]. This was even done in higher dimensions [51].

The coupling of gravity to matter has also been put forward since a long time. Especially popular are scalar-tensor theories. The first paper in this direction was [52], which involved a potential for the scalar and the coupling to gravity described with a function $F(\phi)R$. This was extended to more general functions of the curvature, i.e. $F(\phi, R)$ [53, 54]. Later this was also put in the context of cosmological problems

[55]. The problem in such system is a singularity that occurs at the conformal point. In [56] they tried to circumvent this problem by employing an exponential split of the metric as well as a gauge fixing that is comparable to unimodular gravity. But the problem of the singularity still persists and was just shifted to another point. Scalar-tensor theories are especially interesting due to their cosmological applications. For a detailed discussions see [40].

Graviton-matter interactions can also have severe effects on the matter system itself. For example, graviton loops can generate matter-self-interactions e.g. for scalars [57] and for fermions [24]. A possible question is if gravitons can induce chiral symmetry breaking [58]. Further, graviton-matter interactions enhance cross sections compared to the standard model prediction. This is especially interesting in a scenario with higher dimensional spacetime since this reduces the value of the Planck scale and in consequence enhances the graviton contribution to the cross section. This can be tested for example with muon-muon production [3] or photon-photon scattering [59]. In Yang-Mills theories, the influence of asymptotic safety can be tested with respect to asymptotic freedom. The influence of gravity should not spoil asymptotic freedom. This was investigated in [60] and is explained in more detail in [31, 61].

In this work, we are especially interested in the effect of graviton-matter interactions to the pure quantum gravity system, i.e. what is the influence on the UV fixed point. The question is: Are there constraints on the matter content from the asymptotic safety perspective? The first work on this subject was [25], which determined the sign of the matter contributions to the beta functions. This was continued in [62] and [63] with first bounds on the matter sector. Eventually in [26] and the follow-up paper [27] the complete standard model content was coupled to gravity and the existence of a fixed point investigated. This approach is very closely related to the work of this thesis and is therefore discussed in the next section in detail.

For reviews on asymptotic safety we refer to [15, 17].

4.2 Inclusion of Matter

This thesis is also concerned with the inclusion of matter into the asymptotic safety scenario. In this section, we discuss the effects of matter that are in principle possible. The technical details follow at the end of the next chapter. Further, we recap the latest results from [26].

In Yang-Mills theories it is known that too many fermion flavours can spoil asymptotic freedom. A similar effect can take place in asymptotic safety and hence it is necessary to carefully include matter degrees of freedom into the theory. To get a first feeling for the matter effects we take a look at the beta functions, especially of the beta function of g. A typical shape is

$$\dot{g} = \beta_{g,\text{gravity}} \pm N_f(\dots) \pm N_s(\dots) \pm N_v(\dots)\,, \tag{4.15}$$

where N_f, N_s and N_v are the number of fermion, scalar and vector boson flavours,

respectively. So the contributions are proportional to the flavour number, which is quite obvious considering that each particle can once run in the loop of the diagram that defines the equation for Newton's coupling. The signs of the contribution have been intentionally left undetermined since these signs indicate potentially stabilizing or destabilizing behaviour. To be more precise: If the sign is negative then it is opposite to the canonical running of g, which is cause by its mass dimension, and it has the same sign as the loop corrections from the pure gravity part close to the fixed point. It is necessary that the loop corrections all together get negative enough at some momentum scale in order to encounter the canonical running of g and therefore to ensure the existence of the fixed point. Due to this argument we conclude that a negative sign is potentially stabilizing the UV fixed point and therefore supporting the asymptotic safety scenario, while a positive sign is potentially destabilizing. We want to emphasize that we put the word "potentially" since the system is way more complicated that presented here and the subject of stabilization can not be strictly determined by one sign in the beta function. For example there could ba a stabilizing mechanism, which increases the contribution of the pure gravity loops and therefore compensates the positive contribution of matter fields. Such a stabilizing mechanism is especially effective if it strengthens or weakens the graviton propagator. The graviton propagator with a momentum $q < 1$ has the shape

$$G_{\text{Graviton}} = \frac{1}{\mu_h + 1} \times \text{tensor structure}\,, \tag{4.16}$$

where μ_h is the mass parameter of the graviton. This propagator has a well known pole at $\mu_h = -1$. Evidently the graviton propagator loses strength if the graviton mass is driven to larger values, and gains strength vice versa. Therefore is the sign of the matter contribution in the $\dot{\mu}_h$ equation at least as important as the sign in the $\dot{g}$ equation. A positive sign in the $\dot{\mu}_h$ equation weakens the graviton propagator, thus also the gravity loops in the $\dot{g}$ equation and in consequence destabilizes the UV fixed point.

We now want to recap the results from [26]. They introduced minimally coupled fermions, scalars and vector bosons and derived the beta functions of g and λ via the standard background field flow and improved it with the anomalous dimensions of the graviton, the ghost, and the matter particles. They obtained the following results: Fermions and scalars destabilize the UV fixed point while vector bosons tend to stabilize it. They found critical numbers of flavours, where the fixed point ceases to exist, namely:

$$N_{f,\text{crit}} \approx 10,1 \qquad \text{and} \qquad N_{s,\text{crit}} \approx 27,7\,. \tag{4.17}$$

These are the matter bounds in case of just one matter type. They also checked specific matter models like the standard model (SM) ($N_s = 4$, $N_f = 45/2$ and $N_v = 12$), the SM with right-handed neutrinos and some scalar dark matter ($N_s = 6$, $N_f = 24$ and $N_v = 12$), the minimally supersymmetric standard model (MSSM) ($N_s = 49$, $N_f = 61/2$ and $N_v = 12$) and some grand unified theories (GUTs). Their

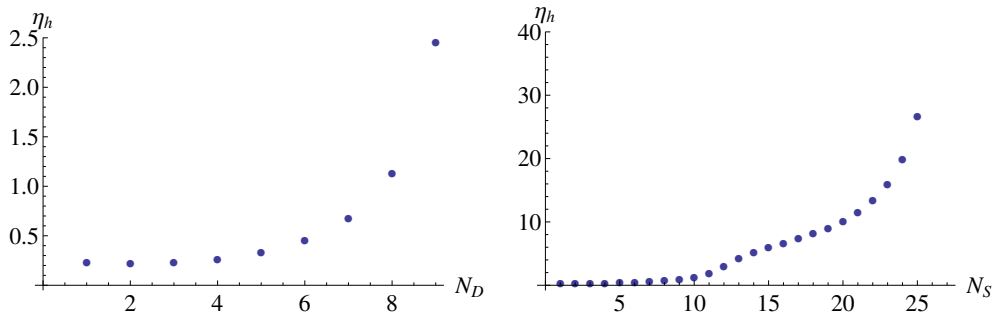

Figure 4.2: The anomalous dimensions of "Matter matters" in the scalar sector is displayed. On the left the fixed point value of the anomalous dimension of the graviton is plotted over the number of fermion flavours, while on right the same is done over scalar flavours. Both anomalous dimensions have too large values from $N_f \approx 9$ and $N_s \approx 10$, respectively, and hence indicate a breakdown of the truncation. Both plots are taken from [26].

claim is that the standard model, also with small extensions, is compatible with asymptotic safety while MSSM and GUTs are not. The fact that the SM particle content can be higher that the single matter bound is explained by the fact that vector bosons are stabilizing the UV fixed point.

This claim is on the one hand quite beautiful since it contains statements that can be verified. But on the other hand, there are quite some rough approximations in their computation that should leave the reader in doubt about the certainty of the statements. First of all, they used the background flow method, which is known to cause unphysical background dependencies in the system. But also the anomalous dimensions, which are for some examples displayed in figure 4.2, have partly incredible large values. A value of $\eta > 2$ is usually considered untrustworthy and a hint towards the breakdown of the truncation, as it is explained in the next section. Furthermore their statement about supersymmetry has to be taken very carefully since their model is simply counting of flavour number and does not include any physics of a supersymmetric model like the cancellation of one loop corrections.

4.3 Upper Bound on the Anomalous Dimension

We are doing a small interlude and discuss an upper bound on anomalous dimensions. For this, we take the definition of the anomalous dimension, which is

$$\eta(k) := -\frac{\dot{Z}(k)}{Z(k)}\,, \tag{4.18}$$

with the approximation that neither the wavefunction renormalization Z nor the anomalous dimension is momentum dependent. This can be evolved to

$$Z(k) = Z(k_0) \exp\left(- \int_{k_0}^{k} \frac{\mathrm{d}k'}{k'} \eta(k') \right) . \tag{4.19}$$

For large k the anomalous dimension is close to a fixed point value and therefore approach the constant η^*. We approximate the anomalous to be that constant since we are just integrating over large values of k. With this approximation the anomalous dimension can be taken out of the integral and the integration can be performed. The result is

$$Z(k) = Z(k_0) \left(\frac{k}{k_0} \right)^{-\eta^*} . \tag{4.20}$$

We defined the regulator via

$$R_k(p^2) = \Gamma_k^{(2)}(p^2)\Big|_{m=0} r\left(\frac{p^2}{k^2}\right) \sim Z(k) p^2 r\left(\frac{p^2}{k^2}\right) , \tag{4.21}$$

which has to fulfil the requirement (2.12), which translates into

$$\lim_{k\to\infty} R_k \sim \lim_{k\to\infty} Z(k) k^2 \propto \lim_{k\to\infty} k^{2-\eta^*} \overset{!}{\to} \infty . \tag{4.22}$$

This requirement is just fulfilled if $\eta^* < 2$. In consequence, we discard solutions with a fixed point value of the anomalous dimension larger than two. These solutions are considered untrustworthy and indicate a breakdown of the truncation.

Part II

Setup and Results

5 Our Setup

In this chapter, we introduce the setup that is used in this thesis. We start from the pure quantum gravity case, explaining the vertex expansion and the vertex construction [21]. This leads to the presentation of our currently best approximation of quantum gravity involving the description of the graviton three-point function. It follows a short recap of the results of [21] and a brief look on their equation for the flow of Newton's coupling, the geometrical flow equation from [20]. Then, we turn to matter inclusions, first fermionic matter and then scalar matter. In case of fermionic matter, we discuss the role of the spin connection and local spin-base invariance [28, 64].

5.1 Pure Quantum Gravity

The matter content of pure quantum gravity is the fluctuating metric $h_{\mu\nu}$, the ghost field c and the anti-ghost field $\bar{c}$. The latter arise from gauge fixing the action. The fluctuating metric originates from splitting the full metric $g_{\mu\nu}$ into a background part $\bar{g}_{\mu\nu}$ and a fluctuating part $h_{\mu\nu}$. We use a linear split

$$g_{\mu\nu} = \delta_{\mu\nu} + h_{\mu\nu} \,, \tag{5.1}$$

with the flat background $\bar{g}_{\mu\nu} = \delta_{\mu\nu}$. We would like to make two comments about these choices. First, we are using a flat Euclidean background and *not* a flat Minkowski background. This implies that at some point we should perform a Wick rotation in order to transform to Minkowski spacetime and restore the settings of classical general relativity. However, it is not clear that the Wick rotation can be performed without any problems. The difference between the two spaces was investigated in [65] for a specific truncation and they found an incredible equivalence between both solutions. They even stated that quantum gravity of both spaces might lay in the same universality class at high energies. Due to these results, we assume in the frame of this thesis that the results of Euclidean spacetime transforms to Minkowski spacetime in a convincing manner. The second comment concerns the type of split. The linear split is not the most general split. Recently many authors have employed the exponential split $g = \bar{g}\mathrm{e}^{h}$ [66–68]. We explain in section 5.1.5 that it is possible to give the fluctuating metric a geometrical meaning. We write all dynamical, fluctuating fields in a super-field vector

$$\Phi = (h, \bar{c}, c) \,. \tag{5.2}$$

Since the regulator is chosen to be diagonal in field space, the Wetterich equation takes the shape

$$\partial_t \Gamma_k[\bar{g}, \Phi] = \frac{1}{2}\mathrm{Tr}\left[\frac{1}{\Gamma_k^{(2h)} + R_{k,h}}\partial_t R_{k,h}\right][\bar{g}, \Phi] - \mathrm{Tr}\left[\frac{1}{\Gamma_k^{(\bar{c}c)} + R_{k,c}}\partial_t R_{k,c}\right][\bar{g}, \Phi]\,. \quad (5.3)$$

As already mentioned we are doing a vertex expansion, also known as level expansion. The expansion takes the following shape, where we have already ignored vertices that are zero:

$$\begin{aligned}\Gamma_k[\bar{g}, \Phi] &= \sum_{n=0}^{\infty} \frac{1}{n!}\Gamma_k^{(n)}[\bar{g}, 0]\Phi^n \\ &= \Gamma_k[\bar{g}, 0] + \Gamma_k^{(h)}[\bar{g}, 0]h + \frac{1}{2}\Gamma_k^{(2h)}[\bar{g}, 0]h^2 + \frac{1}{6}\Gamma_k^{(3h)}[\bar{g}, 0]h^3 + \frac{1}{2}\Gamma_k^{(\bar{c}c)}[\bar{g}, 0]\bar{c}c + \dots\end{aligned} \quad (5.4)$$

The flow equations for each vertex are derived by taking functional derivatives of the Wetterich equation with respect to the fields and then setting all fields to zero. We are presenting the flow of the n-point function in a diagrammatic way. The prefactors of the diagrams are explained below the equations (2.31) and (2.32). We represent graviton propagators with a double line and ghost propagators with a dashed line. The arrow is indicating the ghost flow i.e. if an arrow is going into the vertex it is the anti-ghost and if an arrow is going out of the vertex it is the ghost. So the flow of the graviton two-point function is

∂_t ()$^{-1}$ = 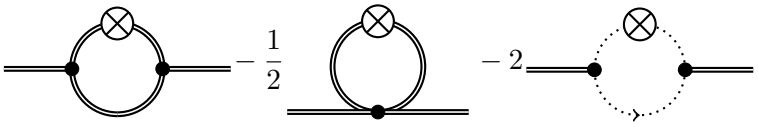

$\equiv \mathrm{Flow}^{(2h)}$ (5.5)

and the flow of the graviton three-point function is

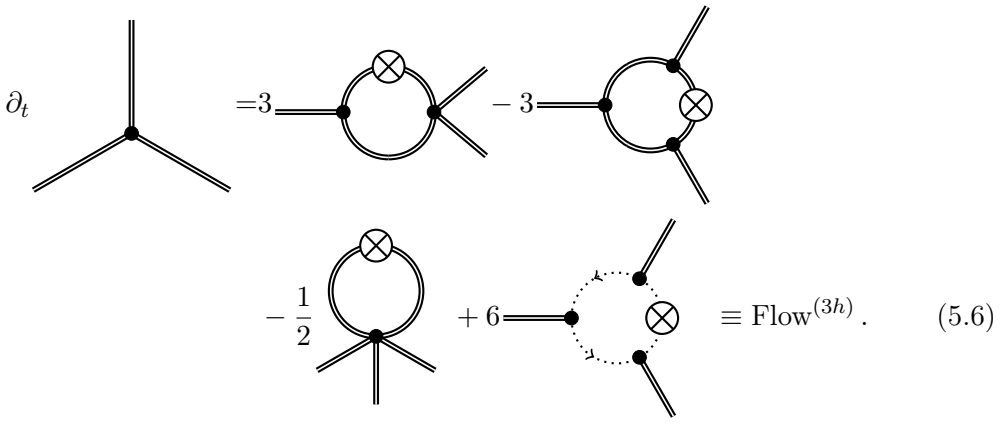

$\equiv \mathrm{Flow}^{(3h)}\,.$ (5.6)

There is also a flow in the ghost sector

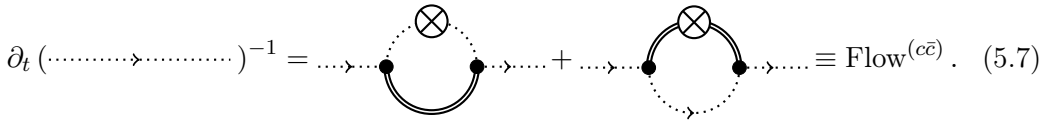

$$\equiv \mathrm{Flow}^{(c\bar{c})} \,. \quad (5.7)$$

Here, we have defined the "Flow", which is just the right hand side of the Wetterich equation. This allows us to distinguish more easily between the left hand side and the right hand side. Note that the two sides of the Wetterich equations are *not* equal anymore as soon as we truncate our system. Therefore different equivalence operations lead to different results and the flow equations become sensible to the point of projection. Contributions of matter are introduced in sections 5.2 and 5.3.

5.1.1 Vertex Construction

We now have to chose an ansatz for our vertex functions in order to evolve the flow equations to differential equations for our coupling parameters. The following ansatz turns out to be convenient:

$$\Gamma^{(\Phi_1 \dots \Phi_n)} = \sqrt{\prod_{i=1}^{n} Z_{\Phi_i}(p_i^2) G_n^{\frac{n}{2}-1}} \mathcal{T}^{(n)} \,, \quad (5.8)$$

where Z_{Φ_i} is the fully momentum dependent wavefunction renormalization of the field Φ_i, G_n is the level n scale dependent Newton's coupling and $\mathcal{T}^{(n)}$ is some tensor structure. Note, that from now on the subscript k, which indicates scale dependence, is dropped for convenience but still all couplings are scale dependent. The term "level n Newton's coupling" expresses the fact that each vertex has its own coupling constant, which is completely independent of all other couplings. In other words, each interaction of n gravitons is determined by its own scale dependent coupling. The power of the Newton's coupling $\frac{n}{2} - 1$ in equation (5.8) takes care of the appropriate dimensional power of the vertex.

The tensor structures can a priori be arbitrarily defined except for some diffeomorphism requirements. But we want to recover general relativity in the IR and hence we choose to derive the tensor structures by taking functional derivatives of the classical action, which is the Einstein-Hilbert action. We have to do some small modifications due our vertex construction, which is

$$\mathcal{T}^{(n)} = S_{\mathrm{EH}}^{(\Phi_1 \dots \Phi_n)}(p_1, \dots, p_n; G_N \to 1, \Lambda \to \Lambda_n) \,. \quad (5.9)$$

So the tensor structures are dependent on all external momenta and also on the "level n cosmological constant" but not on Newton's constant. In other words each vertex has its own scale dependent "cosmological constant". Actually it is not appropriate to call this quantity the cosmological constant. It is rather representing the momentum independent part of the n-th vertex. Let's now have a look at the different vertices.

The one-point function is dependent on G_1 and Λ_1. Further, it is known from the vertex expansion that it completely decouples from the system and gives no feedback at all. This property does not fit to a Newton's coupling but it fits to the cosmological constant. Thus Λ_1 is exactly the well known classical cosmological constant. The two-point function is independent of any Newton's coupling but depends on Λ_2. The first property is intended since a propagation should not carry an interaction coupling. Λ_2 is represents the momentum independent part of the two-point function and thus it is actually a mass term. Consequently, we relate later Λ_2 with the mass of the graviton. The three-point function depends on G_3 and Λ_3. This time we indeed consider an interaction and thus it is appropriate to call G_3 a Newton's coupling. Λ_3 simply represents the momentum independent part of the interaction. As we see now, the three-point function is the first vertex that carries information about the running of Newton's coupling. A fully self-consistent description of quantum theory must therefore include the running of the three-point function. The work of the collaboration, that is presented in this thesis, is the first to compute this running. It is also part of a forthcoming publication [69].

We want to emphasize that due to the distinction of the couplings of the different vertices there exists no action that can generate the vertices. This is already well known from QCD where it is also not possible to write down a defining action. This is based on the fact that it is completely sufficient to define all vertices in order to define a quantum field theory. Hence this flexibility is rather a strength of the theory.

As the generator of the tensor structures we choose the gauge fixed Einstein-Hilbert action

$$S_{\text{EH}} = \frac{1}{16\pi G_N}\int \mathrm{d}^4x\sqrt{g}(2\Lambda - R) + \int \mathrm{d}^4x\sqrt{\bar{g}}\bar{c}^\mu \mathcal{M}_{\mu\nu}c^\nu + \int \mathrm{d}^4x\sqrt{\bar{g}}\frac{1}{2\xi}\bar{g}^{\mu\nu}F_\mu F_\nu\,. \tag{5.10}$$

The gauge fixing condition is chosen linear

$$F_\mu = \bar{\mathcal{D}}^\nu h_{\mu\nu} - \frac{1}{2}\bar{\mathcal{D}}_\mu h^\nu_\nu \tag{5.11}$$

and we furthermore take the limit $\xi \to 0$, which ensures that the flow of ξ is at a fixed point [70]. The resulting Faddeev-Popov operator is of the form

$$\mathcal{M}_{\mu\nu} = \bar{\mathcal{D}}^\rho\left(g_{\mu\nu}\mathcal{D}_\rho + g_{\rho\nu}\mathcal{D}_\mu\right) - \bar{\mathcal{D}}_\mu\mathcal{D}_\nu\,, \tag{5.12}$$

which is linear in the fluctuating field due to the linear gauge fixing condition. Hence only the only ghost graviton interaction is via the $\Gamma_k^{(\bar{c}ch)}$ vertex, explaining the absent diagrams in the equations from (5.5) until (5.7).

5.1.2 Flow of the Graviton Propagator

We are now able to calculate the flow of the graviton propagator. From our vertex construction in equation (5.8) follows

$$\Gamma^{(2h)}(p) = Z_h(p^2) S^{(2h)}_{\mathrm{EH}}(p; G_N \to 1, \Lambda \to \Lambda_2)\,. \tag{5.13}$$

Here $S^{(2h)}_{\mathrm{EH}}$ is a tensor structure with four indices. It is symmetric in the first two indices, in the last two indices and also under exchange of those index pairs. To handle this complicated object one decomposes it into a complete set of tensor structures. This is known as York decomposition [71]. It contains one spin two mode, the transverse traceless mode h^{TT}, one spin one mode, the longitudinal traceless mode h^{LT}, and two scalar modes, the longitudinal h^{LL} and the trace mode h^{Tr}. So in total the decomposition is

$$h_{\mu\nu} = h^{\mathrm{TT}}_{\mu\nu} + \frac{1}{d}\bar{g}_{\mu\nu}h^{\mathrm{Tr}} + 2\bar{\mathcal{D}}_{(\mu}h^{\mathrm{LT}}_{\nu)} + \left(\bar{\mathcal{D}}_\mu\bar{\mathcal{D}}_\nu - \frac{\bar{g}_{\mu\nu}}{d}\bar{\mathcal{D}}^2\right)h^{\mathrm{LL}}\,, \tag{5.14}$$

where $\bar{\mathcal{D}}$ is the covariant derivative on the background, which is in our case just the partial derivative due to the flat background. The flow of each of the components is a scalar quantity and therefore it makes sense to compute each flow separately. However it simplifies the calculation tremendously if one focuses on the most important contribution, which is the transverse traceless part. There are several arguments in favour of the importance of the transverse-traceless part. First of all it can be computed that it is the numerically dominating part. Secondly one can argue that it is less gauge dependent that other parts. For example both longitudinal parts can be set to zero by gauge choice while this is not possible for the transverse-traceless part. The third argument is that in classical general relativity the graviton propagates as spin two excitation.

The decomposition of the two-point function into projectors is also important for the inversion of the propagator since the inversion of a rank four tensor is non trivial. We are postponing this task into the next chapter. For now we just introduce the transverse-traceless projector

$$\Pi^{\mathrm{TT}}_{\mu\nu\rho\sigma} = \frac{1}{2}\left(\Pi^{\mathrm{T}}_{\mu\rho}\Pi^{\mathrm{T}}_{\nu\sigma} + \Pi^{\mathrm{T}}_{\mu\sigma}\Pi^{\mathrm{T}}_{\nu\rho}\right) - \frac{1}{3}\Pi^{\mathrm{T}}_{\mu\nu}\Pi^{\mathrm{T}}_{\rho\sigma}\,, \tag{5.15}$$

with the transverse projector

$$\Pi^{\mathrm{T}}_{\mu\nu} = \delta_{\mu\nu} - \frac{p_\mu p_\nu}{p^2}\,. \tag{5.16}$$

The two-point function from equation (5.13) is now projected on its transverse traceless part with (5.15). The result is

$$\Gamma^{(2h)}_{\mathrm{TT}}(p^2) = \frac{Z_h(p^2)}{32\pi}(p^2 - 2\Lambda_2)\,, \tag{5.17}$$

where it gets evident that Λ_2 is indeed related to the mass parameter of the graviton. To emphasize this fact we rename this parameter and introduce the dimensionless mass parameter of the graviton

$$\mu_h := -2\Lambda_2 k^{-2} \,. \tag{5.18}$$

We are now interested in the flow of the two point function i.e. the flow of the couplings that appear in the two-point function. By taking the scale derivative of equation (5.17) we get

$$\dot{\Gamma}^{(2h)}_{\mathrm{TT}}(p^2) = \frac{1}{32\pi}\left((p^2 + k^2\mu_h)\dot{Z}_h(p^2) + Z_h(p^2)(2k^2\mu_h + k^2\dot{\mu}_h)\right) . \tag{5.19}$$

There are now several possibilities how to project the flow of the propagator onto the flow of the couplings. We show two possibilities, which are both used in this thesis. We want to emphasize that all those projections are leading to different results although we are doing exact manipulations of the Wetterich equation. But the Wetterich equation is already an inequality since the system is truncated. Our task is to choose the best projection scheme and to minimize the error.

In case of a momentum independent wavefunction renormalization the most common and also the most simple projection is the derivative projection at $p = 0$. It also has the advantage that it leads to analytic equations. So once the flow is projected on $p = 0$ and a second time on $p = 0$ after taking a derivative with respect to p^2. This is applied to equation (5.19) and the flow is solved for

$$\dot{\mu}_h = (-2 + \eta_h)\mu_h + \frac{32\pi}{Z_h k^2}\mathrm{Flow}^{(2h)}_{\mathrm{TT}}(p^2 = 0) \,, \tag{5.20}$$

$$\eta_h := -\frac{\dot{Z}_h}{Z_h} = -\frac{32\pi}{Z_h}\partial_{p^2}\mathrm{Flow}^{(2h)}_{\mathrm{TT}}(p^2)\Big|_{p^2=0} \,, \tag{5.21}$$

where we have introduced the anomalous dimension of the graviton η_h, which is in general a momentum and scale dependent quantity but we often approximate it to be momentum independent. The flow of the two-point function is in both cases determined by the diagrams in equation (5.5) contracted with the transverse-traceless projector.

For a momentum dependent wavefunction renormalization this procedure does not lead to nice equations. Instead, we make the same steps as in [21] to get integral equations for the graviton mass and for the anomalous dimension. We start by evaluating equation (5.19) at $p^2 = -k^2\mu_h$, which is the pole of the graviton propagator. Note, that this choice obviously corresponds to $p^2 < 0$ for $\mu_h > 0$. This problem of imaginary momenta is solved by an analytic continuation into the complex plane. Then, the flow is solved for

$$\dot{\mu}_h = -2\mu_h + 32\pi\frac{\mathrm{Flow}^{(2h)}_{\mathrm{TT}}(-k^2\mu_h)}{k^2 Z_h(-k^2\mu_h)} \,. \tag{5.22}$$

It is important to notice that this flow is a functional of only the anomalous dimension and not of the wavefunction renormalization, since isolated factors cancel each other. This equation is inserted back in (5.19) and this time solved for the anomalous dimension

$$\eta_h(p^2) = 32\pi \frac{\frac{\mathrm{Flow}^{(2h)}_{\mathrm{TT}}(-k^2\mu_h)}{k^2 Z_h(-k^2\mu_h)} - \frac{\mathrm{Flow}^{(2h)}_{\mathrm{TT}}(p^2)}{k^2 Z_h(p^2)}}{p^2 + k^2\mu_h} \,. \tag{5.23}$$

Again, this is a functional of only the anomalous dimension. Note that this equation is an integral equation or Fredholm equation of the second type since the right hand side contains the integral over the loop momentum and the anomalous dimension depends on the loop momentum. This equation can also be used for momentum independent anomalous dimension where it simplifies to an ordinary algebraic equation. The results in this approximation are actually more quite convenient that the derivative projection and their analytic equations.

5.1.3 Flow of the Ghost Propagator

The diagrammatic flow of the ghost sector is displayed in equation (5.7). It is a symmetric tensor of rank two. We compute only the transverse part of the flow i.e. we contract it with the transverse projector in equation (5.16) and divide by the norm of the projector, which is three. The resulting two-point function of the ghost is simply

$$\Gamma^{(c\bar{c})}_{\mathrm{T}}(p^2) = Z_c(p^2)p^2 \,, \tag{5.24}$$

where Z_c is the wavefunction renormalization of the ghost. It defines the anomalous dimension of the ghost in the usual way $\eta_c(p^2) := -\dot{Z}_c(p^2)/Z_c(p^2)$. The integral equation for the anomalous dimension is therefore trivially

$$\eta_c(p^2) = -\frac{\mathrm{Flow}^{(c\bar{c})}_{\mathrm{T}}(p^2)}{p^2 Z_c(p^2)} \,, \tag{5.25}$$

which is again a functional of only the anomalous dimensions. The flow of the ghost propagator is determined by the diagrams in equation (5.7). The same formula is used in case of momentum independent anomalous dimensions but evaluated for vanishing external momentum. It then again simplifies to an ordinary algebraic equation. Note that the flow of the ghost propagator is proportional to p^2 and thus the equation is well defined for $p = 0$ and no mass of the ghost is dynamically generated.

5.1.4 Flow of the Graviton Three-Point Function

The diagrammatic flow of the graviton three-point function is shown in equation (5.6) and the construction of the vertex in equation (5.8). The three point function is a rank six tensor and dependent on three external momenta. One momentum can be eliminated via momentum conservation. The tensor structure is very rich, it contains almost any possible combination of metrics. So it is an extraordinary complicated

object, which theoretically should be solved with a complete set of orthogonal rank six projectors and in complete momentum dependence. It is easy to imagine that task is way too extensive. Especially considering that some tensor structures carry non-physical degrees of freedom, it becomes clear that a more simplified ansatz is reasonable. Hence we want to project it on a specific tensor and momentum configuration, trying to catch the leading physical contribution. In the following, we first construct a projector for the tensor structures and afterwards we discuss convenient momentum configurations. We do not claim that our projection methods are unique or a priori favourable but they have turned out to be reasonable choices.

First of all we split the tensor structure from equation (5.9) in a momentum dependent part and a momentum independent part. Since the momentum independent part is simply proportional to Λ_3 this split is

$$\begin{aligned}\mathcal{T}^{(3h)}(p_1,p_2,p_3;\Lambda_3) =&\mathcal{T}^{(3h)}(p_1,p_2,p_3;\Lambda_3=0)\\ &+\mathcal{T}^{(3h)}(p_1=p_2=p_3=0;\Lambda_3)\,.\end{aligned} \tag{5.26}$$

The point of this split is that the first part is now independent of Λ_3 and thus is used to construct the projector for Newton's coupling Π_G while the other part is used to construct the projector for the Λ_3 coupling Π_Λ. From the two-point function we know already that the transverse-traceless part of the graviton is the dominating part and also often considered the physical relevant part. We transfer this knowledge to the three-point function and project each external leg on its transverse-traceless part. Further this enhances the self-consistency of our projection. With this we arrive at the projectors

$$\begin{aligned}\Pi_G^{\alpha\beta\gamma\delta\mu\nu}(p_1,p_2,p_3) :=&\Pi_{\mathrm{TT}}^{\alpha\beta\alpha'\beta'}(p_1)\Pi_{\mathrm{TT}}^{\gamma\delta\gamma'\delta'}(p_2)\Pi_{\mathrm{TT}}^{\mu\nu\mu'\nu'}(p_3)\\ &\times\mathcal{T}^{(3h)}_{\alpha'\beta'\gamma'\delta'\mu'\nu'}(p_1,p_2,p_3;\Lambda_3=0)\,,\end{aligned} \tag{5.27}$$

$$\begin{aligned}\Pi_\Lambda^{\alpha\beta\gamma\delta\mu\nu}(p_1,p_2,p_3) :=&\Pi_{\mathrm{TT}}^{\alpha\beta\alpha'\beta'}(p_1)\Pi_{\mathrm{TT}}^{\gamma\delta\gamma'\delta'}(p_2)\Pi_{\mathrm{TT}}^{\mu\nu\mu'\nu'}(p_3)\\ &\times\mathcal{T}^{(3h)}_{\alpha'\beta'\gamma'\delta'\mu'\nu'}(p_1=p_2=p_3=0;\Lambda_3)\,.\end{aligned} \tag{5.28}$$

These projectors are each applied once to the flow equation of the three-point function. All indices are contracted and the results are two scalar flow equations. We want to emphasize that the projectors can be arbitrary normalized since they are applied on both sides of the flow equation. In the equation for Λ the limit of the external momenta going to zero has to be taken, since it represents the momentum independent part. Thus, the left hand side of the Wetterich equations evolves to

$$\dot{\Gamma}_G^{(3h)} :=\Pi_G\circ\dot{\Gamma}^{(3h)}\,, \tag{5.29}$$

$$\dot{\Gamma}_\Lambda^{(3h)} :=\lim_{p_1,p_2,p_3\to 0}\Pi_\Lambda\circ\dot{\Gamma}^{(3h)} \tag{5.30}$$

where the circle stands for the contraction of all indices. To simplify our task further, we are now deciding for a momentum configuration. In principle any momentum

configuration is possible but in this thesis we are focusing on two configuration, which are especially appealing due to their symmetry properties. The first momentum configuration is simplest possible i.e.

$$p_1 = \begin{pmatrix} p \\ 0 \\ 0 \\ 0 \end{pmatrix}, \qquad p_2 = \begin{pmatrix} -p \\ 0 \\ 0 \\ 0 \end{pmatrix}, \qquad p_3 = \begin{pmatrix} 0 \\ 0 \\ 0 \\ 0 \end{pmatrix}. \tag{5.31}$$

So one external leg is taken to zero momentum. Momentum conservation then forces the remaining momenta to be in opposite direction. It is important to note that the transverse-traceless projector for the zero momentum leg is not well defined i.e. there remain undefined angles between p_3 and p_1 as well as between p_3 and q after all contractions are carried out. Therefore the projector for this leg is replaced with the one-projector

$$\Pi_{\text{one},\mu\nu\rho\sigma} = \frac{1}{2}\left(\delta_{\mu\rho}\delta_{\nu\sigma} + \delta_{\mu\sigma}\delta_{\nu\rho}\right) - \frac{1}{3}\delta_{\mu\nu}\delta_{\rho\sigma}\,. \tag{5.32}$$

The advantage of this configuration is its simplicity. It is important to note that the external legs from the diagrams in equation (5.6) should be symmetrized with respect to the momentum configuration. We call this the asymmetric momentum configuration.

The second momentum configuration is the most symmetric configuration. All momenta have the value and the angle between each pair is $\frac{2\pi}{3}$. We parameterize it as

$$p_1 = \begin{pmatrix} p \\ 0 \\ 0 \\ 0 \end{pmatrix}, \qquad p_2 = \begin{pmatrix} -p/2 \\ \sqrt{3}p/2 \\ 0 \\ 0 \end{pmatrix}, \qquad p_3 = \begin{pmatrix} -p/2 \\ -\sqrt{3}p/2 \\ 0 \\ 0 \end{pmatrix}. \tag{5.33}$$

For the definition of the coordinate system, see section 6.3. We call this the symmetric momentum configuration.

Our system of differential equations is build up amongst others from the graviton two-point function and the graviton three-point function. So in order to decide, which momentum configuration is suitable, it is recommendable to check, which momentum configuration appears most often in the differential equation and choose this one. Here it is crucial how the graviton two-point function is projected. Let's first discuss the $p = 0$ projection for it. In this case the asymmetric momentum configuration appears twice in the self-energy diagram of the graviton two-point function

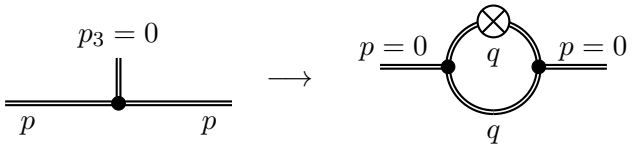

(5.34)

If the graviton two-point function is projected at $p = k$ then the story is different. The best feedback vertex for the self-energy is a complicated one with different momenta on each external leg. But the important information is that all external momenta are non-zero and in consequence we conclude that the symmetric momentum configuration is the best approximation for the feedback i.e.

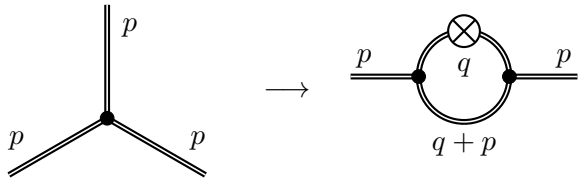

(5.35)

We derive now the flow equations for Newton's coupling and for Λ_3 for each momentum configuration by evaluating the left hand side of the flow equation. We start with the asymmetric configuration. Evaluating all contractions on the left hand side leads to

$$\dot{\Gamma}_G^{(3h)}(p^2) = \frac{1}{32 \cdot 96\pi^2} \partial_t \left[Z_h^{1/2}(0) Z_h(p^2) G_3^{1/2} \left(35p^4 - 65\Lambda_3 p^2 \right) \right] , \tag{5.36}$$

$$\dot{\Gamma}_\Lambda^{(3h)} = \frac{5\Lambda_3}{96\pi^2} \partial_t \left[Z_h^{3/2}(0) G_3^{1/2} \Lambda_3 \right] . \tag{5.37}$$

Note that the overall factor depends on the normalization of the projector. In the second equation almost no work has to be done anymore. We introduce the usual dimensionless variables $g_3 := G_3 k^2$ as well as $\lambda_3 := \Lambda_3 k^{-2}$, evaluate the derivative and solve for $\dot{\lambda}_3$. The result is

$$\dot{\lambda}_3 = -2\lambda_3 + \frac{3}{2}\eta_h(0)\lambda_3 - \frac{1}{2}\left(\frac{\dot{g}_3}{g_3} - 2 \right) \lambda_3 + \frac{96}{5}\pi^2 \mathrm{Flow}_\Lambda^{(3h)}(p^2 = 0) , \tag{5.38}$$

where the flow of the three-point function is given by the diagrams shown in equation (5.6) contracted with the projector from equation (5.28) and taken in the limit $p \to 0$. This equation is universal and does not depend on the momentum configuration. The prefactor of the flow again depends on the normalization of the projector.

In case of equation (5.36), which should lead to the flow of Newton's coupling, there are several reasonable choices since we again have the ambiguity to project on the momentum p. Since we want to project on the momentum dependent part of the flow, we want to project on the coefficient of the p^4 term in the equation. For this, we first of all divide by $Z_h^{1/2}(0) Z_h(p^2) p^2$, since it is part of the norm of the projector and then we employ a finite difference i.e. we evaluate the equation at two different momentum scales p_a and p_b and subtract the resulting flows. Typical

values for those momentum scales are $p_a = k$ and $p_b = 0$ or both $p_a = 0 = p_b$, which means that the finite difference turns into a common derivative. With the same dimensionless variables as before and solved for the flow of Newton's coupling, the resulting equation is

$$\begin{aligned}\dot{g}_3 =& 2g_3 + \eta_h(0)g_3 + 2\frac{\eta_h(p_a^2)p_a^2 - \eta_h(p_b^2)p_b^2}{p_a^2 - p_b^2}g_3 - 2\frac{65}{35}\frac{\eta_h(p_a^2) - \eta_h(p_b^2)}{p_a^2 - p_b^2}\lambda_3 g_3 \\ &+ 32\frac{192}{35}\pi^2\frac{\frac{\text{Flow}_G^{(3h)}(p_a^2)}{Z_h^{1/2}(0)Z_h(p_a^2)p_a^2} - \frac{\text{Flow}_G^{(3h)}(p_b^2)}{Z_h^{1/2}(0)Z_h(p_b^2)p_b^2}}{p_a^2 - p_b^2}\,,\end{aligned} \tag{5.39}$$

where the flow is again taken from equation (5.6) but this time contracted with the projector from equation (5.27). The first three terms are the usual canonical scaling terms where the η_h are evaluated according to the momentum values on the external legs. The third term originates from the momentum independent part of the vertex and vanishes for momentum independent anomalous dimensions. the last term represents the right hand side of the equations. We want to emphasize that this term is just a function of the anomalous dimension and the wavefunction renormalization cancels as usual. In case of a momentum independent anomalous dimension, the equation simplifies to

$$\dot{g}_3 = (2 + 3\eta_h)g_3 + 32\frac{192}{35}\pi^2\frac{\frac{\text{Flow}_G^{(3h)}(p_a^2)}{Z_h^{3/2}p_a^2} - \frac{\text{Flow}_G^{(3h)}(p_b^2)}{Z_h^{3/2}p_b^2}}{p_a^2 - p_b^2}\,. \tag{5.40}$$

In principle we have to repeat all of the last steps for the symmetric momentum configuration. We just present the result, since just the prefactors differ. The equation for g_3 is

$$\begin{aligned}\dot{g}_3 =& 2g_3 + 3\frac{\eta_h(p_a^2)p_a^2 - \eta_h(p_b^2)p_b^2}{p_a^2 - p_b^2}g_3 - 3\frac{8}{19}\frac{\eta_h(p_a^2) - \eta_h(p_b^2)}{p_a^2 - p_b^2}\lambda_3 g_3 \\ &+ 32\frac{2048}{171}\pi^2\frac{\frac{\text{Flow}_G^{(3h)}(p_a^2)}{Z_h^{3/2}(p_a^2)p_a^2} - \frac{\text{Flow}_G^{(3h)}(p_b^2)}{Z_h^{3/2}(p_b^2)p_b^2}}{p_a^2 - p_b^2}\,.\end{aligned} \tag{5.41}$$

The equation for λ_3 is universal and hence displayed in equation (5.38).

5.1.5 Global Flows and the Geometrical Flow Equation

In this section, we briefly recapitulate the results of the paper "Global Flows" [21] since we are directly improving upon their truncation. They made a vertex expansion and introduced the self-consistent vertex construction, that we are using, see equation (5.8). They calculated the full two-point function with fully momentum dependent anomalous dimensions and arrived at the before mentioned integral equations (5.22), (5.23) and (5.25). They did not close the equations with the graviton three-point

function but with the geometric flow equation. The couplings from higher vertex function that appear in the two point function were essentially identified $\lambda_4 = \lambda_3 = -\mu_h/2$ except in the region $\mu_h \to -1$. In this region, which is the IR region, they performed a scaling analysis to catch the dominating powers of $1 + \mu$.

The geometric flow equation is an alternative for the flow of the Newton's coupling, derived in [20]. We shortly describe the basics of the paper without going into details and eventually present the results. It is the aim of the paper to construct a fully diffeomorphism-invariant flow. This is done by considering the geometrical of Vilkovisky-DeWitt effective action. This is basically an improvement of the former introduced linear split $g = \bar{g} + h$ where the fluctuating field h is neither a metric nor a vector and hence bares no geometrical meaning at all. The exponential split $g = \bar{g}e^h$ in turn has already a geometrical meaning and the connection is the trivial one. In [20] the Vilkovisky's connection is used, which defines h as a tangent vector at $\bar{g}$. It is furthermore important that in this paper the difference of the background flow and the dynamical flow is resolved. We have already seen in section 4.1 that in the usual background flow approximation those two are identified, which evidently introduces an error. Here Nielsen identities are used to resolve the difference. The resulting equation can be found in [20] and [21].

We come now to the results of "Global Flows". In figure 5.1, their computed phase diagram is displayed. The phase diagram contains a whole bunch of fixed points, namely the usual Gaussian fixed point, a fully attractive UV fixed point, two IR fixed points where one is massive and one is massless, and a metastable fixed point. These fixed points are located at the coordinates

$$(g^*, \mu_h^*)_{\text{Gauss}} = (0, 0)\,, \tag{5.42}$$
$$(g^*, \mu_h^*)_{\text{UV}} = (0.614, -0.645)\,, \tag{5.43}$$
$$(g^*, \mu_h^*)_{\text{IR,massive}} = (0, \infty)\,, \tag{5.44}$$
$$(g^*, \mu_h^*)_{\text{IR,massless}} = (0, -1)\,, \tag{5.45}$$
$$(g^*, \mu_h^*)_{\text{metastable}} = (0.25, -0.91)\,. \tag{5.46}$$

The first IR fixed point is called massless since the dimensionful quantity $k^2\mu_h$ goes in this case to zero for $k \to 0$. For the second IR fixed point the dimensionless variable goes to infinity for $k \to 0$ and the limit of the dimensionful quantity is something finite i.e. leads a massive graviton. It turns out, that the massless IR fixed point describes well classical general relativity and classical scaling is well fulfilled close to the fixed point. This work was the first to find a global trajectory leading from an IR fixed point to a UV fixed point.

Another important result of the paper is the locality of the two-point function, which was also discussed in their preceding paper, see [22]. The locality of the two-point function causes that the anomalous dimensions of the graviton is going to zero for $p \to \infty$. The locality occurs due to a non-trivial cancellation of two diagrams. Locality is a desired property and we check later if this property also extends to the graviton three-point function.

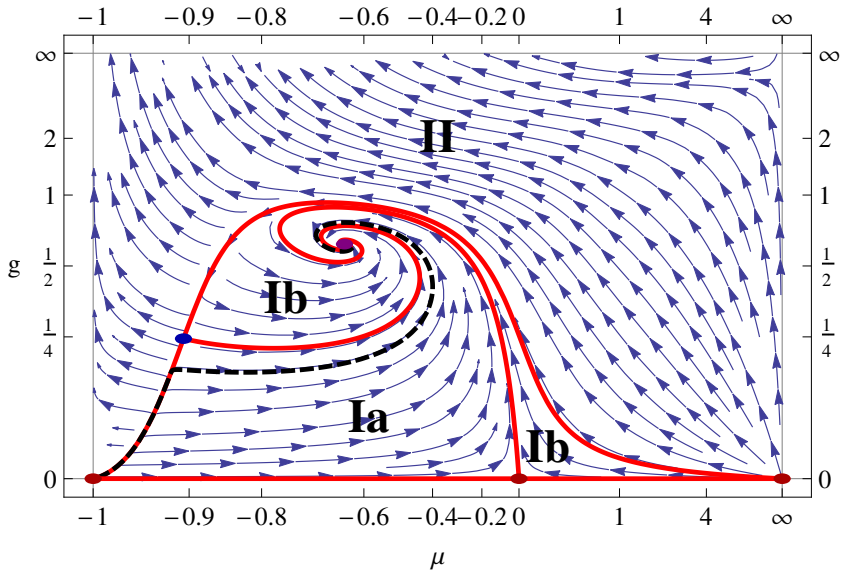

Figure 5.1: The global phase diagram of quantum gravity from [21] is shown. The dimensionless Newton's coupling is plotted over the dimensionless mass parameter of the graviton. The arrows indicate the flow in the UV direction. Besides the Gaussian and the UV fixed point exist two IR fixed points and one metastable fixed point. Region Ia contains trajectories that connect the massless IR fixed point with the UV fixed point, while region Ib contains the trajectories that connect with the massive IR fixed point. Region II only contains trajectories, which don't connect to the UV fixed point. The massless IR fixed point turns out to describe classical general relativity and is therefore region Ia is considered to be the physical one. One specific trajectory of this region is highlighted as example.

In summary, the results of "Global Flows" are very promising. The geometrical flow equation turn out to be a very nice and useful equation. The only downside is, that it is an external input and not as self-consistent as for example the graviton three-point function. That is the reason, why we believe that we can improving on "Global Flows" with our truncation. We hope to keep all the nice features of their global phase diagram and show that the self-consistent three-point function is a useful closure of the equations.

5.2 Inclusion of Fermions

In this section, we introduce fermions in the system of quantum gravity. We only consider minimally coupled fermions, which means means couplings with a negative mass dimension are neglected. Also, matter-self interactions like for example a four-

fermion interaction are not considered. In consequence, our euclidean fermionic action is

$$S_{\text{ferm}}[g, \bar{\psi}, \psi] = \int \mathrm{d}^4x \sqrt{g} \bar{\psi} (\gamma_\mu \nabla^\mu + m_\psi) \psi \,, \tag{5.47}$$

which is simply added to the gauge fixed Einstein-Hilbert action. Here, γ_μ represent the Dirac matrices in some representation and ∇^μ is the Dirac operator. ψ and $\bar{\psi}$ are the fermion and the anti-fermion respectively, where the later one is defined as

$$\bar{\psi} \equiv \psi^\dagger h \,, \tag{5.48}$$

with h as spin metric, not to be confused with the fluctuating part of the metric. We chose this notation to be in accordance with [28]. The spin metric is often represented with the γ^0 matrix.

The mass of the fermion is m_ψ and does not arise from any symmetry breaking like in the standard model. It is simply a parameter put in by hand and destroys chiral symmetry. It is a coupling that exhibits RG running and we use it later to discuss the influence of the mass on the UV fixed point. This approach is a naive first shot since it does not originate from spontaneous symmetry breaking.

The Dirac matrices need to fulfil the Clifford algebra. In Minkowski space $\gamma_{(m),\mu}$ or in the tangent space of a spacetime point on a manifold, this is fulfilled by the usual flat Dirac matrices $\gamma_{(f),a}$ and the relation is

$$\{\gamma_{(f),a}, \gamma_{(f),b}\} = 2\eta_{ab} \mathbb{1} \,, \tag{5.49}$$

where $\{.,.\}$ is the anti-commutator and $\mathbb{1}$ the unity matrix with same dimensionality as the representation of the Dirac matrices. In curved space, this promotes to

$$\{\gamma_\mu, \gamma_\nu\} = 2g_{\mu\nu} \mathbb{1} \,. \tag{5.50}$$

So in consequence, the gamma matrices become spacetime dependent i.e. a functional of the metric. There is no unique solution to equation (5.50). Instead, if one set of Dirac matrices is a solution they can be transformed to a new solution via a spin-base transformation [28].

There are now two possibilities to compensate the appearing spacetime dependence of the Dirac matrices. First, it is possible to introduce a vielbein, which parameterizes the metric as well as the Dirac matrices. Thus, all relevant degrees of freedom are captured with the vielbein. However, it was shown recently that in some special cases this vielbein formalism can lead to trouble and it is more convenient to use the properties of the spin-base transformation to take the metric itself as the relevant degree of freedom [28]. Nevertheless, we shortly present the idea of a vielbein since it helps to introduce the spin connection.

A vielbein e^a_μ is introduced to parameterize the metric and the Dirac matrices, with the outcome

$$g_{\mu\nu} = e_\mu{}^a e_\nu{}^b \eta_{ab} \qquad \text{and} \qquad \gamma_\mu = e_\mu{}^a \gamma_{(f),a} \,. \tag{5.51}$$

With this definition and equation (5.49) it becomes straight forward evident that equation (5.50) is fulfilled. The covariant derivative of the vielbein includes now additionally a spin connection ω since the vielbein needs to capture the dynamics in spacetime as well as in spinor space. This covariant derivative is also used to determine the spin connection i.e.

$$\nabla_\mu e_\nu{}^a = \partial_\mu e_\nu{}^a - \Gamma^\kappa_{\mu\nu} e_\kappa{}^a + \omega_\mu{}^a{}_b e_\nu{}^b = 0 \,, \tag{5.52}$$

where Γ is the Christoffel symbol as defined in equation (3.5) and we have implicitly defined the already before used notation $\nabla_\mu = \mathcal{D}_\mu + \omega_\mu$ i.e. the covariant derivative acting on an object in spinor space can be separated into the spacetime covariant derivative and the spin connection. The covariant derivative of a spinor is then given by

$$\nabla_\mu \psi = \partial_\mu \psi + \frac{1}{8} \omega_\mu{}^{ab} [\gamma_{(f),a}, \gamma_{(f),b}] \psi \,, \tag{5.53}$$

where $[.,.]$ represents the commutator. Now all necessary quantities are defined and can be computed. The path integral is performed over the vielbein and the (anti)-fermion.

Let's return to the alternative that is actually used in this thesis, the spin-base invariance formalism introduced in [28]. The aim is to make the metric the relevant degree of freedom. However simply expressing the Dirac matrices as a functional of the metric and integrating over the metric in the path integral doesn't do the job since the solution to equation (5.50) is not unique and we would introduce multi counting. The symmetry under spin-base transformations has to be taken into account and, in analogy to gauge symmetries, the gauge has to be fixed. This usually introduces ghost in the theory but here it turns out that this integration is trivial, so we can fix the gauge in an arbitrary way.

An important ingredient in order to implement the metric as the relevant degree of freedom is the Weldon theorem [72], which connects an infinitesimal transformation of the Dirac matrices, that preserves the Clifford algebra, to an infinitesimal transformation of the inverse metric plus an infinitesimal transformation of the spin-base group. Details about the further derivation can be found in [28].

Ultimately, we need the variation of the Dirac matrices and the spin connection with respect to the metric. In [28], they presented up to the second variation of those quantities in a fixed gauge. Unfortunately, this is not enough for our purposes since we need the vertex with two fermions and three gravitons and hence the third variation with respect to the metric. Thus, we derived formulas for the n-th variation of the Dirac matrices and the spin connection. But the derivation is quite long and the resulting expressions are quite unhandy and therefore we refer for this to appendix

C.

A comment about our Euclidean setting is necessary. In [28], all results were obtained in Minkowski space. We, however, start in Euclidean space and assume that we can perform at some point a Wick rotation without hitting a pole and without a change in the results. We demand that the flat Dirac matrices fulfil the Euclidean equivalent of equation (5.49) and, furthermore, that our action is real, which was also demanded in [28]. There are almost no changes compared to the paper, except that the spin metric is antihermitean in the Euclidean case i.e. $h^\dagger = -h$.

We are now presenting the contributions to the flows of the gravity sector due to fermion loops. In our diagrammatic representation, fermions are depicted as solid lines. The arrows indicate the fermion flow i.e. if an arrow is going into the vertex it is the anti-fermion and if an arrow is going out of the vertex it is the fermion. Here is the contribution to the flow of the graviton propagator

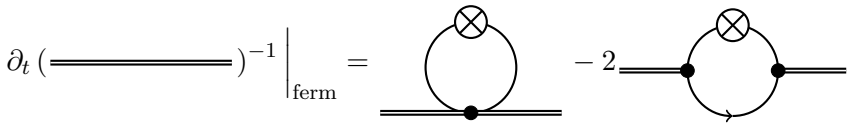

(5.54)

and the contribution to the graviton three-point function

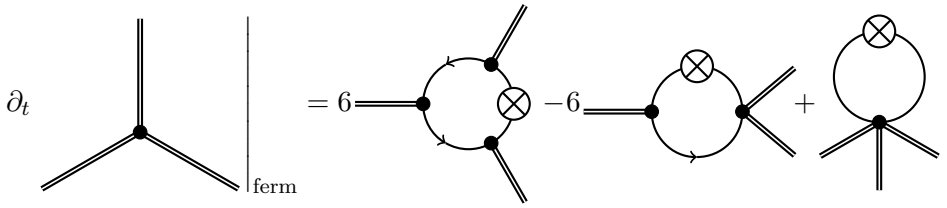

. (5.55)

The flow of the fermion propagator is

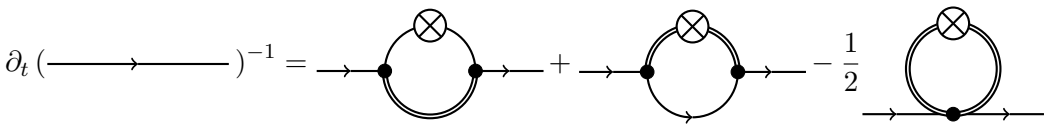

$$\equiv \text{Flow}^{(\psi\bar{\psi})}\,. \tag{5.56}$$

We are not including a four-fermion interaction although it is dynamically generated by graviton-fermion interactions. This is done in other work and we refer to [24] and [58] for gravitationally generated four-fermion interactions or [73] for a review without gravity. One result is that there is no feedback from the four-fermion interaction into the gravity system if it is momentum independent, which is the case in most truncations.[1] Therefore, we can neglect it without any problems. The only remaining fermionic flow is the fermion two-point function, which is in our truncation

$$\Gamma^{\psi\bar{\psi}} = Z_\psi(p^2)(i\not{p} + m_\psi \mathbb{1})\,, \tag{5.57}$$

[1] If the four-fermion interaction is bosonized then there is evidently a feedback e.g. through the running of the scalar in the graviton three-point function.

where $\not{p} = \gamma_\mu p^\mu$. And, in consequence, the fermion propagator is

$$(\Gamma^{\bar{\psi}\psi} + R_k)^{-1} = \frac{1}{Z_\psi(p^2)} \frac{i\not{p}(1 + r(p^2/k^2)) + m_\psi \mathbb{1}}{p^2(1 + r(p^2/k^2))^2 + m_\psi^2} \,. \tag{5.58}$$

The differential equations for the momentum independent anomalous dimension of the fermion $\eta_\psi := -\dot{Z}_\psi / Z_\psi$ and for the dimensionless mass of the fermion $\mu_\psi = m_\psi^2 k^{-2}$ are obtained by taking the derivative with respect to the RG time t and then either the trace is taken at $p = 0$ or the equation is multiplied by $\not{p}$ and then the trace is taken. These manipulations lead to the equations

$$\dot{\mu}_\psi = (2\eta_\psi - 2)\mu_\psi + 2\sqrt{\mu_\psi} \frac{\mathrm{Tr}\left(\mathrm{Flow}^{(\psi\bar{\psi})}(p=0)\right)}{k Z_\psi d} \,, \tag{5.59}$$

$$\eta_\psi = i \left. \frac{\partial_{p^2} \mathrm{Tr}\left(\not{p} \mathrm{Flow}^{(\psi\bar{\psi})}(p^2)\right)}{Z_\psi d} \right|_{p=0} \,, \tag{5.60}$$

where d is the dimension of the representation of the Dirac matrices and $d = 4$ in the present work. This is a typical $p = 0$ projection with the approximation of a momentum independent anomalous dimension. Other momentum projections like $p = k$ are possible and also an equation for the fully momentum dependent anomalous dimension can be realized. However, in this work we stick to the simplest projection since we can obtain analytic equations in this case.

5.3 Inclusion of Scalars

The inclusion of scalars in the theory is much easier compared to fermions. The covariant derivative of a scalar is just a partial derivative. There is neither a Levi-Civita connection nor a spin connection. We again investigate minimally coupled scalars, which corresponds to the action

$$S_{\mathrm{scalar}}[g, \phi] = \int \mathrm{d}^4x \sqrt{g} \left(\frac{1}{2} \partial_\mu \phi \partial^\mu \phi + \frac{1}{2} m_\phi^2 \phi^2 \right) \,. \tag{5.61}$$

It is possible to extend the scalar-graviton coupling by functions like $F(\phi)R$ or even $F(\phi, R)$ [55], to include matter-self-interactions like ϕ^4 [57], or to introduce a complete Yukawa system by coupling it to fermions with terms like $\phi\psi\bar{\psi}$ [58]. But this goes beyond the topic of this thesis.

The contributions to the graviton flows with the scalar depicted as a dashed line are

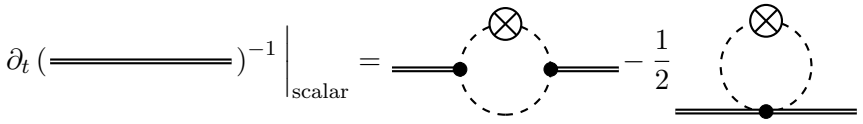

(5.62)

as well as

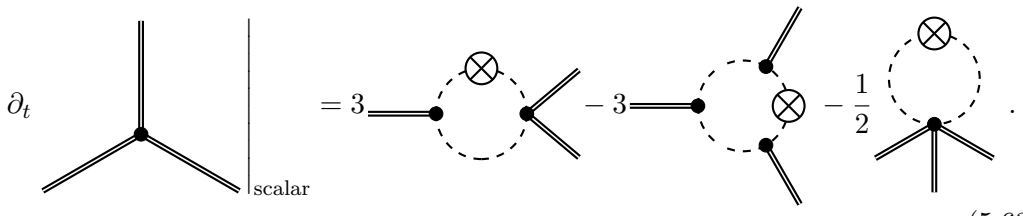

(5.63)

There is no contribution to fermion flow since we do not consider matter-matter interactions. What remains is the scalar flow with

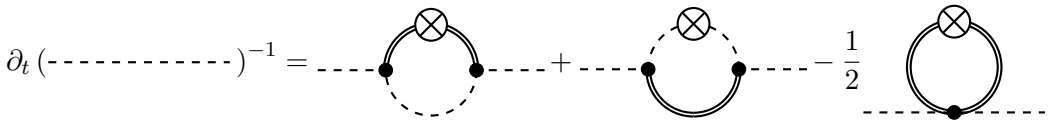

(5.64)

These are all the diagrams that need to be computed. One would have to include a four scalar interaction as well as a Yukawa interaction to have a fully consistent system since those are generated anyway by graviton loops. However, we are still neglecting them for reasons of simplicity.

The scalar two-point function has its typical shape with the wavefunction renormalization due to our vertex construction, which is

$$\Gamma^{(2\phi)}(p^2) = Z_\phi(p^2)(p^2 + m_\phi^2)\,, \tag{5.65}$$

which offers the usual momentum projection possibilities. For example a $p = 0$ projection and for a momentum independent wavefunction renormalization leads to

$$\dot{\mu}_\phi = (-2 + \eta_\phi)\mu_\phi + \frac{\mathrm{Flow}^{(2\phi)}(p=0)}{Z_\phi k^2}\,, \tag{5.66}$$

$$\eta_\phi = -\left.\frac{\partial_{p^2}\mathrm{Flow}^{(2\phi)}(p^2)}{Z_\phi}\right|_{p=0}\,, \tag{5.67}$$

where we have introduced the dimensionless mass of the scalar $\mu_\phi := m_\phi^2 k^{-2}$ and the anomalous dimension of the scalar $\eta_\phi := -\dot{Z}_\phi/Z_\phi$. In this work, we are only using this momentum projection since it is the only one that leads to analytic equations.

6 Methods of Computation

In this chapter, we present the methods of calculations i.e. how the vertices are calculated, how the propagator is inverted and how the contraction of diagrams are evaluated. This is done very briefly since we cannot present here the details of the used programs. Further, we talk about some technical details how we obtain analytic equations and also discuss some properties of these equations.

6.1 Computation of Vertices

The computation of vertices is in principle a straight forward computation i.e it involves just taking functional derivatives of the action. When the functional derivative is taken with respect to a metric one has to remember to symmetrize afterwards. So the result is

$$\frac{\delta g_{\mu\nu}(x_1)}{\delta g_{\alpha\beta}(x_2)} = \delta^{\alpha\beta}_{\mu\nu}\delta(x_1 - x_2)\,, \tag{6.1}$$

with $\delta^{\alpha\beta}_{\mu\nu} = \frac{1}{2}(\delta^\alpha_\mu\delta^\beta_\nu + \delta^\alpha_\nu\delta^\beta_\mu)$. The result of the variation is Fourier transformed and the vertices in momentum space are obtained. The Dirac delta distributions are important since they first kill the integral of the action and then ensure momentum conservation of each vertex.

The problem of the calculation is not the complicated mathematics but rather the large results. The number of terms per n-point function is growing exponentially and the three graviton vertex with 206 terms is maybe the last one that a crazy person could intend to compute by hand. For our setup we need the five graviton vertex as well as the two-fermions-three-graviton-vertex with approximately 66000 and 600 terms respectively. Those are incredible long expressions and obviously computer support is necessary. Fortunately we were able to use already existing technology i.e. the program *TARDIS* created by Andreas Rodigast ([74]), which is a *mathematica* based FRG program, which internally uses packages from *form* ([75]) and *xAct* ([76]). *TARDIS* is in principle able to implement an arbitrary action with all kinds of matter content. The calculation of vertices, especially in the graviton sector, is well tested and incredible fast in handling many terms due to its *form* based method of calculation. The testing of the fermion sector was part of this work and by now we have great confidence that all outputs concerning vertices are correct. In principle *TARDIS* can do more e.g. contraction of diagrams and even work out flow equations. But these parts are not well tested and are anyway not used in this work. For the sake of acknowledgement the logo of the program is shown in figure 6.1.

For the sake of comparison and also as support for the next section, where the graviton propagator is inverted, we give the result of the two graviton vertex. All

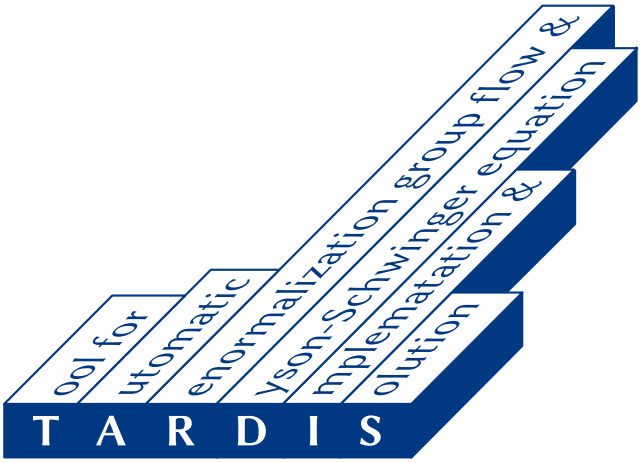

Figure 6.1: Logo of the program TARDIS, which was used to compute all vertices. Author: Andreas Rodigast. [74]

other vertices would be too long to display. The vertex is

$$\begin{aligned}\Gamma^{(2h)}_{\mu\nu\rho\sigma} = \frac{Z_h}{64\pi}\Bigg(&\left(\delta_{\mu\nu}\delta_{\rho\sigma} - \delta_{\mu\sigma}\delta_{\nu\rho} - \delta_{\mu\rho}\delta_{\nu\sigma}\right) 2\Lambda_2 + \left(\delta_{\mu\sigma}\delta_{\nu\rho} + \delta_{\mu\rho}\delta_{\nu\sigma} - 2\delta_{\mu\nu}\delta_{\rho\sigma}\right) p^2 \\ &- \delta_{\mu\sigma}p_\nu p_\rho - \delta_{\nu\rho}p_\mu p_\sigma - \delta_{\nu\sigma}p_\mu p_\rho - \delta_{\mu\rho}p_\nu p_\sigma + 2\delta_{\mu\nu}p_\rho p_\sigma + 2\delta_{\rho\sigma}p_\mu p_\nu \\ &+ \frac{1}{\xi}(\delta_{\mu\nu}\delta_{\rho\sigma}p^2 + \delta_{\mu\sigma}p_\nu p_\rho + \delta_{\nu\rho}p_\mu p_\sigma + \delta_{\nu\sigma}p_\mu p_\rho + \delta_{\mu\rho}p_\nu p_\sigma \\ &- 2\delta_{\mu\nu}p_\rho p_\sigma - 2\delta_{\rho\sigma}p_\mu p_\nu)\Bigg)\,, \end{aligned} \tag{6.2}$$

where ξ is the gauge fixing parameter introduced in section 5.1.1, which we eventually want to set to zero. At this point this not possible but after the inversion the limit will be well defined.

6.2 Computation of the Propagator

In this section, we calculate the propagator from the two-point function. As already mentioned before this is a non-trivial task due to the four indices of the graviton two-point function. A complete set of tensor structures is required. We follow the procedure of [77] and use the Stelle decomposition.

All projectors are constructed from the transversal and the longitudinal projector, which are

$$\Pi^{\mathrm{T}}_{\mu\nu} = \delta_{\mu\nu} - \frac{p_\mu p_\nu}{p^2} \qquad \text{and} \qquad \Pi^{\mathrm{L}}_{\mu\nu} = \frac{p_\mu p_\nu}{p^2}\,. \tag{6.3}$$

The four projectors, which span the space of symmetric rank four tensors, are then

$$\Pi^{(2)}_{\mu\nu\rho\sigma} = \frac{1}{2}\left(\Pi^{\mathrm{T}}_{\mu\rho}\Pi^{\mathrm{T}}_{\nu\sigma} + \Pi^{\mathrm{T}}_{\mu\sigma}\Pi^{\mathrm{T}}_{\nu\rho}\right) - \frac{1}{3}\Pi^{\mathrm{T}}_{\mu\nu}\Pi^{\mathrm{T}}_{\rho\sigma}\,, \tag{6.4}$$

$$\Pi^{(1)}_{\mu\nu\rho\sigma} = \frac{1}{2}\left(\Pi^{\mathrm{T}}_{\mu\rho}\Pi^{\mathrm{L}}_{\nu\sigma} + \Pi^{\mathrm{T}}_{\mu\sigma}\Pi^{\mathrm{L}}_{\nu\rho} + \Pi^{\mathrm{T}}_{\nu\rho}\Pi^{\mathrm{L}}_{\mu\sigma} + \Pi^{\mathrm{T}}_{\nu\sigma}\Pi^{\mathrm{L}}_{\mu\rho}\right)\,, \tag{6.5}$$

$$\Pi^{(0-s)}_{\mu\nu\rho\sigma} = \frac{1}{3}\Pi^{\mathrm{T}}_{\mu\nu}\Pi^{\mathrm{T}}_{\rho\sigma}\,, \tag{6.6}$$

$$\Pi^{(0-w)}_{\mu\nu\rho\sigma} = \Pi^{\mathrm{L}}_{\mu\nu}\Pi^{\mathrm{L}}_{\rho\sigma}\,. \tag{6.7}$$

They are representing a spin two, a spin one and two spin zero particles. The decomposition is evidently equivalent to the York decomposition, which was introduced in equation (5.14). The transverse-traceless projector, see equation (5.15), is also identical to the spin two projector from equation (6.4). The only reason to use the Stelle decomposition instead of the York decomposition is that the two spin-zero transfer operators

$$\Pi^{(0-sw)}_{\mu\nu\rho\sigma} = \frac{1}{\sqrt{3}}\Pi^{\mathrm{T}}_{\mu\nu}\Pi^{\mathrm{L}}_{\rho\sigma} \qquad \text{and} \qquad \Pi^{(0-ws)}_{\mu\nu\rho\sigma} = \frac{1}{\sqrt{3}}\Pi^{\mathrm{L}}_{\mu\nu}\Pi^{\mathrm{T}}_{\rho\sigma} \tag{6.8}$$

are known and they are required for the inversion. The only difference between York and Stelle decomposition is in fact in the spin zero sector.

The two graviton vertex from equation (6.2) is now contracted with each of these six projectors and then respectively divided with the norm of each projector. The scalar results are written in a 4x4 square matrix with the results of (6.4) until (6.7) written on the diagonal in this order and on the side diagonal are the results of (6.8) since they are the transfer operators. The result is

$$\Gamma^{(2h)} = \frac{Z_h}{64\pi}\begin{pmatrix} 2(\mu_h k^2 + p^2) & 0 & 0 & 0 \\ 0 & 2\left(\mu_h k^2 + \frac{p^2}{\xi}\right) & 0 & 0 \\ 0 & 0 & p^2(\frac{3}{\xi} - 4) - \mu_h k^2 & -\sqrt{3}\left(\mu_h k^2 + \frac{p^2}{\xi}\right) \\ 0 & 0 & -\sqrt{3}\left(\mu_h k^2 + \frac{p^2}{\xi}\right) & \mu_h k^2 + \frac{p^2}{\xi} \end{pmatrix}. \tag{6.9}$$

We need to take the inverse of the graviton two-point function plus regulator. The regulator is chosen to be the two-point function at vanishing mass

$$R_{k,\mu\nu\rho\sigma}(p^2) = \Gamma^{(2h)}_{\mu\nu\rho\sigma}(p^2)\Big|_{\mu_h=0} r(k^2/p^2)\,, \tag{6.10}$$

where r is again some dimensionless shape function. So basically we just need to replace $p^2 \to p^2(1 + r(k^2/p^2)) =: \tilde{p}^2$ in equation (6.9). The inversion of equation (6.9) with momentum $\tilde{p}$ is a straight forward matrix inversion. Afterwards, we can safely take the limit $\xi \to 0$.

The result is

$$G \equiv \left(\Gamma^{(2h)} + R_k\right)^{-1} = \frac{16\pi}{Z_h(\mu_h k^2 + \tilde{p}^2)} \begin{pmatrix} 2 & 0 & 0 & 0 \\ 0 & 0 & 0 & 0 \\ 0 & 0 & -1 & -\sqrt{3} \\ 0 & 0 & -\sqrt{3} & -3 \end{pmatrix} . \tag{6.11}$$

Now we can recover the tensor structure by splitting the matrix back into projector coefficients. The limit $\xi \to 0$ is always well defined. In case of the regulator insertion $\dot{R}_k$ it cannot be taken straight away but in the product $G\dot{R}_k G$.

6.3 Evaluation of Diagrams

We have now collected all ingredients to evaluate the diagrams. The evaluation of the diagrams is again a straight forward computation, which involves contractions of large tensor structures and traces over products of Dirac gamma matrices in case of fermion loops or external fermions. As mentioned in the section before, the amount of terms is too high for calculations by hand. Hence we need help by computers. The task was done with self-written *form* programs. *Form* shows in particular good performance when handling many terms and is therefore suitable for our problem.

The loop integration is easiest performed in spherical coordinates. We define the spherical coordinates with

$$\vec{q} = q \begin{pmatrix} \cos(\theta_1) \\ \sin(\theta_1)\cos(\theta_2) \\ \sin(\theta_1)\sin(\theta_2)\cos(\phi) \\ \sin(\theta_1)\sin(\theta_2)\sin(\phi) \end{pmatrix} , \tag{6.12}$$

where $\theta_i \in [0, \pi)$ and $\phi \in [0, 2\pi)$. The integral measure is then given by

$$\begin{aligned} \mathrm{d}^4 q &= \mathrm{d}q\mathrm{d}\phi\mathrm{d}\theta_1\mathrm{d}\theta_2 \sin(\theta_1)^2 \sin(\theta_2) q^3 \\ &= \mathrm{d}q\mathrm{d}\phi\mathrm{d}y\mathrm{d}x \sqrt{1-x^2} q^3 , \end{aligned} \tag{6.13}$$

where we have transformed in the second line with $x := \cos(\theta_1)$ and $y := \cos(\theta_2)$. The angle θ_1 is usually the angle between the first external momentum $\vec{p}_1$ and the loop momentum $\vec{q}$.

6.4 Derivation of Analytic Equations

In this work, analytic equations for all running coupling parameters were derived. This is one of the central results and thus we present in this section some technical details of the derivation. Analytic equations can just be obtained with the optimized regulator, see equation (2.35), and a projection at $p = 0$. In case of the running of g or of the anomalous dimensions the contribution is obtained by taking a derivative

with respect to p^2. Unfortunately, if the task is carried out with *mathematica* the result turns out to be wrong due to the non analytic behaviour of the Litim regulator. The result contains non-trivial products of Heaviside theta functions and Dirac delta distributions, which have to be treated carefully. For this purpose, the following formula is very useful [10, 78]:

$$\delta(x) f(x, \Theta(x)) = \delta(x) \int_0^1 \mathrm{d}u \; f(0, u) \,. \tag{6.14}$$

We show an example, which contributions are missed by *mathematica*. We use the abbreviation $s = p^2 + 2pqx + q^2$. The example is in fact identical to the real calculation for a diagram with a propagator carrying the momentum $\vec{p} + \vec{q}$. The momentum dependence of the remaining diagram is encrypted in the function $f(p)$. Taking the second derivative of such a diagram leads to

$$\begin{aligned}
\frac{\partial^2}{\partial p^2}\,(\text{diagram}) &= \frac{\partial^2}{\partial p^2}\left(\frac{f(p)\Theta(1-q^2)}{m^2+s+(1-s)\Theta(1-s)}\right) \\
&= \frac{\partial^2}{\partial p^2}\left(f(p)\Theta(1-q^2)\left(\frac{\Theta(1-s)}{m^2+1}+\frac{\Theta(s-1)}{m^2+s}\right)\right) \\
&= \frac{\partial}{\partial p}\Bigg(f(p)\Theta(1-q^2)\underbrace{\left(-\frac{\delta(1-s)}{m^2+1}+\frac{\delta(s-1)}{m^2+s}\right)}_{=0}2(p+qx) \\
&\quad + f'(p)\Theta(1-q^2)\left(\frac{\Theta(1-s)}{m^2+1}+\frac{\Theta(s-1)}{m^2+s}\right) \\
&\quad + f(p)\Theta(1-q^2)\frac{-2(p+qx)}{(m^2+s)^2}\Theta(s-1)\Bigg) \\
&\supset f'(p)\Theta(1-q^2)\underbrace{\left(-\frac{\delta(1-s)}{m^2+1}+\frac{\delta(s-1)}{m^2+s}\right)}_{=0}2(p+qx) \\
&\quad - f(p)\frac{2(p+qx)^2}{(m^2+s)^2}\underbrace{\delta(s-1)\Theta(1-q^2)}_{\xrightarrow{p\to 0}\frac{1}{2}\delta(q^2-1)=\frac{1}{4q}\delta(q-1)} \\
&\xrightarrow{p\to 0} -f(0)\frac{x^2}{(m^2+1)^2}\delta(q-1)\,.
\end{aligned} \tag{6.15}$$

In the second to last step just the terms containing a Dirac delta distribution were picked out, since all other terms are well treated by *mathematica*. In the last step equation (6.14) was used. Note that the product $\Theta(1-q^2)\Theta(s-1)$ indeed doesn't give any contribution. The limit $p \to 0$ and the integration can be interchanged in this case since the integrand is not singular. The resulting function $\Theta(1-q^2)\Theta(q^2-1)$ is just non-zero at one point and hence this is a measure-zero set.

Unfortunately in case of fermionic diagrams the problem is a little more tricky since

the propagator appears in a trace. Nevertheless a similar formula was derived and the calculation is shown in appendix A. The difference in the resulting formula is that the result is still a matrix in spinor space and in consequence has to be contracted with the remaining diagram separately. In contrary, the formula in equation (6.15) can be simply applied to the fully contracted diagram.

It is recommendable to check computations like this with a numerical integration. The easiest way to perform this is to express the Heaviside theta functions as an analytic function with a parameter ϵ, which fulfils the limit $\Theta_\epsilon \xrightarrow{\epsilon \to 0} \Theta$. An example for this is the Fermi-Dirac distribution

$$\Theta_\epsilon(x-1) = \frac{1}{\exp\left(\frac{x-1}{\epsilon}\right)+1}\,. \tag{6.16}$$

The Dirac delta distribution is then simply the derivative of Θ_ϵ. With these replacements the derivative with respect to p and the limit $p \to 0$ can easily be applied. Eventually one has to integrate numerically for a small value of ϵ. One has to be careful not to choose a too small value for ϵ since then the error of the integration might dominate. Reasonable values for ϵ are 10^{-1}, 10^{-2} or 10^{-3}.

Now we have everything to obtain analytic equations. A short summary:

- The defining equations are for the running of Newton's coupling and λ_3 are (5.40) and (5.38) in case of the asymmetric momentum configuration and (5.41) and (5.38) in case of the symmetric momentum configuration. For the dimensionless mass parameter of the graviton we use equation (5.20). The anomalous dimensions are determined by the equations (5.21), (5.25), (5.60) and (5.67). The running of the dimensionless matter masses are given by (5.59) and (5.66).

- All evaluations are done with a Limit-shaped cut-off as in equation (2.35).

- The integration is performed in spherical coordinates as in equations (6.12) and (6.13).

- Contributions due to the non-analytic behaviour of the Litim-shaped cut of are taken into account with equations (6.15) and (A.12). Note, that these contributions are always independent of the anomalous dimension due to the overall Dirac delta distribution $\delta(1-q)$ and the integral of the anomalous dimension is exactly zero at $q = 1$. All diagrams are typically proportional to $(n - \eta_i)$ with $n \in \{4, 6, 8, \dots\}$. The contribution can destroy this typical proportionality.

The analytic equations are unfortunately very long expressions and hence just displayed in appendix B. Still, we want to discuss here some important properties of them. First of all, we take a look at the contributions of scalars and fermions for vanishing mass and anomalous dimension. Both contributions to the running of Newton's coupling are negative i.e. potentially stabilizing as explained in section 4.2. This statement is independent of the momentum configuration. This is not

only opposing the results form [26] but also the results from some more general approaches like in [79] and [80]. We already mentioned in section 2.3, that in [33] it was concluded that the sign of the contribution depends on the type of regulator. However, we cannot resolve this issue here due to our flat background and thus, we have to postpone this problem to future investigations.

The matter contribution to the running of the dimensionless mass parameter of the graviton is also important as explained in section 4.2. Here the fermionic contribution has the stabilizing sign, while the scalar contribution has the destabilizing sign. This is again opposing the results of [26], although the comparison is this time not straight forward because their mass of the graviton is simply the cosmological constant. Nevertheless, this is a legit comparison. So in our case, fermions are expected to have a completely stabilizing effect while in the scalar sector a stabilizing and a destabilizing effect encounter each other and it is not clear, which one is stronger.

We want to discuss, if it is possible to change the sign of the matter contribution with the mass or the anomalous dimension of the particle. In the equation for the running of the graviton mass parameter, just the anomalous dimension of the respective matter particle can change the sign if it is larger than six. But this possibility can be ignored because already an anomalous dimension larger that two is untrustworthy as explained in section 4.3. In case of the running of Newton's coupling, the situation is different in the fermionic sector. The mass of the fermion can change the sign of the contribution if $\mu_\psi > 4$ for the asymmetric momentum configuration and if $\mu_\psi > 9$ for the symmetric momentum configuration. Both statements are approximative because it depends on the value of the anomalous dimension. Those are very large values of the mass but we observe later that especially the fermion mass tends to have a finite value at the UV fixed point and thus this possibility of a sign change has to be taken seriously.

The anomalous dimension of the scalar is zero in case of massless scalars. This is surprising and, interestingly, even dependent on the gauge choice in the gravity sector. Our choice of gauge, as described in section 5.1.1, is the one singular gauge where it is zero for massless scalars. This fact is no reason to worry since the anomalous dimension is no observable and has a priori no physical meaning. The effect it has on physical observables can be compensated by other anomalous dimensions, which are as well gauge dependent. In other words, the choice of gauge rotates the value the scalar anomalous dimension into the other anomalous dimensions.

7 Results

In this chapter, we present the results of our setup. We start with general properties of the graviton three-point function, namely its locality, and continue with the fixed points of the pure quantum gravity system. Here, we show on the one hand the results of the asymmetric momentum configuration and on the other hand the ones of the symmetric momentum configuration. Furthermore different momentum projections points are compared, i.e. the difference between a derivative and a finite difference. We also investigate the IR properties of the system. We turn then to the results with matter inclusions for our best approximation, monitor the evolution of the UV fixed point under an increasing amount of scalar and fermion flavours and discuss possible bounds on the matter sector. Further, we investigate the stability of the UV fixed point in the mass direction of the matter particles and show that the possibility of a UV fixed point with a non-vanishing matter mass exists. At last, we return to unimodular quantum gravity, which was very shortly introduced in section 3.1, and analyse its properties in a very basic approximation.

However, we first have to specify how we close the equations, that means how we treat undetermined quantities from higher vertices. For all following analysis, we identify these couplings with the highest know vertex i.e. $g := g_3 \equiv g_4 \equiv g_5$ and $\lambda_3 \equiv \lambda_4 \equiv \lambda_5$.

7.1 Locality of the Graviton Three-Point Function

In this section, we discuss one of the most important properties of the graviton three-point function, namely the locality of its flow in momentum space. The content of this section is also part of forthcoming publication in preparation [69]. Locality in momentum space is a desired property for the flow of all vertices. It is a necessary basic element of the renormalization group, which integrates out momentum shells at some scale k. If a correlation function would be non-local in momentum space then a renormalization group step in the IR influences the physics in the UV, implying that any classical vertex turns into a non-trivial quantum vertex instantly. As a formula this property is expressed for an n-point function as

$$\lim_{\mathbf{p}\to\infty} \frac{|\partial_t \Gamma_k^{(n)}(\mathbf{p})|}{|\Gamma_k^{(n)}(\mathbf{p})|} = 0\,. \tag{7.1}$$

The n-point function is in general of course a tensor and with the notation in equation (7.1) we are referring to components of this tensor. This property is trivially proven for perturbatively renormalizable quantum field theories in four dimensions even

including non-Abelian gauge theories by simple power counting arguments. For graviton vertices this is a highly non-trivial property and the only reason for its origin can be diffeomorphism invariance. In [22] and [21] it was already shown that the flow of the graviton propagator is local. This results in the fact that the anomalous dimension of the graviton is going to zero for large momenta. We present now the steps of the calculation for the graviton three-point function.

We start from the flow displayed in equation (5.6) with arbitrary external momenta p_1, p_2 and p_3. One external momentum can be eliminated via momentum conservation, i.e. $p_3 = -p_1 - p_2$. Then we apply the usual tensorial projection for the flow of Newton's constant shown in equation (5.27). No momentum configuration is chosen since we want to prove it for arbitrary external momenta. The result of the contractions are complicated expressions depending on the norm of the momenta $|p_1|$ and $|p_2|$, on the angle between the momenta θ_{12}, on the angle between the momenta and the integration vector φ_1 and φ_2 and the integration vector q itself. The latter ones are integrated out. For simplicity, we set $p := |p_1| = |p_2|$ and just leave the angle $\theta_{12} \in [0, \pi]$ arbitrary. That means we are checking locality on a single line of the two dimensional parameter space. Since the configurations on this line are by no means significant, we assume that our results extend to the remaining parameter space. We want to emphasize that it is important to symmetrize the diagrams in equation (5.6) with respect to the external momenta.

The next step is to show that the highest power in p cancels in the sum of all diagrams after integration. In case of the graviton three-point this power is p^2. We want to emphasize that this is true for a projector with mass dimension zero. The projector that is described in section 5.1.4 has mass dimension two and in consequence we divide by p^2 to obtain the final projector. We perform the integration as usual in spherical coordinates, see section 6.3 for the definition, and we parameterize the angles between the momenta and the integration vector as

$$\cos\varphi_1 := \cos\theta_1 = x\,, \tag{7.2}$$

$$\cos\varphi_2 := \cos\theta_2 \sin\theta_1 \sin\theta_{12} + \cos\theta_1 \cos\theta_{12} = y\sqrt{1-x^2}\sqrt{1-x_{12}^2} + x x_{12}\,, \tag{7.3}$$

with the usual abbreviations of the spherical coordinates and $x_{12} := \cos\theta_{12}$. To simplify the calculation it is possible to set $\Lambda_n \to 0$ since terms containing these quantities must have a lower power of p. Furthermore all diagrams are proportional to $\frac{\eta_h - 6}{(1+\mu_h)^2}$ in the highest power of p. We skip this prefactor and just give the asymptotes of the diagrams with an overall factor of proportionality missing.

The asymptotes are then

$$\lim_{p\to\infty}\left(-\frac{1}{2p^2}\right.$$ 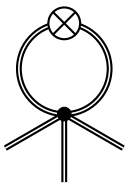 $$\left.\right) \propto 20x_{12}^6 + 8x_{12}^5 + 464x_{12}^4 + 1168x_{12}^3$$

$$+ 1207x_{12}^2 + 1516x_{12} + 1287\,, \tag{7.4}$$

$$\lim_{p\to\infty}\left(-\frac{3}{p^2}\right.$$ 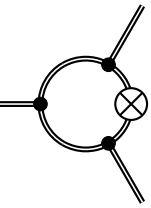 $$\left.\right) \propto -24x_{12}^6 + 48x_{12}^5 + 768x_{12}^4 + 4776x_{12}^3$$

$$+ 13938x_{12}^2 + 11328x_{12} + 3186\,, \tag{7.5}$$

$$\lim_{p\to\infty}\left(\frac{3}{p^2}\right.$$ 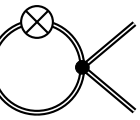 $$\left.\right) \propto 4x_{12}^6 - 56x_{12}^5 - 1232x_{12}^4 - 5944x_{12}^3$$

$$- 15145x_{12}^2 - 12844x_{12} - 4473\,, \tag{7.6}$$

$$\lim_{p\to\infty}\left(\frac{6}{p^2}\right.$$ 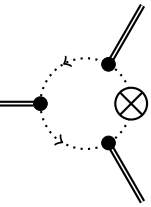 $$\left.\right) = 0\,. \tag{7.7}$$

All factors beautifully cancel and we have shown the highly non-trivial property of locality in momentum space. Note, that the star-diagram and the fish-diagram are already symmetrized with respect to the external momentum legs. The ghost contribution already cancels its highest power in p by itself. We have not checked if those statements are gauge dependent.

The locality is visualized in figure 7.1 where one typical shape of the flow of the three-point function as well as the flow divided by the three-point function itself is plotted. The curves are computed with $\lambda_3 = 0.2$ for the symmetric momentum configuration.

We are further interested in shape of the flow for different values of λ_3 in the symmetric momentum configuration. This is displayed in figure 7.2. All curves are going to a constant for $p \to \infty$ and therefore again confirming locality. Furthermore the plot shows beautifully that the finite difference between $p = k$ and $p = 0$, which leads to the flow of Newton's coupling as explained in section 5.1.4, is the best possible approximation of the physics below the scale $p = k$. Hence, this is the closest we can get the to global information of the flow. A full extraction of the global information would require a fully momentum dependent Newton's coupling.

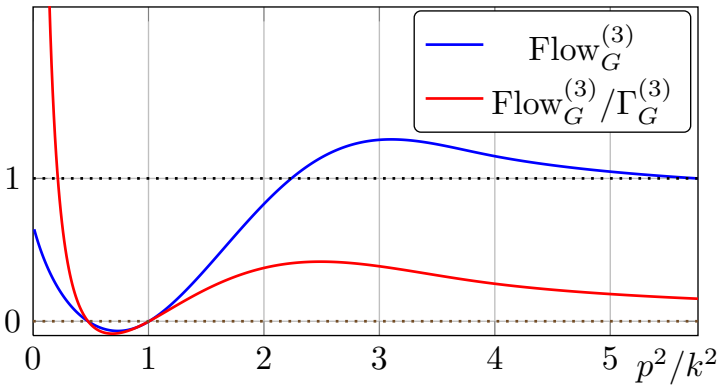

Figure 7.1: A typical shape of the flow of the three point function is shown (blue curve) as well as the flow divided by the three-point function itself (red curve). The blue curve goes to a constant for $p \to \infty$ and the quotient to zero since the vertex itself is proportional to p^2. Hence, this is a confirmation of locality as described in equation (7.1). Both curves are rescaled to be visually appealing.

Also a derivative at $p = k/2$ seems to be reasonable, while a derivative at $p = 0$ is just sufficient for $\lambda_3 \approx 0$ for this particular value of μ_h. Also a derivative at $p = k$ is not very convenient for values $\lambda_3 < 0$. Nevertheless we also investigate the system with a derivative at $p = 0$ since it is the only projection that allows the derivation with analytic equations.

It is important to note that locality does not hold in case of the asymmetric momentum configuration. First of all, our calculation from above is not correct for this limit. We first take the limit $p \to \infty$ and then we set $x_{12} = -1$, which is of course an incorrect order for this special configuration. Computing this configuration in an appropriate way results in non-vanishing terms. Some of these terms are even proportional to Λ_3, since some vertices are completely independent of p in this case. This is neither surprising nor worrying because this is just reflecting that one leg with vanishing momentum is a description of IR physics.

7.2 Pure Gravity Solutions

In this section, we discuss solutions to the pure gravity system without any matter content. We look for UV fixed points and investigate the IR properties of the flow. We show some different systems i.e. we differ between the asymmetric momentum configuration and the symmetric momentum configuration as explained in section 5.1.4. Furthermore, we investigate different momentum projection points for example the asymmetric configuration is just projected with a derivative at $p = 0$ while the symmetric momentum configuration is projected with a finite difference between $p = k$ and $p = 0$ as well as with a derivative at $p = 0$. The reasons for these choices

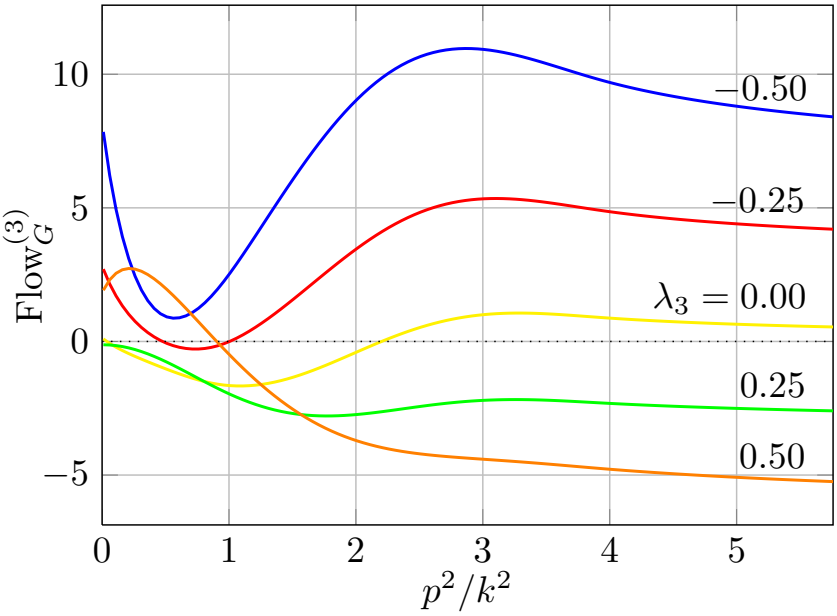

Figure 7.2: The flow of the graviton three-point function is displayed for different values of λ_3 in the setting of the symmetric momentum configuration. All curves are computed for $\mu = -0.3$ and the values for λ_3 are given on each curve. All flows go to a constant for $p \to \infty$ and hence fulfil the locality condition. It shows further that a finite difference between $p = k$ and $p = 0$ is the best approximation for the physics below the scale $p = k$.

were as well explained in section 5.1.4. We start with the asymmetric momentum configuration.

Note, that there are certain requirements for the UV fixed point. The first demand is that $g^* > 0$ since the IR value of g is fixed to be positive and a change of sign is not possible in our truncation. Further, we want $\mu_h > -1$. All equations have pole at $\mu_h = -1$ and hence this value cannot be crossed by any RG flow. Also, we know from earlier analysis the approximate location of the UV fixed point. As long as we don't want to disagree with all previous results, we should stick to that demand. At last, we demand that the UV fixed point has at least two attractive directions, excluding the λ_1 direction. In [21] it was shown that the UV fixed point is fully attractive with respect to the parameters g, μ_h and λ_1 and we don't want to lose attractive directions due to a higher truncation.

7.2.1 Asymmetric Momentum Configuration

The asymmetric momentum configuration is evaluated with a derivative at $p = 0$ and therefore all equations can be obtained analytically. They are displayed in appendix

B. As a first test, we always try to solve the equations with the anomalous dimensions set to zero. This check is reasonable since the anomalous dimension are supposed to be small and the existence of a fixed point shouldn't depend upon the inclusion of the anomalous dimensions.

Unfortunately, the system doesn't contain any physical UV fixed points. This statement also doesn't change after the inclusion of the anomalous dimension. The only fixed point is a completely attractive IR fixed point at the coordinates

$$(g^{*,\mathrm{IR}}, \mu_h^{*,\mathrm{IR}}, \lambda_3^{*,\mathrm{IR}}) = (0.39, -0.47, 0.039) \tag{7.8}$$

and with the critical exponents i.e. eigenvalues of the stability matrix

$$(0.52 \pm 5.3i, 4.7)\,. \tag{7.9}$$

The anomalous dimensions at the fixed point are

$$(\eta_h^{*,\mathrm{IR}}, \eta_c^{*,\mathrm{IR}}) = (1.5, -0.54)\,. \tag{7.10}$$

These results are very questionable in particular since the IR behaviour of gravity is well known. Newton's coupling should become a constant, which is achieved by a quadratic running of the dimensionless parameter i.e. $g_{\mathrm{IR}} \propto k^2$. This is here not the case, instead the g is oscillating around the fixed point value, due to the complex part of the critical exponents, before reaching it. Further, the desired IR fixed point is $(g^{*,\mathrm{IR}}, \mu_h^{*,\mathrm{IR}}) = (0, -1)$ as found in [21].

In summary, this system doesn't give any desired results. There are many arguments that can give an explanation. First of all, the asymmetric momentum configuration doesn't fulfil the condition of locality, described in section 7.1. The reason for this is that one external leg put to zero reflects the physics from the IR. Considering this, it might not be reasonable to look for a physical UV fixed point with a vertex that is evaluated in the IR. But this doesn't explain the failure of the system in the IR and therefore we should also question the projection on the tensor structure we used for the leg with vanishing momentum, which is partly displayed in equation (5.32). We chose this projector because the usual transversal-traceless projector exhibits an ambiguity since the transverse-traceless part of a vanishing momentum is not well defined. But there is no reason why the new projector should capture the leading physical contribution. Unfortunately, in this work was no time to check the dependencies of the results under change of the tensorial projector.

7.2.2 Symmetric Momentum Configuration

The symmetric momentum configuration is most conveniently evaluated with a finite difference between $p = 0$ and $p = k$, as described in section 7.1. The equation for λ_3 is still be evaluated at $p = 0$ since it represents the momentum independent part. The equation for λ_3 is universal and doesn't dependent on the specific momentum configuration. It is the same as in the asymmetric configuration and displayed in

appendix B. The downside of the finite difference is that it is not possible to obtain an analytic equation for the running of Newton's coupling. Due to this fact, we also evaluate the symmetric configuration with a derivative at $p = 0$ although we know that it is not the best projection method.

Finite Difference between $p = 0$ and $p = k$

We again start to analyse the system with the anomalous dimensions set to zero. We include them later and check that the difference is not significant. The equation for the running of Newton's coupling is given by equation (5.41) with the momentum scales $p_a = 0$ and $p_b = k$. This equation requires numeric interpolation in the following way. The flow of the three-point function is sorted in powers of λ_3, the remaining integral is evaluated for certain values of μ_h and the result interpolated as a function of μ_h. The equations for λ_3 and μ_h are the usual analytic ones given in appendix B.

The system exhibits a fully attractive UV fixed point at

$$(g^{*,\mathrm{UV}}, \mu_h^{*,\mathrm{UV}}, \lambda_3^{*,\mathrm{UV}}) = (0.98, -0.33, 0.29) \tag{7.11}$$

and with the critical exponents

$$(-4.0 \pm 0.87i, -3.3)\,. \tag{7.12}$$

These are quite nice results. All directions are attractive, the fixed point values are similar to other investigations and the critical exponents also have reasonable values. Additionally, we find a UV fixed point with just two attractive directions at the coordinates

$$(g^{*,\mathrm{UV},2}, \mu_h^{*,\mathrm{UV},2}, \lambda_3^{*,\mathrm{UV},2}) = (0.96, -0.35, -0.024) \tag{7.13}$$

and with the critical exponents

$$(-2.1 \pm 2.4i, 5.8)\,. \tag{7.14}$$

The eigenvector that belongs to the positive eigenvalue is mainly directed in the λ_3 direction hence the flow leads to the fully attractive fixed point. Further, we find the following IR behaviour

$$(g, \mu_h, \lambda_3) \xrightarrow{k\to 0} (0, -1, \infty)\,, \tag{7.15}$$

which is exactly what was predicted by the scaling analysis from Christiansen et al. in [21]. We phrase these facts carefully since we cannot fully integrate the flow down to $k = 0$ due to numerical problems. The problems become quite obvious considering that all equations have a pole at $\mu_h = 0$ and so in this region $(1 + \mu_h)^{-1}$ going to infinity competes with g going to zero. It is evident that a numerical integration is not suitable for such a limit. For an integration down to $k = 0$ a careful investigation of the scaling behaviours in this region has to be done similar as in [21].

In figure 7.3, we show trajectories connecting the IR region with the UV fixed point. All plotted trajectories end on the fully attractive UV fixed point but they have different IR regimes. Most of them flow toward the classical IR fixed point as described in equation (7.15) but some trajectories also flow towards $(g, \mu_h, \lambda_3) \to (0, \infty, -\infty)$. This nicely agrees with the lower truncation from [21] where the same IR fixed point without λ_3 was found. The second IR behaviour corresponds to a non-physical part of the phase diagram where the graviton is massive in the IR. Note, that the trajectories that flow into the physical IR fixed point can flow infinitely close past the Gaussian fixed point.

We now have to include the anomalous dimensions. The best and only consistent way to do this is the fully momentum dependent anomalous dimension as described in equation (5.23) and in [21]. However, this involves a lot of numerical work since the anomalous dimension has to be solved for each point in theory space with an iterative scheme and unfortunately the computation was not finished yet at the end of this thesis. Instead, we display results of a more simple computation. The most simple solution is a completely momentum independent anomalous dimension, which results in analytic equations as presented in appendix B. However, it was shown that this solution does not consistent results [22]. It is more convenient to differ between $\eta_h(0)$ and $\eta_h(k^2)$ since they both appear on the left hand side of the flow equation. The difference between these to point is usually quite significant and since their contribution on the left hand side is not suppressed like on the right hand side, the errors would cause serious impact on the system. In consequence, we need to calculate the anomalous dimension with a finite difference between some reference scale and p. We decide for the reference scale $p = -\mu_h$ as in [21].

Eventually, we want to compute the anomalous dimension at two points, $p = 0$ and $p = k$. The question remains how we treat the anomalous dimension that appears in the integral i.e. $\int \mathrm{d}q f(q)\eta_h(q)$ for some function f. Here, we use our knowledge that the integral has its maximum at $q = k$ due to the factor q^3 from the integral measure. Furthermore, the anomalous dimension is also peaked at $p \approx k$ and therefore the integral is well approximated by evaluating the anomalous dimension at $p = k$ and taking it out of the integral. This way, we over estimate the integral slightly and the approximation can be improved by including a factor smaller, but close to one.

With this system, we find a UV fixed point at the coordinates

$$(g^{*,\mathrm{UV}}, \mu_h^{*,\mathrm{UV}}, \lambda_3^{*,\mathrm{UV}}) = (0.60, -0.57, 0.097) \tag{7.16}$$

and with the critical exponents

$$(-0.52 \pm 4.1i, 12)\,. \tag{7.17}$$

So this fixed point has just two attractive directions, similar to the second, metastable fixed point before. The fact itself is not alarming since we expect that for some n the λ_n directions becomes repulsive. But in combination with the previous results

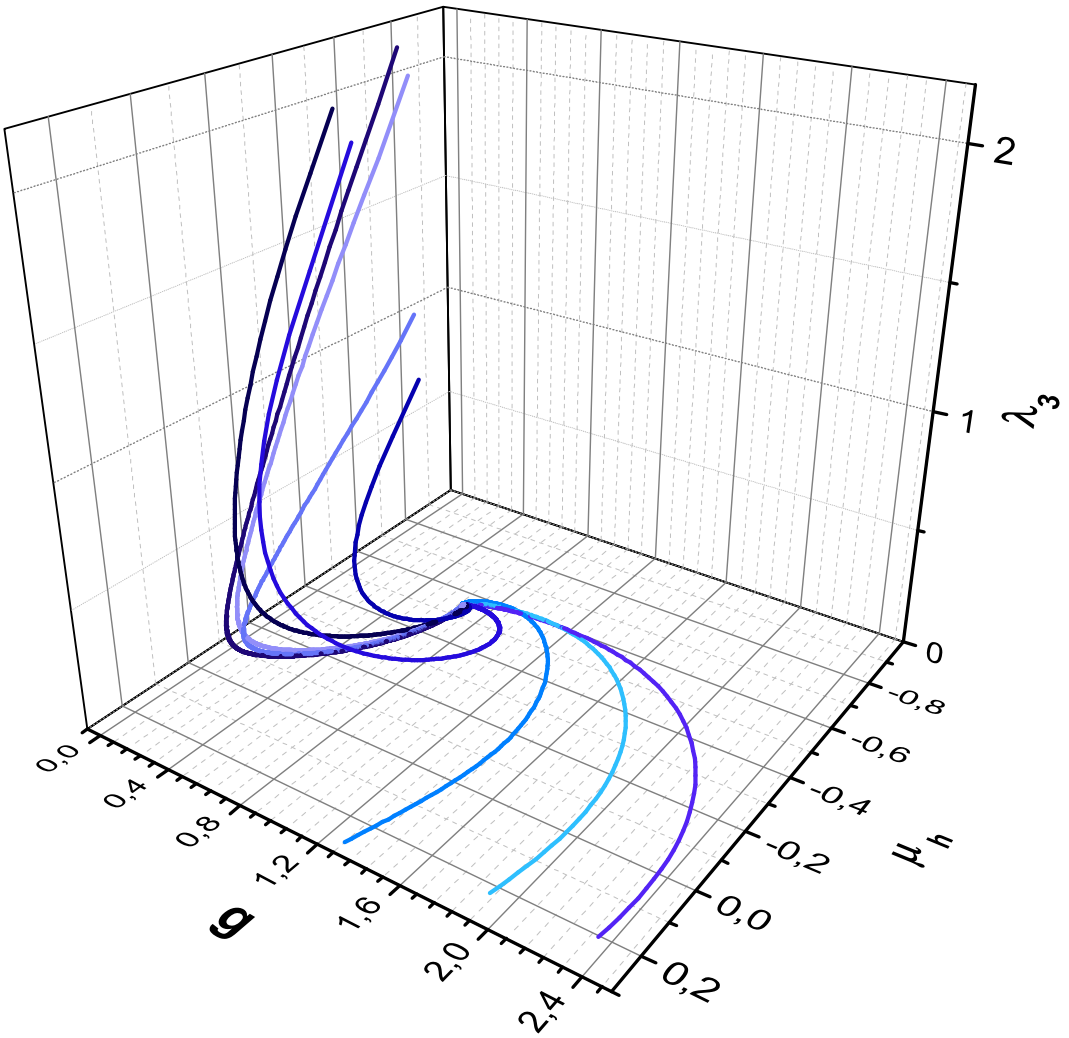

Figure 7.3: The plot shows trajectories in the three dimensional theory space of g, μ_h, λ_3. The fully attractive UV fixed point is visible. Most trajectories flow into the IR direction described in equation (7.15) but some also flow into a massive IR fixed point with $\mu_{\text{IR}} = \infty$. Both IR regions nicely correspond with the results from [21] where it was argued that only the massless IR fixed point is physical. The trajectories can flow infinitely close past the Gaussian fixed point and afterwards head towards the physical IR region.

this is slightly surprising. Even more suspicious are the anomalous dimensions at the UV fixed point, which have the values

$$(\eta_h^{*,\mathrm{UV}}(0), \eta_h^{*,\mathrm{UV}}(k^2), \eta_c^{*,\mathrm{UV}}) = (1.5, 0.43, -1.4)\,. \tag{7.18}$$

The the anomalous dimension of the graviton is larger at $p = 0$ that at $p = k$, disagreeing with our assumption from before and contradicting results obtained in [21]. Thus, we conclude that our approximation for the anomalous dimension is simply insufficient and only a fully momentum dependent anomalous dimension can solve the problem.

At last, we want to use the IR behaviour of the system to express the RG scale k in units of the Planck mass. As already mentioned, in the IR Newton's coupling is proportional to k^2 and therefore it becomes a constant. The constant of proportionality, lets call it C, is just Newton's constant itself, because

$$G_N = gk^{-2} = Ck^2k^{-2} = C\,. \tag{7.19}$$

In natural units the Planck mass is just $M_{\mathrm{Pl}}^2 = G_N^{-1}$ and therefore we can gauge the RG scale to the Planck scale for each trajectory by determining the constant of proportionality. In figure 7.4, this identification was done for an example trajectory that flows into the physical IR region described in equation (7.15). It nicely displays the classical scaling of g and λ_3. For μ_h no classical scaling is expected, instead it flows towards -1 the massless physical IR fixed point. Unfortunately, μ_h is speeding up towards the IR fixed point due to missing scaling input of the higher vertices. The classical scaling stops around the Planck scale and effects of quantum gravity start dominating. Soon afterwards, the flow of all running couplings stops and the UV fixed point is reached. The exact scale where classical scaling stops depends on the selected trajectory.

Derivative at $p = 0$

With a derivative at $p = 0$ it is possible to obtain analytic equations. These are again given in appendix B. We already know from figure 7.2 that the derivative doesn't work in the whole parameter space and in this section we are basically testing if the analytic equations still give reasonable results. As usual, we first solve the system with the anomalous dimensions set to zero. Again, we only find a UV fixed point with two attractive directions at the coordinates

$$(g^{*,\mathrm{UV}}, \mu_h^{*,\mathrm{UV}}, \lambda_3^{*,\mathrm{UV}}) = (0.57, -0.16, -0.16) \tag{7.20}$$

and with the critical exponents

$$(-1.5 \pm 1.8i, 1.6)\,. \tag{7.21}$$

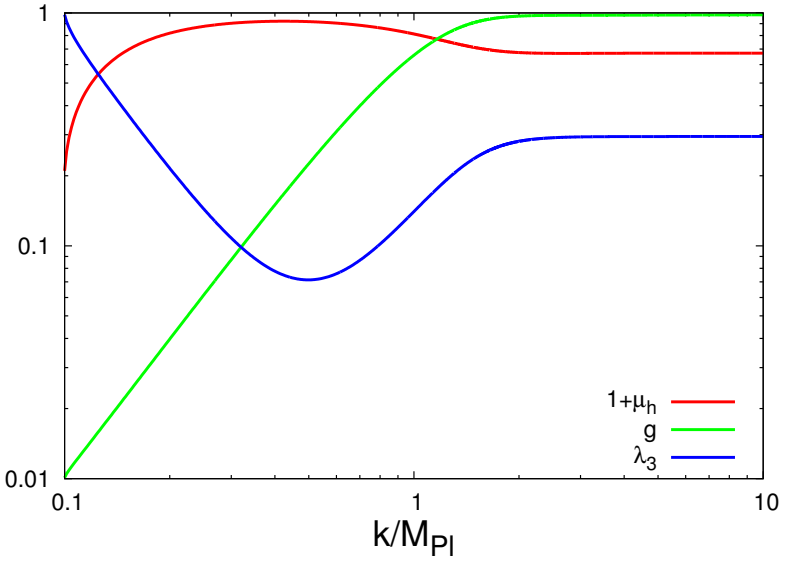

Figure 7.4: The running of the couplings g, μ_h, λ_3 as a function of the RG scale k in units of the Planck mass is displayed. In the IR, g and λ_3 show nice classical scaling while μ_h runs towards minus one. At the Planck scale the effects of quantum gravity take over and the classical scaling stops. Soon afterwards, the UV fixed point is reached and all running couplings become a constant.

The result is surprisingly similar to the metastable fixed points from the section before. We tested if the results persist after the inclusion of the anomalous dimension. This time, we use the anomalous dimension evaluated at vanishing momentum since the equation for g is as well projected at $p = 0$. Nevertheless, we don't want to use the analytic equation for the anomalous dimension since it was shown to be very inaccurate. Instead we use a finite difference with expansion around $p = -\mu_h$. Indeed, we again find a UV fixed point with two attractive directions at the coordinates

$$(g^{*,\mathrm{UV}}, \mu_h^{*,\mathrm{UV}}, \lambda_3^{*,\mathrm{UV}}) = (0.61, -0.43, 0.021) \tag{7.22}$$

and with the critical exponents

$$(-1.3 \pm 4.6i, 5.9)\,. \tag{7.23}$$

The anomalous dimensions at the UV fixed point are

$$(\eta_h^{*,\mathrm{UV}}, \eta_c^{*,\mathrm{UV}}) = (1.0, -0.80)\,. \tag{7.24}$$

So, the results don't change a lot and the anomalous dimensions have reasonable moderate values.

	Without anomalous dimensions		With anomalous dimensions	
	Finite difference	Analytic eq.	Finite difference	Analytic eq.
g^*	0.96	0.57	0.60	0.61
μ_h^*	-0.35	-0.16	-0.57	-0.43
λ_3^*	-0.024	-0.16	0.097	0.021
EV	$(-2.1 \pm 2.4i, 5.8)$	$(-1.5 \pm 1.8i, 1.6)$	$(-0.52 \pm 4.1i, 12)$	$(-1.3 \pm 4.6i, 5.9)$

Table 7.1: The coordinates of the metastable fixed point in different approximations is displayed. The position of the fixed point is quite stable, which might hint towards the physical relevance of the fixed point.

7.3 Summary of the Pure Gravity Results

We shortly summarize the results from the previous sections. Unfortunately, we didn't manage to obtain a complete consistent picture from the different projection procedures. In the asymmetric momentum configuration, we didn't find a single physical UV fixed point and also the IR behaviour was convenient. But we have already argued that the asymmetric configuration is questionable due to its missing property of locality and the ambiguity in the projection procedure. In the symmetric momentum configuration, we found a consistent IR behaviour with classical scaling and a UV fixed point with two attractive directions in all approximations. These metastable fixed points are displayed in table 7.3 and it shows that they are all located very close to each other in theory space. This is a hint towards its possible physical relevance. Nevertheless, their remain doubts due to the strange behaviour of the anomalous dimension in case of the finite difference as explained below equation (7.18). Further, the system with the finite difference and no anomalous dimension showed a fully attractive fixed point, which was not visible in any other approximation. The question, if this is the true physical fixed point or just an artefact of the truncation can sadly just be resolved with the full system involving the fully momentum dependent anomalous dimension.

7.4 UV Fixed Points with Matter

The content of this section is part of an upcoming publication in preparation [81].

We analyse the system with matter just for our best available approximation. The best existing approximation involves the full momentum dependence of the anomalous dimension. This computation was unfortunately not finished in time for this work. In consequence, we stick to the approximation where the anomalous dimension is set to zero. The graviton three-point function is evaluated with a finite difference between $p = 0$ and $p = k$ and the remaining equations are evaluated at $p = 0$ and therefore they can be displayed analytically and are given in appendix B. Furthermore, we consider in this section only massless matter particles i.e. $\mu_\psi = 0 = \mu_\phi$. The inclusion of mass is discussed in section 7.5.

Since we are setting the anomalous dimensions to zero and ignore the mass parameter for the moment, the only relevant equations are the contributions to the flow of the graviton propagator, see (5.54) and (5.62), and to the flow of the graviton three-point function, see (5.55) and (5.63). These contributions are just numbers proportional to the number of flavours. While the contribution to the equations of μ_h and λ_3 can be derived analytically, the contribution to the running of g has to be numerically integrated. The contributions are:

$$\dot{g} = \beta_g\Big|_{\text{Gravity}} - 0.030g^2N_f - 0.013g^2N_s\,, \tag{7.25}$$

$$\dot{\lambda}_3 = \beta_{\lambda_3}\Big|_{\text{Gravity}} + \frac{47}{140\pi}gN_f - \frac{1}{60\pi}gN_s\,, \tag{7.26}$$

$$\dot{\mu}_h = \beta_{\mu_h}\Big|_{\text{Gravity}} - \frac{8}{9\pi}gN_f + \frac{1}{12\pi}gN_s\,. \tag{7.27}$$

The sign of the contribution for g doesn't change in comparison with the analytic equation and thus all arguments from section 6.4 are also valid here. We want to emphasize, that the fermionic contributions are approximately one order of magnitude larger than the scalar contributions. Now, we want to investigate the behaviour of the UV fixed point under an increasing number of matter flavours. We start with fermions.

In figure 7.5, the evolution of the fully attractive UV fixed point from section 7.2.2 is shown. As expected from the equations, the UV fixed point is pushed towards $(g^*, \mu_h^*) = (0, -1)$. The coupling λ_3 almost doesn't change at all and is just slightly pushed towards the value $\frac{1}{2}$. Interestingly, the canonical identification $-\frac{1}{2}\mu_h \equiv \lambda_2 = \lambda_3$, which was for example used in [21], is well fulfilled for large numbers of fermion flavours. This behaviour of the fixed point is a general one and for example also valid for the metastable fixed point from the same section. The fixed points persist for arbitrary numbers of fermion flavours. Thus, we can conclude that fermions indeed are stabilizing the existence of the UV fixed point and therefore confirming our guess from section 6.4. Further it can be concluded that fermions are weakening the gravitational force since g is driven to lower values. To complete our analysis of the influence of fermions, we need to look at the critical exponents to check if the fixed points keep their attractive behaviour.

In figure 7.6, the evolution of the critical exponents of both UV fixed points, the fully attractive and the metastable, are displayed. In case of the fully attractive fixed point, two eigenvalues are getting more and more negative. The critical exponents are usually close to their canonical value, which is just the mass dimension. Evidently, the quantum corrections at the UV fixed point are large and therefore it is not surprising that they change the critical exponent with a leading contribution. Nevertheless, such a dramatic change about many orders of magnitude is queer. For the metastable fixed point such a dramatic change of eigenvalues is not observed. Instead, all eigenvalues remain almost constant. Somehow, a stabilizing mechanism

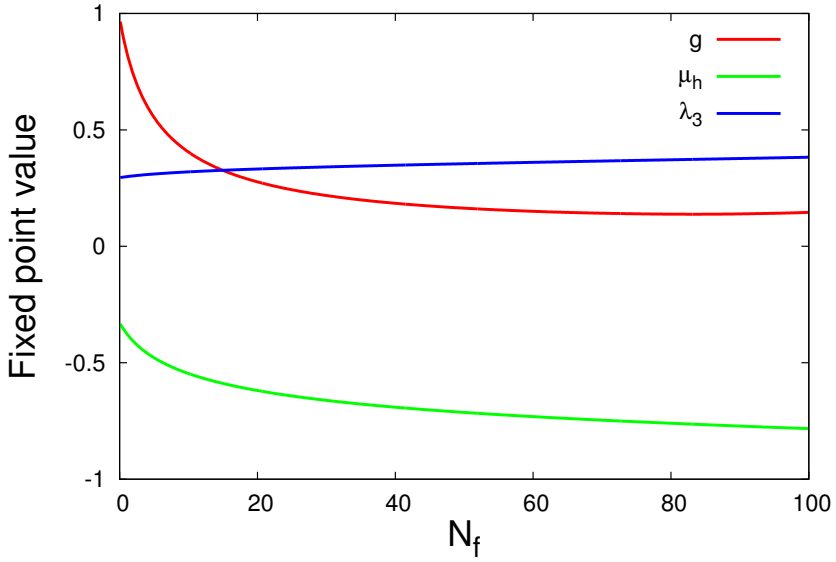

Figure 7.5: The evolution of the UV fixed point values under an increasing amount of fermion flavours are plotted. Fermions have a stabilizing effect on the UV fixed point and move it towards $(g^*, \mu_h^*) = (0, -1)$. Interestingly, the fixed point value for λ_3 is pushed towards $\frac{1}{2}$ and hence the relation $-\frac{1}{2}\mu_h \equiv \lambda_2 = \lambda_3$ is almost exactly fulfilled for a large number of fermions.

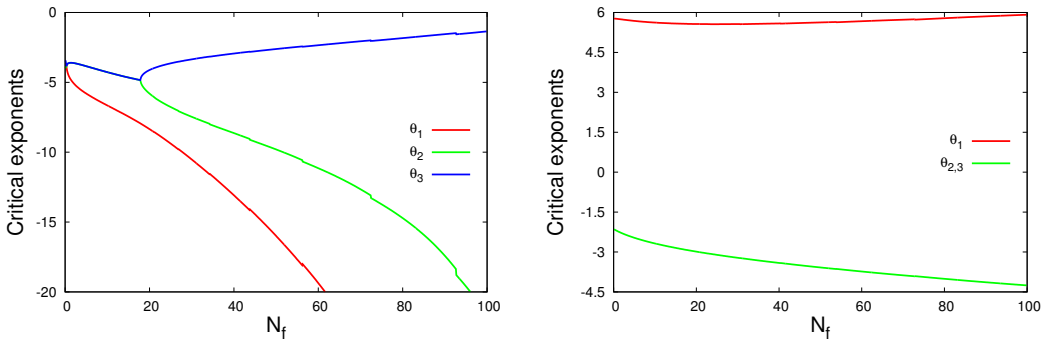

Figure 7.6: The evolution of the real parts of the critical exponents at the UV fixed points under an increasing amount of fermion flavours are plotted. On the left side, the fully attractive UV fixed point is displayed and it remains fully attractive for all plotted number of fermions. From $N_f \approx 17.8$ all exponents are real, before a complex conjugate pair was formed by two eigenvalues. Two eigenvalues get more and more negative, which can be explained by the evolution of the fixed point. On the right side, the metastable fixed point is displayed. Here, the eigenvalues almost don't change over the whole range and the fixed point keeps all its properties.

must take place.

Next, we discuss the inclusion of scalar degrees of freedom. Again, we are interested in the evolution of UV fixed points under an increasing number of scalar flavours. This behaviour is displayed in figure 7.7. Interestingly, the UV fixed point is moved to larger values of g^*. We already discuss in section 6.4 that there are two competing contributions, the scalar contribution in the $\dot{g}$ equation is stabilizing and the one in the $\dot{\mu}_h$ equation is destabilizing. Now, we know that the latter contribution is dominating and we see that the most important sign is actually not the one in the $\dot{g}$ equation but rather in the $\dot{\mu}_h$ equation. Indeed we also observed the this dominance the other way round: A matter particle with a positive sign in the $\dot{g}$ equation and a negative sign in the $\dot{\mu}_h$ equation drives the fixed point towards the physical IR fixed point $(g^*, \mu_h^*) = (0, -1)$. The influence of scalars on the fixed point value of λ_3 is negligible. Again, all these statements hold for all UV fixed points i.e. also for the metastable fixed point.

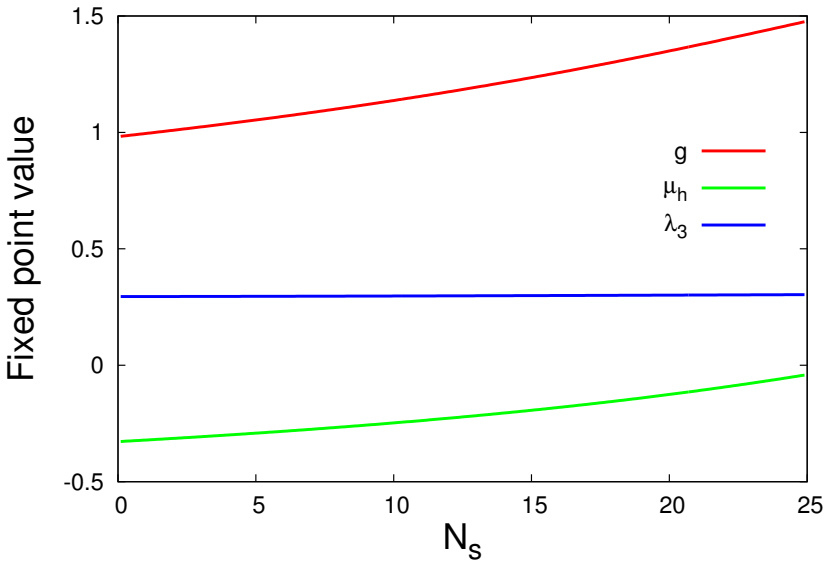

Figure 7.7: The evolution of the UV fixed point values under an increasing amount of scalar flavours are plotted. Scalars have a destabilizing effect on the UV fixed point and move it towards larger values of g. This shows, that the sign in the $\dot{\mu}_h$ equation is more important that the sign in the $\dot{g}$ equation.

In figure 7.8, we show the evolution of the critical exponents of both UV fixed points. In both cases, the eigenvalues remain quite stable. Nevertheless, in case of the fully attractive UV fixed point, one eigenvalue is monotonically growing and might at some point cross the zero line. In this case, the fixed point either loses an attractive direction or it might even complete disappear. Just complex conjugate pairs can easily cross the zero line, others evidently encounter a singularity.

At last, we discuss the inclusion of fermionic and scalar degrees of freedom at

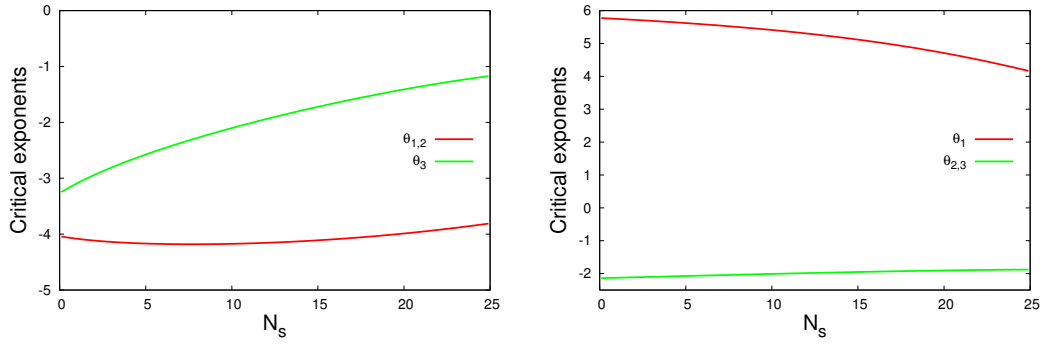

Figure 7.8: The evolution of the real parts of the critical exponents at the UV fixed points under an increasing amount of scalar flavours are plotted. The left plot shows the fully attractive fixed point while the right plot shows the metastable fixed point. In both cases the values of the critical exponents remain quite stable. Two eigenvalues in both cases always form a complex conjugate pair. In the left plot, one eigenvalue is getting monotonically larger and might eventually cross zero, i.e. the fixed point might lose one attractive direction.

the same time. However, this is not particularly exciting since the fermionic contribution is one order of magnitude larger that the scalar contribution. Further, if we are interested in investigating physical matter models like the standard model then, additionally to this a priori dominance of fermions, the number of fermions is even larger than the number of scalars. Also in supersymmetric matter models the dominance of the fermionic contribution is enough to ensure no major difference to the pure fermionic system. Even in GUT theories with five times as many scalars than fermions we observe the same behaviour of the UV fixed point as in the pure fermionic case.

To summarize the matter results, we found that fermions are stabilizing all UV fixed points, i.e. pushing them towards $(g^*, \mu_h^*) = (0, -1)$, while scalars destabilize the UV fixed point. This behaviour is independent of the specific truncation of the pure gravity system, but it might change slightly after the inclusion of the anomalous dimensions. Further, fermionic degrees of freedom completely dominate over scalar ones.

7.5 UV Fixed Points with non-vanishing Mass

In the last section, we have only considered massless particles although we have derived all equations for arbitrary particle masses. We turn now to the question if an interacting UV fixed point with non-vanishing particle masses is possible. It is simply possible to evaluate the stability of the fixed points from the last sections in the mass direction. However, we first want do a more general analysis and investigate,

which area in theory space leads to instabilities in the mass direction. So we look at the equations for the flow of the masses, which are defined through equations (5.59) and (5.66) and are given with fully contracted and integrated diagrams in (B.6) and (B.7).

We are ultimately interested if the UV fixed point with vanishing particle masses, i.e. $\mu_\psi^* = 0 = \mu_\phi^*$ is stable or unstable in direction of the particle mass. If the fixed point is unstable in the mass direction it is necessary to investigate if there is a UV fixed point with a non-vanishing particle mass. This fixed point is then the physical one because even if we start with a massless particle in the IR the quantum fluctuations will drive the flow eventually towards the UV fixed point with a non-vanishing particle mass. From now on this fixed point will be called a massive fixed point while a UV fixed point with vanishing matter masses will be called a massless fixed point. The condition for the stability in the mass direction is

$$\frac{\partial}{\partial \mu_i} \dot{\mu}_i \bigg|_{\mathrm{FP}} < 0 \,, \tag{7.28}$$

where the index $i \in \{\psi, \phi\}$ is labelling scalars and fermions. Unfortunately, the flows of the masses are depending on a lot of parameters. A priori, we have the functions

$$\dot{\mu}_i \equiv \dot{\mu}_i(g, \mu_h, \mu_i, \eta_h, \eta_i) \,, \tag{7.29}$$

but the anomalous dimensions are in turn functions of g, μ_h, λ_3, N_s, N_f, μ_ϕ and μ_ψ. The masses of the particles are set to zero since we are first investigating the stability of the massless fixed point. Nevertheless, we are left with an five dimensional parameter space, which is too much to display. As a first approximation, we set the anomalous dimensions to zero, which can be justified since they are supposed to be small as explained in section 4.3. Otherwise the truncation is considered untrustworthy. For this approximation, the two equations from (7.28) can easily be solved for the separatrices that divide the two dimensional theory space into a part with a stable massless fixed point and a part with an unstable massless fixed point. The separatrices are given by

$$g^* = -\frac{40\pi(\mu_h^* + 1)^2}{19\mu_h^* - 58} \tag{7.30}$$

for the fermions and by

$$g^* = -\frac{2\pi(\mu_h^* + 1)^2}{3(2\mu_h^* + 1)} \tag{7.31}$$

for the scalars. These separatrices are shown in figure 7.9 and it can be concluded that it is far more likely to have a UV fixed point with massive fermions that with massive scalars.

Now, we want to include the evolution of the UV fixed points from section 7.4. This is shown in figure 7.10. Already the fixed point with no matter is located in the area

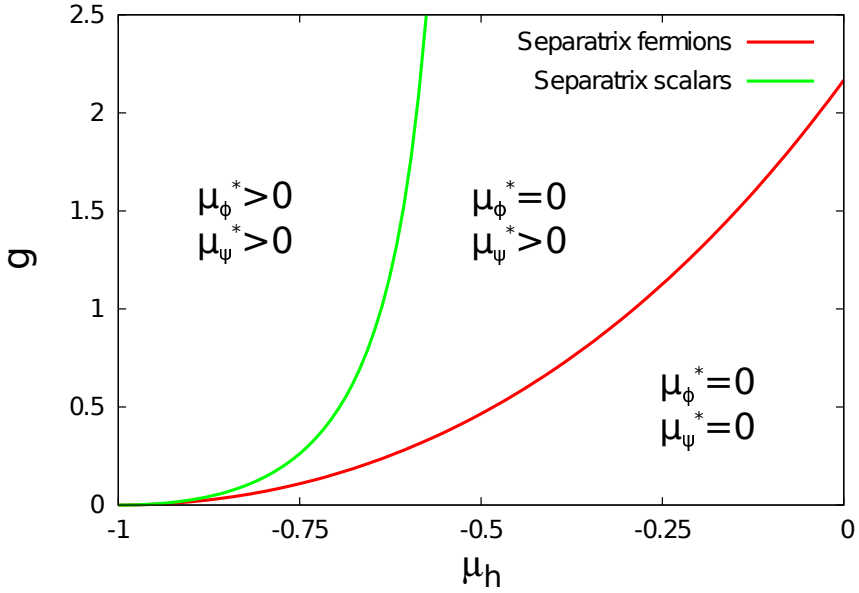

Figure 7.9: The separatrices, which distinguish between areas with $\mu_i^* > 0$ and $\mu_i^* = 0$ for fermions (red curve) and for scalars (green curve), are displayed. The defining equations are (7.30) and (7.31). A UV fixed point with massive fermions is more likely than with massive scalars.

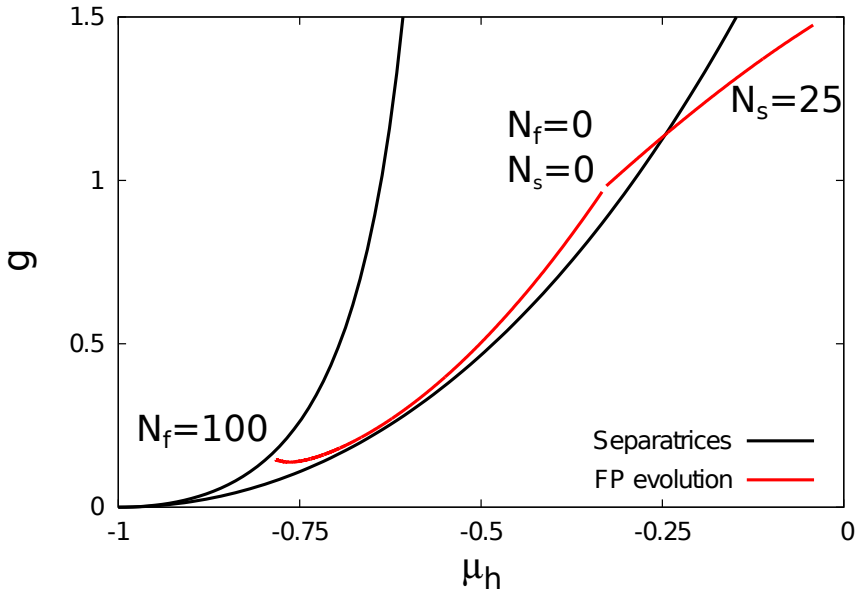

Figure 7.10: The evolution of the fully attractive UV fixed point under increasing matter flavours is plotted together with the mass separatrices. Almost all fixed points are located in the area with a massive fermionic fixed point.

where the mass direction of the fermion is unstable. This does not change with the inclusion of fermion flavours and all fixed points have a massive counterpart. When scalar degrees of freedom are included this pictures changes and the mass direction of the fermion becomes stable. This picture is self-consistent although we have neglected the anomalous dimensions for the separatrices. The simple reason for self-consistency is that we also neglected the anomalous dimensions for the calculation of the fixed points. Nevertheless, the inclusion of anomalous dimensions might change the outcome since the anomalous dimensions influence the separatrices and the fixed points in very different ways.

7.6 Unimodular Quantum Gravity

In this section, we display our results for unimodular quantum gravity, which was introduced in section 3.1. Unimodular quantum gravity is completely different than the Einstein-Hilbert quantum gravity. In consequence, we have to start again from zero, derive new vertices, contract all diagrams and derive new flow equations. To do this in detail could be the work of a whole new Master's thesis and thus we just present here a very rough approximation of the system.

First of all, it is important to realize that due to the unimodular setting, i.e. $\sqrt{g}$ =const., the cosmological constant decouples in the Einstein-Hilbert action and there is no momentum independent part of the n-th graviton vertex. So there is no flow of e.g. the graviton mass parameter. This is not fully true since it is dynamically generated after one RG step but to simplify our task we force its value to be zero for this computation. It could be argued that this procedure restores diffeomorphism invariance in this setting. In consequence, we only have to derive two equations, namely the anomalous dimension and the running of Newton's coupling. This is done in the usual way with the vertex construction in equation (5.8) and via the diagrams of the two- and three-point functions in equations (5.5) and (5.6). We also employ the same projection procedure for the three-point function, i.e. equation (5.27) for the tensorial projection and further a finite difference between $p = 0$ and $p = k$ within the symmetric momentum configuration. In order to simplify our task further, we completely neglect ghost contributions.

An important difference is that we use an exponential split of the metric in order to go along the same lines as [67]. That means

$$g_{\mu\nu} = \bar{g}_{\mu\rho}[\mathrm{e}^h]^\rho_\nu = \delta_{\mu\nu} + h_{\mu\nu} + \frac{1}{2}h_{\mu\lambda}h^\lambda_\nu + \dots \tag{7.32}$$

First of all, we checked the locality of the vertices. Neither the graviton propagator nor the graviton three-point function turn out to be local in momentum space. Nevertheless, we went on and computed the anomalous dimension and the flow of Newton's coupling. The anomalous dimension was set to be momentum independent. Both quantities were computed with a finite difference between $p = 0$ and $p = k$. The nice property of this setting is that the anomalous dimension is just a

function of g, while the running of g is also just a function of g and η_h. The very simple resulting equations are then

$$\eta_h = -\frac{0.55g}{1-0.084g}\,, \tag{7.33}$$

$$\dot{g} = g\frac{0.23g^2+27g-24}{g-12}\,, \tag{7.34}$$

where we have already inserted η_h into the equation of $\dot{g}$. The running of g is displayed in figure 7.11 and evidently there is the standard IR Gaussian fixed point $g^* = 0$ and an attractive UV fixed point. The fixed point coordinate and the anomalous dimension at the fixed point are

$$(g^*, \eta_h^*) = (0.88, -0.52)\,. \tag{7.35}$$

This fixed point value is interestingly exactly identical to the one found in [67]. The anomalous dimension has a nice, small value. The critical exponent at the UV fixed point is

$$\left.\frac{\partial\dot{g}}{\partial g}\right|_{g=0.88} = -2.2\,. \tag{7.36}$$

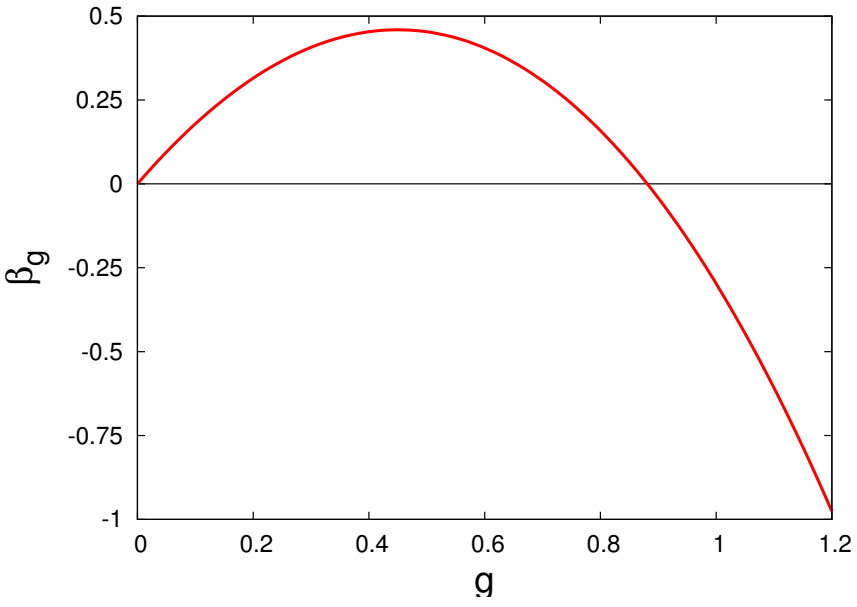

Figure 7.11: The beta function of g for unimodular quantum gravity is plotted. At $g = 0$, the Gaussian fixed point is visible, and at $g \approx 0.88$, an attractive UV fixed point is located.

In summary, already in this simple approximation we obtain a very reasonable fixed point. This doesn't necessarily mean anything since it fist of all has to be checked

in a better truncation. In contrary, the non-locality of the vertices is actually a bad sign the unimodular quantum gravity. Still, it would be interesting to see how other results, like the inclusion of matter, translates into this setting. It should also be mentioned, that in this work there was no time to investigate, which influence destroyed the locality of the flow e.g. it could lay in the basic definition of the unimodular gravity or in the definition of the linear split in equation (7.32) or even something else.

8 Summary and Outlook

We applied a self-consistent vertex expansion as a systematic approximation scheme to the Wetterich equation of a Einstein-Hilbert like theory of quantum gravity. The vertex construction and the projection scheme for the graviton an the ghost propagator were taken from [21]. For the graviton three-point function a procedure of tensorial and momentum projection was introduced. With this a running of Newton's coupling was derived. It was shown that the graviton three-point function is local in momentum space for any momentum projection, which is a necessary condition for the renormalization group flow. Together with the locality of the graviton propagator, which was proven in [22], this can lead towards a well-defined local theory of quantum gravity. All higher vertices should also fulfil the demand of locality.

Analytic equations were derived for all running couplings, but it was shown that they are not adequate in all cases. Some couplings, like the Newton's coupling and the anomalous dimension, require the full momentum information of the flow and therefore the preferred method of calculation involves the full momentum dependence. Furthermore it was shown, that the next best approximation involves a finite difference instead of a derivative. These statements were checked explicitly for the anomalous dimension of the graviton. In case of the anomalous dimension of the matter particles, we have to leave this check for future projects.

The search for a UV fixed point was carried out in different momentum projections. It was shown, that there are preferable momentum configurations for the three-point function. These are the ones, that do not involve zero momentum at any external leg, i.e. the asymmetric momentum configuration should be discarded. This statement is closely related to the statement of locality, where the cancellation for large momenta just takes place if all external momenta become large. In all local momentum projections a UV fixed point with two attractive and one repulsive direction was found, which might hint towards its physical relevance. Unfortunately, we couldn't settle the debate if this is the only physical fixed point, because in one of our best approximations also a fully attractive UV fixed point was found. The results of the computation with fully momentum dependent anomalous dimensions should clarify the picture.

As a second topic, we included minimally coupled scalar and fermionic matter to our best approximation of the pure quantum gravity system. For the description of the fermions we used the spin-base invariance formalism instead of the usual vielbein formalism. The evolution of the UV fixed point under an increasing number of matter flavours was described. It was shown that fermions are stabilizing the existence of the UV fixed point and are weakening the gravitational force while scalars have a destabilizing and strengthening effect. The effect on the critical exponents was investigated and no inclusion induced a change of sign, neither in the scalar nor in

the fermionic case. Thus, all attractive directions of any UV fixed point remained attractive and equivalently for repulsive directions. In consequence, there is no upper bound on the number of fermion flavours, i.e. all numbers of fermions are compatible with the asymptotic safety scenario. However, there is an upper bound on the number of scalars, but we didn't determine this number since the result of the best approximation, which involves the fully momentum dependent anomalous dimension, is still missing.

At last, unimodular quantum gravity was investigated, which is a completely different theory than quantum Einstein gravity. As a first difference, we found that neither the graviton propagator nor the graviton three-point function are respecting the demand of locality. Despite this, we looked for an attractive UV fixed point in a very basic approximation. We indeed found one with all desired properties. However, these results have to be checked in a more elaborate truncation.

There are many possible improvements upon the current work. First of all, the solutions of the best approximation are not yet computed. It will give new insights, which quantities can be approximated for future computations. Then, we truncated our system by identifying the couplings from the four- and five-point functions with the ones from the three-point function. These identification can be checked and the level of truncation increased by an inclusion of the graviton four-point function. The technical possibilities to compute at least one certain tensorial and momentum projection are available.

We have learnt in this thesis, that the topic of projection is very important. Thus, the dependence of the three-point function upon tensorial projection and on the momentum has to be checked in great detail for consistency. There are two ultimate goals: First, the solution of the equations with a fully momentum dependent Newton's coupling in order to drop the momentum projection. Second, a complete set of tensorial projections for the three point function that exhibit independent running. This is however very extensive and cannot be done in the near future.

In the matter sector, our contributions to the gravitational flows have exactly the opposite signs as in other works. The origin of sign change should be investigated and the physical sign determined. In section 2.3, we cited a paper, which showed that different signs can occur between type I and type II regulators. We cannot differ between those regulators, because of we are using a flat background, but the issue should nevertheless be investigated, maybe with a non-flat background. As another future task, it should be tested if the matter contributions to the gravitational flows respect the demand of locality on the one hand for the graviton propagator and on the other hand for the graviton three-point function. Furthermore, gauge bosons can be introduced to have a complete set of Standard Model matter particles. Together with the possible introduction of matter-matter and matter-self interactions, this can lead in the far future to a theory of quantum gravity that is coupled to the complete Standard Model.

In section 6.4, we stated, that we picked the one singular gauge, where the anomalous dimension of the massless scalar is zero. We further stated, that the gauge choice can be understood as a rotation between the different anomalous dimensions

and physical observables are unaffected by the gauge choice. This, however, was rather a rough observation than a well proofed argument. Thus, it would be very interesting to study the influence on the gravitational gauge choice on the whole matter sector. Similar studies have already been done before only for the gravitational sector itself. Also, a study of the regulator dependence is a reasonable possibility to strengthen the statements of this work.

In unimodular quantum gravity, the first steps should be to improve the truncation of the pure gravity system e.g. ghost should be included and the gravitationally generated momentum independent part of each vertex should be treated carefully. It should be investigated if the demand of locality can somehow be recovered, for example by including the ghost contributions. Afterwards, the inclusion of matter particles can be studied. Especially in the scalar sector, the couplings are getting drastically simplified in the unimodular setting compared to the usual Einstein-Hilbert gravity. Thus, it would be interesting to see if the matter particles have similar effects.

Part III

Appendix

A Technicalities for Fermion Loops at zero Momentum

In equation 6.15 we have derived the contributions to the second derivative of the scalar propagator, which are forgotten by *mathematica* because it contains products of distributions. In this section we want to do the same but with the fermion propagator. The task gets more difficult in this case since the propagator is a matrix in spinor space. Our procedure is the following. First we split the propagator into two Heaviside step functions, similar to the scalar case and then we take the derivatives before the overall trace is performed. The result is a new propagator, which is hit by the derivative twice and which gives the new contributions when contracted with the remaining diagram. Remember that this contribution only appears with the Litim-type shape-function, here in case for fermions:

$$r(\vec{p}) = \left(\frac{1}{p} - 1\right)\theta(1-p^2)\,. \tag{A.1}$$

As shorthand notation we introduce $\vec{s} = \vec{p}+\vec{q}$ as well as $s = |\vec{p}+\vec{q}| = \sqrt{p^2+2pqx+q^2}$ and $\not{s} = \gamma_\mu s^\mu$. First, we split the fermion propagator

$$\begin{aligned} G_{\text{ferm}}(\vec{s}) &= \frac{1}{-i\not{s}\left(1+\left(\frac{1}{s}-1\right)\Theta\left(1-s^2\right)\right)+m\mathbb{1}} \\ &= \frac{\theta(1-s^2)}{-i\frac{\not{s}}{s}+m\mathbb{1}} + \frac{\theta(s^2-1)}{-i\not{s}+m\mathbb{1}} \\ &= \frac{\theta(1-s^2)}{1+m^2}\left(i\frac{\not{s}}{s}+m\mathbb{1}\right) + \frac{\theta(s^2-1)}{s^2+m^2}(i\not{s}+m\mathbb{1})\,. \end{aligned} \tag{A.2}$$

This we write as

$$\begin{aligned} G_{\text{ferm}}(\vec{s}) &= f_1(s)\theta(1-s^2) + f_2(s)\underbrace{\theta(s^2-1)}_{1-\theta(1-s^2)} \\ &= (f_1(s)-f_2(s))\theta(1-s^2) - f_2(s)\,, \end{aligned} \tag{A.3}$$

with

$$f_1(s) = \frac{\left(i\frac{\not{s}}{s}+m\mathbb{1}\right)}{1+m^2} \tag{A.4}$$

and

$$f_2(s) = \frac{i\not{s} + m\mathbb{1}}{s^2 + m^2}\,, \tag{A.5}$$

where it is important to notice that

$$f_1(s=1) = f_2(s=1)\,. \tag{A.6}$$

Since we are only interested in the contribution that are forgotten by *mathematica*, we can forget about the second term in A.3. Now, we take the first derivative of the remaining part with respect to p. As usual the Dirac delta distributions are vanishing and we arrive at

$$\begin{aligned}\partial_p G_{\text{ferm}}(s) &\supset \underbrace{-(f_1(s) - f_2(s))\delta(1-s^2)2(p+qx)}_{=0} + \frac{p+qx}{s}(f_1'(s) - f_2'(s))\theta(1-s^2) \\ &= \frac{p+qx}{s}(f_1'(s) - f_2'(s))\theta(1-s^2)\,. \end{aligned}\tag{A.7}$$

We take another derivative of equation (A.7) and only keep the terms proportional to a Dirac delta distribution since all other terms are covered by *mathematica*. The result is

$$\partial_p^2 G_{\text{ferm}}(s) \supset -2\frac{(p+qx)^2}{s}(f_1'(s) - f_2'(s))\delta(1-s^2)\,. \tag{A.8}$$

There is an overall Heaviside step function $\Theta(1-q^2)$ from the regulator insertion. The product of those can be evaluated with the Salmhofer formula from equation (6.14) in the limit $p \to 0$. This gives the sought after contribution.

$$\begin{aligned}\theta(1-q^2)\partial_p^2 G_{\text{ferm}}(s)\Big|_{p=0} &\supset -qx^2(f_1'(q) - f_2'(q))\delta(1-q^2) \\ &= -\frac{1}{2}x^2(f_1'(1) - f_2'(1))\delta(1-q)\end{aligned}\tag{A.9}$$

Only the derivatives of the functions f_1 and f_2 are missing. The derivatives have to be evaluated at $p = 0$ and $q = 1$, which corresponds to $s = 1$.

$$f_1'(q=1) = \frac{i\partial_q\left(\frac{\not{q}}{q}\right)}{1+m^2}\bigg|_{q=1} = \frac{i(\frac{\not{q}}{q} - \not{q})}{1+m^2}\bigg|_{q=1} \tag{A.10}$$

$$f_2'(q=1) = \frac{i\partial_q\not{q}(q^2+m^2) - (i\not{q}+m\mathbb{1})2q}{(q^2+m^2)^2}\bigg|_{q=1} = \frac{i\frac{\not{q}}{q}}{1+m^2} - \frac{2(i\not{q}+m\mathbb{1})}{(1+m^2)^2}\bigg|_{q=1} \tag{A.11}$$

Finally, we arrive at

$$\begin{aligned}\theta(1-q^2)\partial_p^2 G_{\text{ferm}}(s)\Big|_{p=0} &\supset -\frac{1}{2}x^2\left(\frac{i(-\not{q})}{1+m^2}+\frac{2(i\not{q}+m\mathbb{1})}{(1+m^2)^2}\right)\delta(1-q)\\ &= -\frac{x^2}{2(1+m^2)^2}\left((1-m^2)i\not{q}+2m\mathbb{1}\right)\delta(1-q)\,. \qquad \text{(A.12)}\end{aligned}$$

It is important to note that the derivatives ∂_p^2 differs to the derivative ∂_{p^2} if evaluated at $p=0$ about a factor two

$$\frac{1}{2}\partial_p^2\Big|_{p=0} = \partial_{p^2}\Big|_{p=0}\,. \qquad \text{(A.13)}$$

B Analytic Equations

We present the analytic equations of the system. The technicalities are described in section 6.4 and chapter B. For the flow of Newton's coupling we present two possibilities, one from the asymmetric momentum configuration and one from the symmetric momentum configuration. All other equations are unique. Note that the identification

$$g := g_3 \equiv g_4 \equiv g_5 \tag{B.1}$$

has already been performed.

B.1 Flow of the Couplings

Asymmetric momentum configuration:

$$\begin{aligned}
\dot{g} =&(2+3\eta_h)g + \frac{g^2}{\pi}\Bigg(- \frac{5(6-\eta_h)}{42(\mu_h+1)^2} \\
&+ \frac{2\lambda_4(62(6-\eta_h) - 195(4-\eta_h)\lambda_3) + 62(6-\eta_h)\lambda_3 - 15(8-\eta_h)}{63(\mu_h+1)^3} \\
&+ \frac{39(8-\eta_h) - 232(6-\eta_h)\lambda_3}{252(\mu_h+1)^3} + \frac{17 + 272\lambda_4 - 4\lambda_3(161\lambda_4+8)}{42(\mu_h+1)^4} \\
&+ \frac{2772(4-\eta_h)\lambda_3^3 + 1000(6-\eta_h)\lambda_3^2 - 705(8-\eta_h)\lambda_3 + 90(10-\eta_h)}{210(\mu_h+1)^4} \\
&- \frac{523 - 2\lambda_3(4\lambda_3(374\lambda_3 - 615) + 1415)}{105(\mu_h+1)^5} + \frac{3(190+13\eta_c)}{140}\Bigg) \\
&+ \frac{g^2 N_f}{14\pi}\Bigg(- \frac{5(5-\eta_\psi)\,(1-\mu_\psi)}{6\,(1+\mu_\psi)^3} - \frac{5\left(1+6\mu_\psi+\mu_\psi^2\right)}{3\,(1+\mu_\psi)^4} \\
&+ \frac{147(6-\eta_\psi) + (543-128\eta_\psi)\mu_\psi - 75(5-\eta_\psi)\mu_\psi^2}{600\,(1+\mu_\psi)^4} \\
&+ \frac{31 + 148\mu_\psi + 31\mu_\psi^2 + 10\mu_\psi^3}{40\,(1+\mu_\psi)^5}\Bigg) \\
&+ \frac{g^2 N_s}{28\pi}\left(\frac{17+5\mu_\phi}{10\,(1+\mu_\phi)^5} - \frac{13}{3\,(1+\mu_\phi)^4}\right)
\end{aligned} \tag{B.2}$$

Symmetric momentum configuration:

$$\begin{aligned}\dot{g} =&(2+3\eta_h)g+\frac{g^2}{19\pi}\Bigg(-\frac{47(6-\eta_h)}{6(1+\mu_h)^2}+\frac{16(1-3\lambda_3)\lambda_4}{(1+\mu_h)^4}\\&+\frac{45(8-\eta_h)+472(6-\eta_h)\lambda_4-120\lambda_3(2(6-\eta_h)+3(4-\eta_h)\lambda_4)}{18(1+\mu_h)^3}\\&+\frac{147(10-\eta_h)-1860(8-\eta_h)\lambda_3+3380(6-\eta_h)\lambda_3^2+25920(4-\eta_h)\lambda_3^3}{90(1+\mu_h)^4}\\&+2\frac{-299+1780\lambda_3-3640\lambda_3^2+2336\lambda_3^3}{15(1+\mu_h)^5}-\frac{50-53\eta_c}{10}\Bigg)\\&-\frac{g^2N_f}{38\pi}\Bigg(\frac{3(5-\eta_\psi)\,(1-\mu_\psi)}{4\,(1+\mu_\psi)^3}+\frac{3\left(1+6\mu_\psi+\mu_\psi^2\right)}{2\,(1+\mu_\psi)^4}\\&+\frac{(6-\eta_\psi)\,(521+529\mu_\psi)}{450\,(1+\mu_\psi)^4}-\frac{1-32\mu_\psi-9\mu_\psi^2}{5\,(1+\mu_\psi)^5}\Bigg)\\&-\frac{g^2N_s}{95\pi}\left(\frac{50+\eta_\phi}{12\,(1+\mu_\phi)^4}+\frac{3}{(1+\mu_\phi)^5}\right)\end{aligned}\tag{B.3}$$

Universal equation for λ_3 for all momentum configurations:

$$\begin{aligned}\dot{\lambda}_3 =&-\left(1-\frac{3}{2}\eta_h+\frac{\dot{g}}{2g}\right)\lambda_3+\frac{g}{2\pi}\Bigg(\frac{12-\eta_c}{5}+\frac{8-\eta_h-4(6-\eta_h)\lambda_5}{4(1+\mu_h)^2}\\&+\frac{3(8-\eta_h)\lambda_4-16(6-\eta_h)\lambda_3\lambda_4}{3(1+\mu_h)^3}\\&-\frac{11(12-\eta_h)-72(10-\eta_h)\lambda_3+120(8-\eta_h)\lambda_3^2-80(6-\eta_h)\lambda_3^3}{120(1+\mu_h)^4}\Bigg)\\&+\frac{gN_f}{8\pi}\Bigg(\frac{17(6-\eta_\psi)+(378-79\eta_\psi)\mu_\psi}{30\,(1+\mu_\psi)^2}-\frac{(7-\eta_\psi)\,(1+5\mu_\psi)}{7\,(1+\mu_\psi)^3}\\&+\frac{(8-\eta_\psi)\left(1+4\mu_\psi-\mu_\psi^2\right)}{28\,(1+\mu_\psi)^4}\Bigg)\\&+\frac{gN_s}{16\pi}\left(\frac{8-\eta_\phi-4(6-\eta_\phi)\mu_\phi}{6\,(1+\mu_\phi)^2}-\frac{10-\eta_\phi}{5\,(1+\mu_\phi)^3}+\frac{12-\eta_\phi}{30\,(1+\mu_\phi)^4}\right)\end{aligned}\tag{B.4}$$

B.2 Flow of the Masses

$$\begin{aligned}\dot{\mu}_h =&(\eta_h-2)\mu_h+\frac{g}{\pi}\left(\frac{8(6-\eta_h)\lambda_4-3(8-\eta_h)}{12(1+\mu_h)^2}\right.\\&\left.+\frac{21(10-\eta_h)-120(8-\eta_h)\lambda_3+320(6-\eta_h)\lambda_3^2}{180(1+\mu_h)^3}-\frac{10-\eta_c}{5}\right)\\&+\frac{gN_f}{3\pi}\left(-\frac{5(6-\eta_\psi)+(90-19\eta_\psi)\mu_\psi}{10\left(1+\mu_\psi\right)^2}+\frac{(7-\eta_\psi)\left(1+5\mu_\psi\right)}{21\left(1+\mu_\psi\right)^3}\right)\\&+\frac{gN_s}{12\pi}\left(\frac{(6-\eta_\phi)\mu_\phi}{\left(1+\mu_\phi\right)^2}+\frac{10-\eta_\phi}{10\left(1+\mu_\phi\right)^3}\right)\end{aligned}\tag{B.5}$$

$$\begin{aligned}\dot{\mu}_\psi =&(2\eta_\psi-2)\mu_\psi+\frac{g\mu_\psi}{\pi}\left(\frac{6-\eta_h}{(1+\mu_h)^2}\right.\\&\left.-\frac{2408-349\eta_h+1120(6-\eta_h)\mu_\psi}{1120\left(1+\mu_\psi\right)(1+\mu_h)^2}-\frac{133-23\eta_\psi+28(24-5\eta_\psi)\mu_\psi}{140\left(1+\mu_\psi\right)^2(1+\mu_h)}\right)\end{aligned}\tag{B.6}$$

$$\begin{aligned}\dot{\mu}_\phi =&(\eta_\phi-2)\mu_\phi\\&+\frac{g\mu_\phi}{2\pi}\left(\frac{6-\eta_h}{(1+\mu_h)^2}-\frac{(6-\eta_h)\mu_\phi}{(1+\mu_h)^2\left(1+\mu_\phi\right)}-\frac{(6-\eta_\phi)\mu_\phi}{(1+\mu_h)\left(1+\mu_\phi\right)^2}\right)\end{aligned}\tag{B.7}$$

B.3 Anomalous Dimensions

$$\begin{aligned}\eta_h =&\frac{g}{4\pi}\left(\frac{6-\eta_h}{(1+\mu_h)^2}-\frac{6(8-\eta_h)+8(6-\eta_h)\lambda_3-36(4-\eta_h)\lambda_3^2}{9(1+\mu_h)^3}\right.\\&\left.+\frac{17+8\lambda_3(9\lambda_3-8)}{3(1+\mu_h)^4}-\eta_c\right)\\&+\frac{gN_f}{24\pi}\left(\frac{(5-\eta_\psi)\left(1-\mu_\psi\right)}{2\left(1+\mu_\psi\right)^3}+\frac{1+6\mu_\psi+\mu_\psi^2}{\left(1+\mu_\psi\right)^4}\right)\\&-\frac{32gN_s}{315\pi\left(1+\mu_\phi\right)^4}\end{aligned}\tag{B.8}$$

$$\eta_c =-\frac{g}{9\pi}\left(\frac{8-\eta_h}{(1+\mu_h)^2}+\frac{8-\eta_c}{1+\mu_h}\right)\tag{B.9}$$

$$\begin{aligned}\eta_\psi =&\frac{g}{4\pi}\left(\frac{9(7-\eta_h)+12(10-\eta_h)\mu_\psi}{20\left(1+\mu_\psi\right)(1+\mu_h)^2}-\frac{9(6-\eta_h)}{8(1+\mu_h)^2}\right.\\&\left.+\frac{6-\eta_\psi+(54-11\eta_\psi)\mu_\psi}{5\left(1+\mu_\psi\right)^2(1+\mu_h)}\right)\end{aligned}\tag{B.10}$$

$$\eta_\phi = \frac{g\mu_\phi}{2\pi}\left(\frac{6-\eta_h}{(1+\mu_h)^2(1+\mu_\phi)} + \frac{6-\eta_\phi}{(1+\mu_h)(1+\mu_\phi)^2} - \frac{6\mu_\phi}{(1+\mu_h)^2(1+\mu_\phi)^2}\right) \tag{B.11}$$

C Formula for nth-Derivative of the Spin Connection

In this chapter we will compute the n-th functional derivative of the Dirac matrices and of the spin connection with respect to the metric. As usual we work with the linear split of the metric on flat Euclidean background

$$g_{\mu\nu} = \delta_{\mu\nu} + h_{\mu\nu}\,, \tag{C.1}$$

i.e. the only non-vanishing variation of the metric is $\delta g_{\mu\nu} = h_{\mu\nu}$. We start now with derivation of the variation of the Dirac matrices. We make an ansatz for the n-th variation

$$\delta^n \gamma_\mu = b^n_{\mu\nu} \bar{\gamma}^\nu\,, \tag{C.2}$$

where $\bar{\gamma}$ are the background Dirac matrices and $b_{\mu\nu}$ is some symmetric tensor. The variation depends on the choice of the spin-base and therefore it is likely that the ansatz is justified for some gauge. Now we can take variations of the Clifford algebra (5.50). As an easy example to visualize the process the first take one variation and evaluate it on the background

$$\begin{aligned}
\delta\{\gamma_\mu, \gamma_\nu\} &= \{\delta\gamma_\mu, \bar{\gamma}_\nu\} + \{\bar{\gamma}_\mu, \delta\gamma_\nu\} \\
&= b^1_{\rho\mu}\{\bar{\gamma}^\rho, \bar{\gamma}_\nu\} + b^1_{\rho\nu}\{\bar{\gamma}_\mu, \bar{\gamma}^\rho\} \\
&= 4b^1_{\mu\nu}\mathbb{1} \overset{!}{=} 2\delta g_{\mu\nu}\mathbb{1}\,,
\end{aligned} \tag{C.3}$$

where we have used the flat Clifford algebra (5.49) in the next to last step and the exclamation mark indicates where we switch to the right hand side. In consequence we can conclude

$$b^1_{\mu\nu} = \frac{1}{2}\delta g_{\mu\nu} \equiv \frac{1}{2} h_{\mu\nu}\,. \tag{C.4}$$

We take now n variations of the Clifford algebra. The right hand side evidently vanishes for $n \geq 2$. For the left hand side we find

$$\begin{aligned}
\delta^n\{\gamma_\mu, \gamma_\nu\} &= \sum_{k=0}^{n} \frac{n!}{k!(n-k)!}\{\delta^{n-k}\gamma_\mu, \delta^k\gamma_\nu\} = \sum_{k=0}^{n} \frac{2n!}{k!(n-k)!} b^{n-k}_{\mu\rho} b^{k\rho}_{\nu}\mathbb{1} \\
&= \left(4b^n_{\mu\nu} + \sum_{k=1}^{n-1} \frac{2n!}{k!(n-k)!} b^{n-k}_{\mu\rho} b^{k\rho}_{\nu}\right)\mathbb{1} \overset{!}{=} 0\,.
\end{aligned} \tag{C.5}$$

In the next to last step the first and the last term of the sum was taken out with the aim to get a recursive formula for b^n, which is then

$$b^n_{\mu\nu} = -\frac{1}{2}\sum_{k=1}^{n-1} \frac{n!}{k!(n-k)!} b^{n-k}_{\mu\rho} b^{k\rho}_{\nu} \,. \tag{C.6}$$

The structure of the iteration suggest that the solution is of the form

$$h^n_{\mu\nu} = h_{\mu\rho} h^{\rho}_{\sigma} h^{\sigma}_{\tau} \dots h^{\lambda}_{\nu} \tag{C.7}$$

and indeed plugging the ansatz

$$b^n_{\mu\nu} = n! \lambda_n h^n_{\mu\nu} \tag{C.8}$$

into equation (C.6) leads to

$$\lambda_n = -\frac{1}{2}\sum_{k=1}^{n-1} \lambda_{n-k}\lambda_k \,, \tag{C.9}$$

which has the solution

$$\lambda_n = -\frac{(-1)^n \Gamma(n-\frac{1}{2})}{2\sqrt{\pi}\Gamma(n+1)} \,. \tag{C.10}$$

With this all variations are fixed. We can now write the Dirac matrices as an expansion of variations with respect to the metric. Note that the factor $n!$ from equation C.8 drops out with the usual $1/n!$ from the expansion. So the result is

$$\gamma_\mu = \underbrace{\sum_{n=0} \lambda_n h^n_{\mu\nu}}_{=:B_{\mu\nu}} \bar{\gamma}^\nu \,. \tag{C.11}$$

where we have for defined the quantity B the later use. Note that B depends on the fluctuating metric and hence the full metric can not be used to raise or lower indices. We have to do more computation Dirac matrix $\gamma^\mu = g^{\mu\nu}\gamma_\nu$. This becomes evident when the inverse metric $g^{\mu\nu}$ is expanded in variations of the metric e.g. the first variation of the inverse metric is

$$\delta g^{\mu\nu} = -\bar{g}^{\mu\rho}\delta g_{\rho\sigma}\bar{g}^{\sigma\nu} = -h^{\mu\nu} \,. \tag{C.12}$$

And the second variation is

$$\begin{aligned} \delta^2 g^{\mu\nu} &= -\delta\left(g^{\mu\rho}\delta g_{\rho\sigma} g^{\sigma\nu}\right) \\ &= \bar{g}^{\mu\alpha}\delta g_{\alpha\lambda}\bar{g}^{\lambda\rho}\delta g_{\rho\sigma}\bar{g}^{\sigma\nu} + \bar{g}^{\mu\rho}\delta g_{\rho\sigma}\bar{g}^{\sigma\lambda}\delta g_{\lambda\alpha}\bar{g}^{\alpha\nu} \\ &= 2h^{\mu\rho}h^{\nu}_{\rho} = 2h^2_{\mu\nu} \,. \end{aligned} \tag{C.13}$$

The continuation of this iteration is obvious. Again, the $n!$ just cancels the $1/n!$ from the expansion and we end up with

$$g^{\mu\nu} = \sum_{n=0} (-1)^n h^{n\mu\nu} \tag{C.14}$$

With this input it is easy to compute the variation of γ^μ i.e.

$$\begin{aligned} \gamma^\mu = g^{\mu\nu}\gamma_\nu &= \sum_{n=0} (-1)^n h^{n\mu\nu} \sum_{m=0} \lambda_m h^m_{\nu\rho} \bar{\gamma}^\rho \\ &= \sum_{j=0} \underbrace{\sum_{k=0}^{j} (-1)^{j-k} \lambda_k \, h^{j\mu}_{\ \ \nu}}_{=:\bar{\lambda}_j} \bar{\gamma}^\nu \,. \end{aligned} \tag{C.15}$$

The sum that is defining $\bar{\lambda}$ can be solved with the result

$$\bar{\lambda}_n = \frac{(-1)^n (n+1)\Gamma(n+\frac{1}{2})}{\sqrt{\pi}\Gamma(n+2)} \,. \tag{C.16}$$

It is evident that equation (C.15) can be written in analogy to equation (C.11) with an object similar to B. We decide to call this object $\bar{B}$

$$\gamma^\mu = \bar{B}^{\mu\nu}\gamma_\nu \,. \tag{C.17}$$

From the Clifford algebra

$$\{\gamma^\mu, \gamma_\nu\} = 2\delta^\mu_\nu \tag{C.18}$$

it follows directly by plugging in equations (C.11) and (C.17) that B and $\bar{B}$ are inverse to each other i.e.

$$\bar{B}^{\mu\rho} B_{\rho\nu} = \delta^\mu_\nu \,. \tag{C.19}$$

We are done with the variation of the Dirac matrices and turn now to the variation of the spin connection. The starting point is equation (26) in [28] i.e.

$$\mathcal{D}_\mu \gamma^\nu = -[\Gamma_\mu, \gamma^\nu] \,, \tag{C.20}$$

where $\mathcal{D}$ is the spacetime covariant derivative and hence not including the spin connection. The equation is just holds if the spacetime contorsions part is set to zero and a certain spin connection gauge is chosen. Both choices are acceptable for the computation we are doing. We start by splitting the covariant derivative in equation (C.20) into a background part and a fluctuating part. On the right hand side we introduce an artificial split of the spin connection $\Gamma = \Gamma^{(1)} + \Gamma^{(2)}$, which exactly copies the split on the left hand side. Therefore we obtain two equations

$$\bar{\mathcal{D}}_\mu \gamma^\nu = -[\Gamma^{(1)}_\mu, \gamma^\nu] \qquad \text{and} \qquad \tilde{\Gamma}^\nu_{\mu\rho}\gamma^\rho = -[\Gamma^{(2)}_\mu, \gamma^\nu] \,, \tag{C.21}$$

where $\tilde{\Gamma}$ is the difference between the full Christoffel symbol and the Christoffel symbol on the background. We will first work with the first equation and use equations (C.11) and (C.17). In consequence the equation evolves to

$$\bar{\mathcal{D}}_\mu(\bar{B}^{\nu\rho}\bar{\gamma}_\rho) = -\bar{B}^{\nu\rho}[\Gamma^{(1)}_\mu, \bar{\gamma}_\rho]\,. \tag{C.22}$$

We multiply the equation with $B_{\sigma\nu}$, apply the covariant derivative on the left hand side and split the spin connection into a background and a fluctuating part. The background part of the spin connection is the equal to the background part of the full spin connection. The result is

$$\bar{\mathcal{D}}_\mu\bar{\gamma}_\sigma + B_{\sigma\nu}(\bar{\mathcal{D}}_\mu\bar{B}^{\nu\rho})\bar{\gamma}_\rho = -[\hat{\Gamma}^{(1)}_\mu, \bar{\gamma}_\sigma] - [\bar{\Gamma}_\mu, \bar{\gamma}_\sigma]\,. \tag{C.23}$$

We can identify the background part of equation (C.20) and cancel this part on both sides. To solve the remaining equation it is useful to look on the dependencies of the Dirac matrices on both sides. The left hand side is proportional to $\bar{\gamma}$ and the right hand side to $[.,\bar{\gamma}]$ and therefore the spin connection has to be proportional to $[\bar{\gamma},\bar{\gamma}]$ otherwise the Dirac matrices will not match. This can be proven by splitting the spin connection into a complete basis of complex 4x4 matrices, which is build up of Dirac matrices and the identity matrix. Thus we make the ansatz

$$\Gamma^{(1)}_\mu = t^{\alpha\beta}_\mu[\bar{\gamma}_\alpha, \bar{\gamma}_\beta]\,. \tag{C.24}$$

Inserting this into equation (C.23) and solving for t results in

$$t^{\alpha\beta}_\mu = \frac{1}{8}\bar{g}^{\sigma\alpha}B_{\sigma\nu}\bar{\mathcal{D}}_\mu\bar{B}^{\nu\beta}\,. \tag{C.25}$$

Together with the definition of B in equation (C.11) this is the expansion around the background metric of the first part of the spin connection. We can put in the definition of B and pick the n-th variation of it by choosing the terms that contain n powers of h. The result is the complicated expression

$$\delta^n t^{\alpha\beta}_\mu = -\frac{1}{8}\sum_{k=0}^{n-1}(-1)^k\binom{n-1}{k}\frac{\Gamma(\frac{3}{2}+k)}{\Gamma(\frac{3}{2}+k-n)}h^{n-k-1,\alpha\nu}(\bar{\mathcal{D}}_\mu h_{\nu\rho})h^{k,\rho\beta}\,. \tag{C.26}$$

Now we can turn to the second part of equation (C.21). We again apply the same argument as before that the spin connection has to be proportional to $[\gamma,\gamma]$ and make the same ansatz as in equation (C.24). This time we call the factor s. Inserting this ansatz and solving for s results in

$$s_{\mu,\alpha\beta} = -\frac{1}{8}g_{\rho\beta}\tilde{\Gamma}^\rho_{\mu\alpha}\,. \tag{C.27}$$

The fluctuating part of the Christoffel symbol is inserted and the antisymmetry of s under the exchange of the indices α and β is used. The result is the simple expression

$$s_{\mu,\alpha\beta} = -\frac{1}{8}\bar{\mathcal{D}}_\alpha h_{\mu\beta}\,. \tag{C.28}$$

With this also the second part of the spin connection is written as expansion. Finally we want to present the full n-th variation of the spin connection:

$$\begin{aligned}\delta^n\Gamma_\mu = -\frac{1}{8}\Bigg(&\sum_{k=0}^{n-1}(-1)^k\binom{n-1}{k}\frac{\Gamma(\frac{3}{2}+k)}{\Gamma(\frac{3}{2}+k-n)}h^{n-k-1,\alpha\nu}(\bar{\mathcal{D}}_\mu h_{\nu\rho})h^{k,\rho\beta}[\bar{\gamma}_\alpha,\bar{\gamma}_\beta]\\ &+ n\bar{\mathcal{D}}_\alpha h_{\mu\beta}\delta^{n-1}[\gamma^\alpha,\gamma^\beta]\Bigg)\,.\end{aligned} \tag{C.29}$$

This is the formula that is implemented in *TARDIS*. Together with the variations of the Dirac matrices this gives for a computer an easy computable formula. For computation by hand this formula can be simplified a little further by plugging in the known expressions for the Dirac matrices and by using symmetry arguments. The resulting formula is unfortunately quite long and unhandy:

$$\begin{aligned}\delta^n\Gamma_\mu = -\frac{1}{8}[\bar{\gamma}_\alpha,\bar{\gamma}_\beta]\Bigg(&\sum_{k=1}^{\leq n/2} f_1(n,k)h^{k-1,\alpha\nu}h^{n-k,\beta\varrho}\left(f_2(n,k)\bar{D}_\mu h_{\nu\varrho} + 2\bar{D}_{[\nu}h_{\varrho]\mu}\right)\\ &+ f_3(n)\bar{D}_\nu h_{\varrho\mu}h^{(n-1)/2,\alpha\nu}h^{(n-1)/2,\beta\varrho}\Bigg)\,,\end{aligned} \tag{C.30}$$

with

$$f_1(n,k) = (-1)^{k-1}k\binom{n}{k}\frac{\Gamma(k-\frac{1}{2})}{\Gamma(k-n+\frac{1}{2})} \tag{C.31}$$

$$f_2(n,k) = 3 + \frac{1-2k}{n} + \frac{n}{1/2-k} \tag{C.32}$$

$$f_3(n) = \begin{cases}0, & \text{if } n \text{ even},\\ (-1)^{(n-1)/2}\frac{(2n)!}{2((n-1)/2)!((n+1)/2)!}, & \text{if } n \text{ odd}.\end{cases} \tag{C.33}$$

Acknowledgements

First of all, I want to thank my supervisor Prof. Jan Pawlowski for giving me the opportunity to work on this project and for his excellent supervision. It was a great pleasure to work in his group and I gained a lot of physical insights during the work. It was very nice, that the door for discussions was always opened. Then, I want to thank Prof. Tilman Plehn for doing the second correction of this thesis. Also, I want to thank all my collaborators for nice atmosphere and great teamwork. In my humble opinion, this teamwork was the key that we achieved quite some nice results. Further, I want to thank my office mates, Jan and Tobias, for perfect atmosphere in the office, that allowed working when it was necessary and fun when it was possible. I want to thank Andreas, Celia, Nic, Tobias and Zhanna for proof reading my introduction and giving useful hints on it. Zhanna deserves further credits for the help on the three-dimensional plot. At last, I want to thank my family, my friends and especially my girlfriend, Zhanna, for constant support during the whole time. Further, I want to thank my friends for the nice distractions in the evenings.

D Lists

D.1 List of Figures

D.2 List of Tables

E Bibliography

[1] Steven Weinberg. Asymptotically Safe Inflation. *Phys. Rev.*, D81:083535, 2010. doi: 10.1103/PhysRevD.81.083535.

[2] Kevin Falls, Daniel F. Litim, and Aarti Raghuraman. Black Holes and Asymptotically Safe Gravity. *Int.J.Mod.Phys.*, A27:1250019, 2012. doi: 10.1142/S0217751X12500194.

[3] Erik Gerwick, Daniel Litim, and Tilman Plehn. Asymptotic safety and Kaluza-Klein gravitons at the LHC. *Phys.Rev.*, D83:084048, 2011. doi: 10.1103/PhysRevD.83.084048.

[4] Gerard 't Hooft and M.J.G. Veltman. One loop divergencies in the theory of gravitation. *Annales Poincare Phys.Theor.*, A20:69–94, 1974.

[5] Steven Weinberg. Ultraviolet Divergences in Quantum Theories of Gravitation. *General Relativity: An Einstein centenary survey, Eds. Hawking, S.W., Israel, W; Cambridge University Press*, pages 790–831, 1979.

[6] Kenneth G. Wilson. The Renormalization Group and Strong Interactions. *Phys.Rev.*, D3:1818, 1971. doi: 10.1103/PhysRevD.3.1818.

[7] Joseph Polchinski. Renormalization and Effective Lagrangians. *Nucl.Phys.*, B231:269–295, 1984. doi: 10.1016/0550-3213(84)90287-6.

[8] Christof Wetterich. Exact evolution equation for the effective potential. *Phys.Lett.*, B301:90–94, 1993. doi: 10.1016/0370-2693(93)90726-X.

[9] M. Reuter and C. Wetterich. Effective average action for gauge theories and exact evolution equations. *Nucl.Phys.*, B417:181–214, 1994. doi: 10.1016/0550-3213(94)90543-6.

[10] Tim R. Morris. The Exact renormalization group and approximate solutions. *Int. J. Mod. Phys.*, A9:2411–2450, 1994. doi: 10.1142/S0217751X94000972.

[11] Jan M. Pawlowski, Daniel F. Litim, Sergei Nedelko, and Lorenz von Smekal. Infrared behavior and fixed points in Landau gauge QCD. *Phys.Rev.Lett.*, 93: 152002, 2004. doi: 10.1103/PhysRevLett.93.152002.

[12] M. Reuter. Nonperturbative Evolution Equation for Quantum Gravity. *Phys. Rev.*, D57:971–985, 1998. doi: 10.1103/PhysRevD.57.971.

[13] Wataru Souma. Nontrivial ultraviolet fixed point in quantum gravity. *Prog.Theor.Phys.*, 102:181–195, 1999. doi: 10.1143/PTP.102.181.

[14] M. Reuter and Frank Saueressig. Renormalization group flow of quantum gravity in the Einstein-Hilbert truncation. *Phys.Rev.*, D65:065016, 2002. doi: 10.1103/PhysRevD.65.065016.

[15] Max Niedermaier and Martin Reuter. The Asymptotic Safety Scenario in Quantum Gravity. *Living Rev.Rel.*, 9:5, 2006.

[16] Alessandro Codello, Roberto Percacci, and Christoph Rahmede. Investigating the Ultraviolet Properties of Gravity with a Wilsonian Renormalization Group Equation. *Annals Phys.*, 324:414–469, 2009. doi: 10.1016/j.aop.2008.08.008.

[17] Roberto Percacci. Asymptotic Safety. 2007. to appear in 'Approaches to Quantum Gravity: Towards a New Understanding of Space, Time and Matter' ed. D. Oriti, Cambridge University Press.

[18] Alessandro Codello, Roberto Percacci, and Christoph Rahmede. Ultraviolet properties of f(R)-gravity. *Int. J. Mod. Phys.*, A23:143–150, 2008. doi: 10.1142/S0217751X08038135.

[19] Elisa Manrique, Martin Reuter, and Frank Saueressig. Bimetric Renormalization Group Flows in Quantum Einstein Gravity. *Annals Phys.*, 326:463–485, 2011. doi: 10.1016/j.aop.2010.11.006.

[20] Ivan Donkin and Jan M. Pawlowski. The phase diagram of quantum gravity from diffeomorphism-invariant RG-flows. 2012.

[21] Nicolai Christiansen, Benjamin Knorr, Jan M. Pawlowski, and Andreas Rodigast. Global Flows in Quantum Gravity. 2014.

[22] Nicolai Christiansen, Daniel F. Litim, Jan M. Pawlowski, and Andreas Rodigast. Fixed points and infrared completion of quantum gravity. *Phys.Lett.*, B728:114–117, 2014. doi: 10.1016/j.physletb.2013.11.025.

[23] U. Harst and M. Reuter. QED coupled to QEG. *JHEP*, 05:119, 2011. doi: 10.1007/JHEP05(2011)119.

[24] Astrid Eichhorn and Holger Gies. Light fermions in quantum gravity. 2011.

[25] Djamel Dou and Roberto Percacci. The running gravitational couplings. *Class.Quant.Grav.*, 15:3449–3468, 1998. doi: 10.1088/0264-9381/15/11/011.

[26] Pietro Donà, Astrid Eichhorn, and Roberto Percacci. Matter matters in asymptotically safe quantum gravity. *Phys.Rev.*, D89:084035, 2014. doi: 10.1103/PhysRevD.89.084035.

[27] P. Donà, Astrid Eichhorn, and Roberto Percacci. Consistency of matter models with asymptotically safe quantum gravity. 2014.

[28] Holger Gies and Stefan Lippoldt. Fermions in gravity with local spin-base invariance. *Phys.Rev.*, D89:064040, 2014. doi: 10.1103/PhysRevD.89.064040.

[29] Holger Gies. Introduction to the functional RG and applications to gauge theories. *Lect.Notes Phys.*, 852:287–348, 2012. doi: 10.1007/978-3-642-27320-9_6.

[30] Juergen Berges, Nikolaos Tetradis, and Christof Wetterich. Non-perturbative renormalization flow in quantum field theory and statistical physics. *Phys. Rept.*, 363:223–386, 2002. doi: 10.1016/S0370-1573(01)00098-9.

[31] Nicolai Christiansen. Towards Ultraviolet Stability in Quantum Gravity. Master's thesis, Heidelberg University, 2011.

[32] Benjamin Knorr. Towards Global Completeness in Asymtotically Safe Gravity. Master's thesis, Heidelberg University, 2013.

[33] Pietro Dona and Roberto Percacci. Functional renormalization with fermions and tetrads. *Phys.Rev.*, D87(4):045002, 2013. doi: 10.1103/PhysRevD.87.045002.

[34] Daniel F. Litim. Optimization of the exact renormalization group. *Phys.Lett.*, B486:92–99, 2000. doi: 10.1016/S0370-2693(00)00748-6.

[35] W.G. Unruh. A Unimodular Theory of Canonical Quantum Gravity. *Phys.Rev.*, D40:1048, 1989. doi: 10.1103/PhysRevD.40.1048.

[36] Steven Weinberg. The Cosmological Constant Problem. *Rev.Mod.Phys.*, 61:1–23, 1989. doi: 10.1103/RevModPhys.61.1.

[37] Astrid Eichhorn. The Renormalization Group flow of unimodular f(R) gravity. 2015.

[38] K. Falls, D.F. Litim, K. Nikolakopoulos, and C. Rahmede. A bootstrap towards asymptotic safety. 2013.

[39] Kevin Falls, Daniel F. Litim, Konstantinos Nikolakopoulos, and Christoph Rahmede. Further evidence for asymptotic safety of quantum gravity. 2014.

[40] Tobias Henz. Dilaton Symmetric Scalar-Tensor Theories of Quantum Gravity. Master's thesis, Heidelberg University, 2012.

[41] Dario Benedetti, Kai Groh, Pedro F. Machado, and Frank Saueressig. The Universal RG Machine. *JHEP*, 1106:079, 2011. doi: 10.1007/JHEP06(2011)079.

[42] O. Lauscher and M. Reuter. Flow equation of quantum Einstein gravity in a higher- derivative truncation. *Phys. Rev.*, D66:025026, 2002. doi: 10.1103/PhysRevD.66.025026.

[43] Stefan Rechenberger and Frank Saueressig. The R^2 phase-diagram of QEG and its spectral dimension. *Phys.Rev.*, D86:024018, 2012. doi: 10.1103/PhysRevD.86.024018.

[44] Astrid Eichhorn, Holger Gies, and Michael M. Scherer. Asymptotically free scalar curvature-ghost coupling in Quantum Einstein Gravity. *Phys. Rev.*, D80:104003, 2009. doi: 10.1103/PhysRevD.80.104003.

[45] Kai Groh and Frank Saueressig. Ghost wave-function renormalization in Asymptotically Safe Quantum Gravity. *J. Phys.*, A43:365403, 2010. doi: 10.1088/1751-8113/43/36/365403.

[46] Astrid Eichhorn and Holger Gies. Ghost anomalous dimension in asymptotically safe quantum gravity. *Phys. Rev.*, D81:104010, 2010. doi: 10.1103/PhysRevD.81.104010.

[47] Elisa Manrique and Martin Reuter. Bimetric Truncations for Quantum Einstein Gravity and Asymptotic Safety. *Annals Phys.*, 325:785–815, 2010. doi: 10.1016/j.aop.2009.11.009.

[48] Elisa Manrique, Martin Reuter, and Frank Saueressig. Matter Induced Bimetric Actions for Gravity. *Annals Phys.*, 326:440–462, 2011. doi: 10.1016/j.aop.2010.11.003.

[49] Martin Reuter and Holger Weyer. Background Independence and Asymptotic Safety in Conformally Reduced Gravity. *Phys. Rev.*, D79:105005, 2009. doi: 10.1103/PhysRevD.79.105005.

[50] Peter Fischer and Daniel F. Litim. Fixed points of quantum gravity in extra dimensions. *Phys.Lett.*, B638:497–502, 2006. doi: 10.1016/j.physletb.2006.05.073.

[51] Kevin Falls and Daniel F. Litim. Black hole thermodynamics under the microscope. 2012.

[52] Roberto Percacci and Daniele Perini. Asymptotic safety of gravity coupled to matter. *Phys. Rev.*, D68:044018, 2003. doi: 10.1103/PhysRevD.68.044018.

[53] Gaurav Narain and Roberto Percacci. Renormalization Group Flow in Scalar-Tensor Theories. I. *Class. Quant. Grav.*, 27:075001, 2010. doi: 10.1088/0264-9381/27/7/075001.

[54] Gaurav Narain and Christoph Rahmede. Renormalization Group Flow in Scalar-Tensor Theories. II. *Class. Quant. Grav.*, 27:075002, 2010. doi: 10.1088/0264-9381/27/7/075002.

[55] Tobias Henz, Jan Martin Pawlowski, Andreas Rodigast, and Christof Wetterich. Dilaton Quantum Gravity. 2013.

[56] Roberto Percacci and Gian Paolo Vacca. Search of scaling solutions in scalar-tensor gravity. 2015.

[57] Astrid Eichhorn. Quantum-gravity-induced matter self-interactions in the asymptotic-safety scenario. *Phys.Rev.*, D86:105021, 2012. doi: 10.1103/PhysRevD.86.105021.

[58] Jan Meibohm. Matter in Asymptotically Safe Quantum Gravity. Master's thesis, Heidelberg University, 2015.

[59] Astrid Eichhorn. Experimentally testing asymptotically safe quantum gravity with photon-photon scattering. pages 2233–2235, 2015. doi: 10.1142/9789814623995_0406.

[60] Sarah Folkerts, Daniel F. Litim, and Jan M. Pawlowski. Asymptotic freedom of Yang-Mills theory with gravity. *Phys.Lett.*, B709:234–241, 2012. doi: 10.1016/j.physletb.2012.02.002.

[61] Sarah Folkerts. Asymptotic Safety for Gravity coupled to Yang-Mills Theory: an RG Study. Master's thesis, Heidelberg University, 2009.

[62] Roberto Percacci and Daniele Perini. Constraints on matter from asymptotic safety. *Phys. Rev.*, D67:081503, 2003. doi: 10.1103/PhysRevD.67.081503.

[63] Alessandro Codello. Large N Quantum Gravity. *New J.Phys.*, 14:015009, 2012. doi: 10.1088/1367-2630/14/1/015009.

[64] Holger Gies and Stefan Lippoldt. Global surpluses of spin-base invariant fermions. 2015.

[65] Elisa Manrique, Stefan Rechenberger, and Frank Saueressig. Asymptotically Safe Lorentzian Gravity. *Phys.Rev.Lett.*, 106:251302, 2011. doi: 10.1103/PhysRevLett.106.251302.

[66] Kevin Falls. On the renormalisation of Newton's constant. 2015.

[67] Astrid Eichhorn. On unimodular quantum gravity. *Class.Quant.Grav.*, 30:115016, 2013. doi: 10.1088/0264-9381/30/11/115016.

[68] Andreas Nink. Field Parametrization Dependence in Asymptotically Safe Quantum Gravity. 2014.

[69] Nicolai Christiansen, Benjamin Knorr, Jan Meibohm, Jan Martin Pawlowski, Manuel Reichert, and Andreas Rodigast. Local Quantum Gravity. 2015.

[70] Daniel F. Litim and Jan M. Pawlowski. On general axial gauges for QCD. *Nucl.Phys.Proc.Suppl.*, 74:329–332, 1999. doi: 10.1016/S0920-5632(99)00188-7.

[71] James W. Jr. York. Conformatlly invariant orthogonal decomposition of symmetric tensors on Riemannian manifolds and the initial value problem of general relativity. *J.Math.Phys.*, 14:456–464, 1973. doi: 10.1063/1.1666338.

[72] H. Arthur Weldon. Fermions without vierbeins in curved space-time. *Phys.Rev.*, D63:104010, 2001. doi: 10.1103/PhysRevD.63.104010.

[73] Jens Braun. Fermion Interactions and Universal Behavior in Strongly Interacting Theories. *J.Phys.*, G39:033001, 2012. doi: 10.1088/0954-3899/39/3/033001.

[74] Andreas Rodigast. TARDIS.

[75] Jos Vermaseren. Form. URL `http://www.nikhef.nl/~form`.

[76] José M. Martín-García. xAct. URL `http://www.xact.es`.

[77] K.S. Stelle. Renormalization of Higher Derivative Quantum Gravity. *Phys.Rev.*, D16:953–969, 1977. doi: 10.1103/PhysRevD.16.953.

[78] Walter Metzner, Manfred Salmhofer, Carsten Honerkamp, Volker Meden, and Kurt Schonhammer. Functional renormalization group approach to correlated fermion systems. 2011.

[79] Finn Larsen and Frank Wilczek. Renormalization of black hole entropy and of the gravitational coupling constant. *Nucl.Phys.*, B458:249–266, 1996. doi: 10.1016/0550-3213(95)00548-X.

[80] Xavier Calmet, Stephen D. H. Hsu, and David Reeb. Quantum gravity at a TeV and the renormalization of Newton's constant. *Phys. Rev.*, D77:125015, 2008. doi: 10.1103/PhysRevD.77.125015.

[81] Nicolai Christiansen, Jan Meibohm, Jan Martin Pawlowski, and Manuel Reichert. Gravity Rules. 2015.

Erklärung:

Ich versichere, dass ich diese Arbeit selbstständig verfasst habe und keine anderen als die angegebenen Quellen und Hilfsmittel benutzt habe.

Heidelberg, den 01. April 2015 .....